NATIONAL ADVISORY COMMITTEE FOR AERONAUTICS

TECHNICAL NOTE 3307

AN INVESTIGATION OF A WING-PROPELLER CONFIGURATION EMPLOYING LARGE-CHORD PLAIN FLAPS AND LARGE-DIAMETER PROPELLERS FOR LOW-SPEED FLIGHT AND VERTICAL TAKE-OFF

By Richard E. Kuhn and John W. Draper

Langley Aeronautical Laboratory
Langley Field, Va.

Washington
December 1954

NATIONAL ADVISORY COMMITTEE FOR AERONAUTICS

TECHNICAL NOTE 3307

AN INVESTIGATION OF A WING-PROPELLER CONFIGURATION EMPLOYING LARGE-CHORD PLAIN FLAPS AND LARGE-DIAMETER PROPELLERS FOR LOW-SPEED FLIGHT AND VERTICAL TAKE-OFF

By Richard E. Kuhn and John W. Draper

SUMMARY

An investigation of the effectiveness of a wing equipped with large-chord plain flaps and auxiliary vanes in rotating the thrust vector of two large-diameter propellers through the large angles required for vertical take-off and low-speed flight has been conducted in the Langley 300 MPH 7- by 10-foot tunnel. The semispan model used was equipped with a 60-percent-chord flap, a 30-percent-chord flap, and two large-diameter overlapping propellers.

Under static-thrust conditions, a maximum upward rotation of the effective thrust vector of 45° was obtained with the 60-percent-chord flap deflected 30° and the 30-percent-chord flap deflected 50°. With the addition of two auxiliary vanes, the upward deflection of the thrust vector was increased to 67°. With this configuration, vertical take-off could be made with a take-off attitude of 23° and at airplane weights up to 95 percent of the thrust. A method is presented for calculating the lift due to flap deflection and slipstream for small flap deflections if the lift due to flap deflection at zero thrust and the lift due to flap deflection at zero forward speed are known.

INTRODUCTION

The practical utilization of the helicopter has indicated the usefulness of aircraft that are capable of operating from very small bases. The advantages to be gained with aircraft that incorporate the small-field capabilities of the helicopter and the high-speed potential of conventional airplanes are readily apparent. Numerous designs have been proposed for achieving these advantages. If lift is to be produced, it is necessary to give a mass of air per unit time a downward velocity.

The helicopter uses a large rotor to deflect a large mass of air per unit time downward at a relatively low velocity; however, the consequence of having the rotor axis approximately perpendicular to the flight path seriously limits the high-speed potential of the helicopter.

Reference 1 reports satisfactory flight tests of a configuration with which hovering and vertical landings and take-offs were made possible by turning the slipstream of relatively large-diameter propellers downward by means of a cascade of vanes. The configuration was designed solely to demonstrate the feasibility of this approach and to study the stability and control problems in hovering and in vertical take-off and landing. No provision was made for forward flight.

The present investigation was undertaken to determine the effectiveness of a monoplane wing equipped with plain flaps for deflecting the slipstream through large angles and thereby providing appreciable lift at low forward speeds. The effectiveness of auxiliary vanes, in combination with the plain flaps, in deflection of the slipstream through the large turning angles required for vertical take-off was also investigated.

COEFFICIENTS AND SYMBOLS

When a wing is located in the slipstream of a propeller, large forces and moments can be produced even though the free-stream velocity decreases to zero. For this condition, coefficients based on the free-stream dynamic pressure approach infinity and therefore become meaningless. It appears appropriate, therefore, to base the coefficients on the dynamic pressure in the slipstream. The coefficients based on this principle are indicated in the present paper by the use of a double prime and are defined in this section. The positive sense of the forces, moments, and angles determined for the static-thrust tests is shown in figure 1. For the tests at forward speeds, the usual convention for forces was used; that is, the lift and longitudinal force were taken perpendicular and parallel, respectively, to the free stream.

C_L lift coefficient based on free-stream dynamic pressure, $\frac{L}{qS/2}$

C_L'' lift coefficient, $\frac{L}{q''S/2}$

C_m'' pitching-moment coefficient, $\frac{\text{Pitching moment}}{q''\bar{c}S/2}$

C_{m_p}'' propeller pitching-moment coefficient, $\frac{\text{Propeller pitching moment}}{q''S\bar{c}}$

C_{N_p}'' propeller normal-force coefficient, $\frac{\text{Propeller normal force}}{q''S}$

C_X'' longitudinal-force coefficient, $\frac{\text{Longitudinal force}}{q''S/2}$

T_c'' thrust coefficient, $\frac{T}{q'' \frac{\pi}{4} D^2}$

A aspect ratio

b wing span, ft; also, propeller blade chord, ft

c wing chord, ft

$\bar{c}$ mean aerodynamic chord, $\frac{2}{S} \int_0^{b/2} c^2 dy$, ft

d slipstream diameter at leading edge of wing, ft

D propeller diameter, ft

h propeller-blade thickness, ft

L lift, lb

N number of propellers

q free-stream dynamic pressure, $\frac{\rho V^2}{2}$, lb/sq ft

q'' dynamic pressure in slipstream, $q + \frac{T}{\frac{\pi}{4} D^2}$, lb/sq ft

r radius to propeller blade element, ft

R radius to propeller tip, ft

S	twice semispan-wing area, sq ft
T	thrust per propeller, lb
V	free-stream velocity, ft/sec
ΔV	increment of velocity in slipstream due to thrust
W	airplane weight, lb.
y	spanwise distance from wing root
α	angle of attack, deg
β	propeller-blade angle, deg
$\beta_{.75R}$	propeller-blade angle at 0.75 radius, deg
δ_f	flap deflection, deg
θ	inclination of resultant force vector at zero forward speed, $\arctan \frac{C_L''}{C_X''}$, deg
ϵ	downwash angle without slipstream, deg
ϵ''	downwash angle at any value of T_c'', deg
ρ	mass density of air, slugs/cu ft

Subscripts:

30	30-percent-chord flap
60	60-percent-chord flap
$\alpha=0$	at zero angle of attack
p	for forces and moments acting on propeller
T_c''	at any value of T_c''
mph	in miles per hour

MODEL AND APPARATUS

The semispan wing used in this investigation had an aspect ratio of 4.55, a taper ratio of 0.714, and an NACA 0015 airfoil section. A drawing of the model is presented in figure 2 and photographs of the model are shown in figures 3 and 4. The geometric characteristics of the model are given in the following table:

Wing:	
Area (semispan), sq ft	5.125
Semispan, ft	3.416
Mean aerodynamic chord, ft	1.514
Root chord, ft	1.75
Tip chord, ft	1.25
Airfoil section	NACA 0015
Aspect ratio	4.55
Taper ratio	0.714
Propellers:	
Diameter, ft	2.0
Disk area, sq ft	3.14
Nacelle diameter, ft	0.33

The wing was constructed of mahogany supported by a steel spar and was equipped with plain flaps of 60 and 30 percent chord supported by two internal hinge brackets. The juncture between wing and flap was sealed and faired with aluminum cover plates and cellulose tape.

For some tests, two auxiliary vanes were used in addition to the flaps. The auxiliary-vane configuration is shown in figure 5. The vanes were made of 1/8-inch sheet steel rolled into a 90° arc to a radius of 15 percent of the chord.

The geometric characteristics of the three-blade propellers are given in figure 6. The blades were constructed of aluminum alloy and utilized Clark Y sections. The propellers were driven by variable-frequency electric motors that were rated at 20 horsepower at 18,000 rpm. The large propeller diameter prevented use of this high rotational speed, and during tests the propeller speed seldom exceeded 6,000 rpm. The rotational speed was determined by observing a stroboscopic-type instrument that indicated the output frequency of a small alternator connected to the motor shaft. The outboard propeller rotated clockwise and the inboard propeller rotated counterclockwise. The wing was tested as a right-hand wing.

The motors were mounted inside the aluminum-alloy nacelles through strain-gage beams so that the thrust, torque, lift, and pitching moment

of the propeller and spinner could be measured. The total forces and moments of the configuration were measured on a balance system at the root of the semispan wing.

TESTS

The investigation used two different experimental setups and included tests with both propellers operating. A few tests were also made with only the inboard propeller operating. The tests at zero forward speed were conducted in one end of a large storage room as shown in figures 4 and 7. The model was first set up with the propeller slipstream directed down the long axis of the room toward the far end with the flaps set at zero. With this arrangement, a substantial positive pitching moment was indicated on each propeller. Reversing the orientation of the model to that shown in figure 7 appreciably reduced the indicated propeller pitching moment. This pitching moment was believed to be due to some asymmetrical inflow to the propellers caused by the recirculation of air in the room and obstructions caused by miscellaneous equipment stored in the room. This recirculation had no noticeable effect on the forces existing on the complete semispan model.

The tests with forward velocity were conducted with the semispan model mounted from the ceiling of the Langley 300 MPH 7- by 10-foot tunnel as shown in figure 3. For these tests the shaft thrust of the propellers was held constant throughout the angle-of-attack range and was chosen to give a dynamic pressure of 8 pounds per square foot in the slipstream at zero angle of attack. The corresponding thrust and free-stream dynamic pressures and propeller blade angles for various thrust coefficients are tabulated below:

T_c''	V + ΔV, ft/sec	V, ft/sec	q", lb/sq ft	q, lb/sq ft	T, lb	$\beta_{.75R}$, deg
0	82	82.0	8	8.00	0	Off
.2	↓	73.2	↓	6.40	5.03	20
.5		57.9		4.00	12.5	8
.71		44.2		2.32	17.6	8
.91		24.6		.72	22.6	8
1.00	↓	0	↓	0	25	8

The Reynolds number in the slipstream, based on the mean aerodynamic chord of 1.514 ft, is 0.8×10^6.

In order to minimize the time required for the tests, the operating conditions were chosen so that only two propeller blade-angle settings were required. A blade angle of 8° was found to be satisfactory for thrust coefficients of 0.91, 0.71, and 0.50 and a blade angle of 20° was used for the thrust coefficient of 0.20.

CORRECTIONS

Approximate corrections for the effects of the tunnel walls on the velocity in the tunnel and in the slipstream were derived and are presented in reference 2. These corrections were applied to the results presented in the present paper.

The jet-boundary corrections which were applied to the angle of attack and the longitudinal force were estimated by the method of reference 3. The following corrections were applied to the data:

$$\alpha = \alpha_{measured} + 0.50 C_L''_{(T_c''=0)} \frac{q}{q''}$$

$$C_X'' = C_X''_{measured} - 0.008 \left[C_L''_{(T_c''=0)} \right]^2 \frac{q}{q''}$$

The correction to the pitching moment was estimated and was found to be negligible.

These corrections are strictly applicable only in the low angle-of-attack range; however, they have been applied throughout the entire angle-of-attack range. The lift coefficient for the power-off condition was used in correcting all data.

Corrections to the free-stream dynamic pressure for the effects of the model blockage have not been applied in reducing the data. These corrections are negligible in the low angle-of-attack range but become of increasing importance as the drag increases at the higher angles of attack and higher flap deflections. The correction can be estimated by the method of reference 4 and applied as follows:

$$q_{corrected} = q_{measured} \left[1 + \frac{0.036}{1 - T_c''} \left(C_X'' - T_c'' \cos \alpha \, N(0.613) \right) \right]$$

REDUCTION OF DATA

The data obtained in this investigation would be applicable to the type of flight operation illustrated in figure 8. A flight of this type involves zero forward speed for take-off and landing, where the generated lift is obtained from the thrust of the propellers. In this flight condition, the use of free-stream dynamic pressure in reducing the data to coefficient form would result in extremely high coefficients as the free-stream dynamic pressure is reduced to low values. At zero forward speed, the coefficients would always be infinite and therefore meaningless. For the condition in which the wing is largely immersed in the slipstream of a propeller, the forces would be expected to be largely determined by the dynamic pressure in the slipstream. It appears appropriate, therefore, to base the coefficients on the dynamic pressure in the slipstream. With this system the coefficients approach their normal value as the speed is increased and also have a finite value at zero forward speed. The thrust coefficient T_c'' approaches zero as the speed is increased and is equal to unity at zero forward speed.

The dynamic pressure in the slipstream can be computed from the propeller thrust by the simple momentum theory as follows:

$$T = M_p \, \Delta V_{\alpha=0} = \rho \frac{\pi}{4} D^2 \left(V + \frac{\Delta V_{\alpha=0}}{2} \right) \Delta V_{\alpha=0}$$

where M_p is the mass flow through the propeller and $\Delta V_{\alpha=0}$ is the increment of velocity due to thrust at a great distance behind the propeller at zero angle of attack. The terms can be rearranged as follows:

$$\frac{(\Delta V_{\alpha=0})^2}{2} + V \, \Delta V_{\alpha=0} - \frac{T}{\rho \frac{\pi}{4} D^2} = 0$$

Solving by the quadratic equation yields

$$\Delta V_{\alpha=0} = -V \pm \sqrt{V^2 + 2 \frac{T}{\rho \frac{\pi}{4} D^2}}$$

$$\left(\Delta V_{\alpha=0} + V \right)^2 = V^2 + 2 \frac{T}{\rho \frac{\pi}{4} D^2}$$

$$q''_{\alpha=0} = q + \frac{T}{\frac{\pi}{4} D^2} \tag{1}$$

By definition,

$$T_c'' = \frac{T}{q'' \frac{\pi}{4} D^2}$$

Some other useful relationships can be expressed as:

$$\left(\frac{q}{q''}\right)_{\alpha=0} = 1 - T_c'' \tag{2}$$

$$\left(\frac{V}{V + \Delta V}\right)_{\alpha=0} = \sqrt{1 - T_c''} \tag{3}$$

$$\left(\frac{\Delta V}{V}\right)_{\alpha=0} = \frac{1 - \sqrt{1 - T_c''}}{\sqrt{1 - T_c''}} \tag{4}$$

The above relations have been derived for an angle of attack of 0° but have been applied to the data through the angle-of-attack range.

RESULTS AND DISCUSSION

The results of the investigation are presented in the following figures:

Static Thrust Conditions

In order to obtain vertical take-off, it is necessary to satisfy the conditions that the lift be greater than the weight and the net longitudinal force be equal to zero. One method of satisfying these conditions would involve placement of the thrust axis in the vertical plane, as was considered in reference 2. After take-off, the thrust axis then could be mechanically rotated into the horizontal plane to convert to the cruising configuration. Another approach to the problem is illustrated in reference 1, in which the propeller axis is always essentially horizontal and the thrust is rotated to a near-vertical position aerodynamically by turning the slipstream by means of four turning vanes. The cascade configuration of reference 1 was designed only for exploratory studies of hovering and vertical take-off and landing and was not intended to be a configuration that could easily be converted for cruising flight.

The present investigation was undertaken to determine the extent to which the effective propeller-thrust vector can be rotated by the use of large-chord flaps and to determine what other modifications (such as auxiliary vanes) would be required with the propeller axis essentially horizontal to rotate the thrust vector sufficiently to make vertical take-off possible. In general, it is not necessary to rotate the thrust vector through a full 90° since, if a ground attitude at take-off were 15° to 20°, the wing configuration would be required to rotate the thrust vector only 70° to 75°.

The angle through which the thrust vector has been rotated can easily be deduced by plotting the data as indicated in figure 1. For any particular flap setting, the lift is plotted against the longitudinal force to represent the resultant-force vector and indicate the angle θ through which the thrust vector has been rotated. The ratio of the resultant force to the thrust represents the effectiveness of the turning.

Plain-flap configuration.- With plain flaps alone, the thrust vector could be rotated upward as much as 45° and this rotation could be obtained with a turning efficiency of 90 percent with flap deflections of 30° and 50° on the 60-percent-chord and 30-percent-chord flap, respectively (fig. 9(e)). This rotation of the thrust vector fell far short of the 70° to 75° desired for vertical take-off. Higher flap deflections, in general, resulted in decreases in both turning effectiveness and the angle through which the thrust vector was rotated.

Two apparent eccentricities in the data of figure 9 are worthy of discussion. Figures 9(d) and 9(f) indicate that, with the flaps neutral, the longitudinal force is greater than the thrust, so that the wing drag is negative. This result can probably be attributed to recovery by the wing of some of the rotational energy in the slipstream. The rotation in the slipstream causes a local positive angle of attack on one side of the thrust axis and the lift vector associated with this local flow is inclined forward. The negative lift vector associated with downflow on the other side of the thrust axis is also inclined forward. Both vectors produce a component of force in the negative drag direction.

The small turning angle indicated in figure 9(f) with flaps retracted is probably due to the upflow between the propellers, which produces a lift that is not fully counteracted by the downflow outside of the slipstream due to losses at the wing tip.

The effects of the number of propellers on the aerodynamic characteristics of the wing with only the 30-percent-chord flap deflected are illustrated in figure 10. For this configuration, the number of propellers used is seen to have little effect on the turning effectiveness (fig. 10(f)).

Auxiliary-vane configuration.- In an attempt to increase the angle through which the thrust vector could be rotated, some exploratory tests were conducted with auxiliary vanes. The configuration presented in figure 5 was judged to be reasonable on the basis of maximum turning angle and the ratio of resultant force to thrust obtained. No attempt was made to determine an optimum configuration from the standpoint of vane size.

For the configuration with the auxiliary vanes extended, for example, vertical take-off could be achieved with a ground attitude of 23° and at airplane weights up to 95 percent of the propeller thrust (fig. 11(f)).

The use of only the inboard propeller materially reduced the angle through which the thrust vector could be rotated (fig. 11). Figure 12 shows a summary plot of the turning effectiveness of the wing with the optimum combinations of plain flaps and flaps with vanes.

Tests With Forward Speed

Basic data.- The tests of the model with forward speed for the range of thrust coefficients were made in the Langley 300 MPH 7- by 10-foot tunnel. The basic data for the various flap configurations with both propellers operating are presented in figures 13 to 22 and with only the inboard propeller operating, in figures 23 to 26. It should be kept in mind that, for these data, the shaft thrust of the propellers was held constant throughout the angle-of-attack range. Also, all the direct propeller forces were included in these data. Results presented for configurations with zero flap deflection (figs. 13 and 23) were obtained from reference 2. The characteristics of the wing alone and the effects of the nacelles on the aerodynamic characteristics are presented in reference 2. It should be remembered that the coefficients are based on the dynamic pressure in the slipstream as indicated by the double prime used with the symbols.

Effect of flap deflection and thrust coefficient on lift characteristics.- The application of power is seen to increase the angle of attack for maximum lift and decrease the variation of lift with angle of attack above maximum lift. The variation of lift-curve slope with thrust coefficient (flaps neutral) is discussed in reference 2. The variation of lift coefficient with flap deflection is presented in figure 27 and the variation of $\frac{\partial C_L''}{\partial \delta_f}$ with thrust coefficient is presented in figure 28. The decrease in $\frac{\partial C_L''}{\partial \delta_f}$ at the higher thrust coefficients is due to the decrease in the mass flow of air that the wing had available to deflect at the lower speeds (high T_c'').

In an attempt to calculate the value of $\frac{\partial C_L''}{\partial \delta_f}$ through the thrust-coefficient range, the following analysis was found to be successful for small flap deflections. The momentum theory of lift states that lift is produced by imparting a downward velocity to the mass of air contained in a stream tube of diameter equal to the wing span. In the case of a wing in the presence of a slipstream, the lift would be made up of two parts - that due to deflecting the mass of air in the slipstream and that due to deflecting the mass flow in the stream tube but external to the slipstreams.

At zero thrust, the lift can be written as

$$L_{T_c''=0} = \rho \frac{\pi}{4} b^2 V^2 \sin \epsilon$$

At other values of T_c'',

$$L_{T_c''} = \rho \frac{\pi}{4}\left(b^2V^2 \sin \epsilon'' - Nd^2V^2 \sin \epsilon''\right) + N\rho \frac{\pi}{4} D^2\left(V + \frac{\Delta V}{2}\right)(V + \Delta V)\sin \epsilon''$$

where the first term represents the lift due to deflecting the mass of air external to the propeller slipstreams and the second term represents the lift due to deflecting the slipstreams themselves. For small angles of downwash, $\sin \epsilon'' = \frac{\epsilon''}{57.3}$ and in coefficient form

$$\left(\frac{\partial C_L''}{\partial \delta_f}\right)_{T_c''} = \left(\frac{\partial C_L''}{\partial \delta_f}\right)_{T_c''=0} (1 - T_c'') \frac{\rho \frac{\pi}{4}\left(b^2V^2 \frac{\partial \epsilon''}{\partial \delta_f} - Nd^2V^2 \frac{\partial \epsilon''}{\partial \delta_f}\right) + N\rho \frac{\pi}{4} D^2\left(V + \frac{\Delta V}{2}\right)(V + \Delta V)\frac{\partial \epsilon''}{\partial \delta_f}}{\rho \frac{\pi}{4} b^2V^2 \frac{\partial \epsilon}{\partial \delta_f}}$$

where d is the propeller slipstream diameter at the wing (ref. 2).

In terms of the thrust coefficient,

$$\left(\frac{\partial C_L''}{\partial \delta_f}\right)_{T_c''} = \left(\frac{\partial C_L}{\partial \delta_f}\right)_{T_c''=0} \left(1 - T_c''\right) \frac{\partial \epsilon''/\partial \delta_f}{\partial \epsilon/\partial \delta_f} \left\{1 - \frac{Nd^2}{b^2} + \frac{ND^2}{b^2}\left[\frac{1 + \sqrt{1 - T_c''}}{2(1 - T_c'')}\right]\right\}$$

At $T_c'' = 0$,

$$\tan \frac{\epsilon}{2} = \frac{C_{D_i}}{C_L}$$

where C_{D_i} is the induced-drag coefficient given by

$$C_{D_i} = \frac{C_L^2}{\pi A}$$

For small angles, then,

$$\epsilon = 2(57.3)\frac{C_L^2/\pi A}{C_L}$$

$$\frac{\partial \epsilon}{\partial \delta_f} = \frac{2(57.3)\frac{\partial C_L}{\partial \delta_f}}{\pi A} \tag{5}$$

At $T_c'' = 1.0$ and small flap deflections,

$$\frac{\partial \epsilon''}{\partial \delta_f} = \frac{\partial \theta}{\partial \delta_f}$$

The variation of ϵ'' with thrust coefficient can be derived if the flow in the slipstreams and the flow external to the slipstreams mix according to the strength of their velocity vectors as indicated in the following sketch:

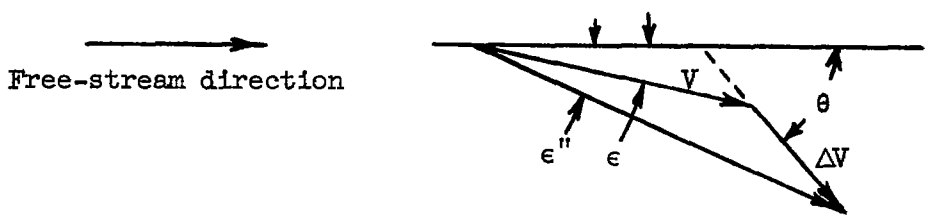

In this sketch, ϵ is the downwash angle if the propeller slipstreams are not present ($T_c'' = 0$) and θ is the downwash angle of the slipstream ($T_c'' = 1$). Then,

$$\tan \epsilon'' = \frac{(\sin \theta)\Delta V + (\sin \epsilon)V}{(\cos \theta)\Delta V + (\cos \epsilon)V}$$

For small angles,

$$\frac{\epsilon''}{\epsilon} = \frac{V}{V + \Delta V} + \frac{\Delta V}{V + \Delta V}\frac{\theta}{\epsilon}$$

and, from equations (3) and (4),

$$\frac{\partial \epsilon'' / \partial \delta_f}{\partial \epsilon / \partial \delta_f} = \sqrt{1 - T_c''} + \frac{\partial \theta / \partial \delta_f}{\partial \epsilon / \partial \delta_f}\left(1 - \sqrt{1 - T_c''}\right)$$

The resulting expression for lift coefficient due to flap deflection is

$$\frac{\partial C_L''}{\partial \delta_f} = \left(\frac{\partial C_L}{\partial \delta_f}\right)_{T_c''=0}\left[\sqrt{1 - T_c''} + \frac{\partial\theta/\partial\delta_f}{\partial\epsilon/\partial\delta_f}\left(1 - \sqrt{1 - T_c''}\right)\right]\left[\left(1 - T_c''\right)\left(1 - \frac{ND^2}{b^2}\right) + \frac{ND^2}{b^2}\left(\frac{1 + \sqrt{1 - T_c''}}{2}\right)\right] \tag{6}$$

For the 30-percent-chord-flap configuration (fig. 9(e)),

$$\frac{\partial\theta}{\partial\delta_f} = 0.5$$

and substituting the value for $\partial C_L''/\partial\delta_f$ from figure 27 at small deflections and $T_c'' = 0$ into equation (5) gives

$$\frac{\partial\epsilon}{\partial\delta_f} = 0.28$$

Application of the foregoing analysis gives reasonably good agreement with the experimental data (fig. 28).

Effect of flap deflection on propeller characteristics.- The effect of angle of attack on the aerodynamic characteristics of the isolated propeller and of both propellers operating in the presence of the wing has been discussed in reference 2. Consequently, only the effects of flap deflection and angle of attack are presented herein. The effects of these parameters on C_{N_p}'' and C_{m_p}'' are presented in figures 29 and 30, respectively. As mentioned in reference 2, some difficulties were experienced with the instrumentation for the inboard propeller that resulted in excessive scatter and large shifts in the wind-off readings. The scatter in the data of figures 29 and 30 can be attributed to this cause.

The normal-force data show appreciable scatter (fig. 29); however, flap deflection appears to have no consistent effect on the normal-force

coefficient. The propellers of the test model were located relatively far ahead of the wing where the upwash due to the wing would be small.

The operation of the propeller in the presence of the wing is seen almost to double the pitching moment of the propeller as compared with that of the isolated propeller (fig. 30). Deflection of the flaps produces a further increase in the propeller pitching moment. These increases cannot be attributed to an increase in wing-induced upwash at the propeller disk because an increase in upwash should produce corresponding increases in propeller normal force. It is probable that these increases in pitching moment are due to a change in the velocity through the upper and lower portions (relative to the wing-chord plane) of the propeller disk. An increase in velocity over the wing (upper part of the propeller disk) would tend to decrease the thrust from the upper part of the disk. Conversely, a decrease in velocity through the lower half of the disk would increase the thrust of this part of the propeller, which results in an increase in the nose-up pitching moment of the propeller with increasing angle of attack and with increasing flap deflection.

The propeller pitching moment can be regarded as an effective displacement of the thrust of the propeller axis. The effective location of the thrust vector is presented in figure 31 and was determined from the pitching-moment data of figure 30 by the following relationship:

$$\frac{r}{R} = \frac{C_{m_p} "S\bar{c}}{T_c " \frac{\pi D^3}{8}}$$

For the most extreme conditions the thrust vector is seen to move downward more than one-fourth of the propeller radius.

Application of Results

Some performance calculations have been made for an assumed airplane in order to illustrate the application of the data and to permit a more thorough analysis of the results. A wing loading W/S of 40 pounds per square foot and a drag coefficient of 0.01 for the fuselage and other parts of the airplane not represented by the model were assumed. The flight plan was assumed to start with the auxiliary vanes extended and flaps deflected $\left(\delta_{f_{30}} = 20^\circ \text{ and } \delta_{f_{60}} = 60^\circ\right)$ for vertical take-off at an airplane attitude of 23° (data of fig. 11). The airplane attitude was then reduced to a lower angle, for example 5°, after which the vanes, the 60-percent-chord flap, and the 30-percent-chord flap were retracted, in that order.

The thrust coefficient required for zero longitudinal force and the lift coefficient available for various flap configurations were determined by cross-plotting the longitudinal force and lift coefficients against thrust coefficient as in figure 32. The forward velocities associated with these conditions are calculated by the expression

$$V_{mph} = \frac{60}{88}\sqrt{\frac{W/S}{C_L''}\left(1 - T_c''\right)\frac{2}{\rho}}$$

The thrust coefficient required and lift coefficient available are plotted against forward speed in figure 33. Unfortunately, the failure of one of the blades in the outboard propeller terminated the test in the tunnel before the tests of the auxiliary-vane configuration at the intermediate thrust coefficients could be performed.

The performance of the present configuration, in which the propeller thrust is used for vertical take-off by deflecting the slipstream downward with the wing and vanes, is compared in figures 33 to 35 with the performance of the configuration of reference 2 in which the entire wing and propeller are rotated from vertical for take-off to horizontal for cruising flight. The present configuration requires somewhat lower thrust coefficients and lower thrust horsepower for level flight at low forward speeds (figs. 33 and 34). The power required was calculated by the method of reference 2. The power required for take-off is somewhat higher for the present configuration because of the losses associated with turning the slipstream downward. These losses do not appear excessive, however, and can probably be reduced in a more efficient design. For either configuration, if a high-speed propeller efficiency of 0.85 and a static thrust efficiency of 0.65 is assumed, there will be sufficient power available for take-off if the airplane is designed for a speed of the order of 400 mph.

The pitching moments that would have to be balanced by some auxiliary means are presented in figure 35, along with the corresponding effective moment arm of the center of lift $\partial C_m''/\partial C_L''$. The diving moments associated with the present configuration are appreciably larger than the nose-up moments for the configuration of reference 2. Also, at zero forward speed, the present configuration has a large diving moment while the pitching moment for the configuration of reference 2 would, of course, be zero. Both are presented with reference to an assumed center of gravity at the quarter chord of the mean aerodynamic chord.

CONCLUSIONS

An investigation of a wing-propeller configuration employing large-diameter propellers and large-chord plain flaps for low-speed flight and vertical take-off indicates the following conclusions:

1. Under static thrust conditions, the use of plain flaps alone (60-percent-chord flap deflected 30° and the 30-percent-chord flap deflected 50°) were effective in rotating the thrust vector upward only about 45°.

2. The configuration with two auxiliary vanes in combination with the plain flaps rotated the thrust vector upward 67°. With this configuration, vertical take-off could be made with an initial attitude of 23° and at airplane weights up to 95 percent of the thrust of the propellers.

3. It is shown that the lift due to flap deflection and slipstream can be calculated for the configurations tested for small flap deflections if the lift due to flap deflection at zero thrust and the lift due to flap deflection at zero forward speed are known.

4. Application of the results to a hypothetical airplane having the same ratio of propeller-disk area to wing area as the model tested and designed for a wing loading of 40 pounds per square foot and a speed of 400 miles per hour indicates that sufficient power would be available for this configuration to achieve vertical take-off. Also, at zero forward speed, large diving moments are shown to be associated with this configuration.

Langley Aeronautical Laboratory,
National Advisory Committee for Aeronautics,
Langley Field, Va., August 26, 1954.

REFERENCES

1. McKinney, Marion O., Tosti, Louis P., and Davenport, Edwin E.: Dynamic Stability and Control Characteristics of a Cascade-Wing Vertically Rising Airplane Model in Take-Offs, Landings, and Hovering Flight. NACA TN 3198, 1954.

2. Draper, John W., and Kuhn, Richard E.: Investigation of the Aerodynamic Characteristics of a Model Wing-Propeller Combination and of the Wing and Propeller Separately at Angles of Attack up to 90°. NACA TN 3304, 1954.

3. Gillis, Clarence L., Polhamus, Edward C., and Gray, Joseph L., Jr.: Charts for Determining Jet-Boundary Corrections for Complete Models in 7- by 10-Foot Closed Rectangular Wind Tunnels. NACA WR L-123, 1945. (Formerly NACA ARR L5G31.)

4. Herriot, John G.: Blockage Corrections for Three-Dimensional-Flow Closed-Throat Wind Tunnels, With Consideration of the Effect of Compressibility. NACA Rep. 995, 1950. (Supersedes NACA RM A7B28.)

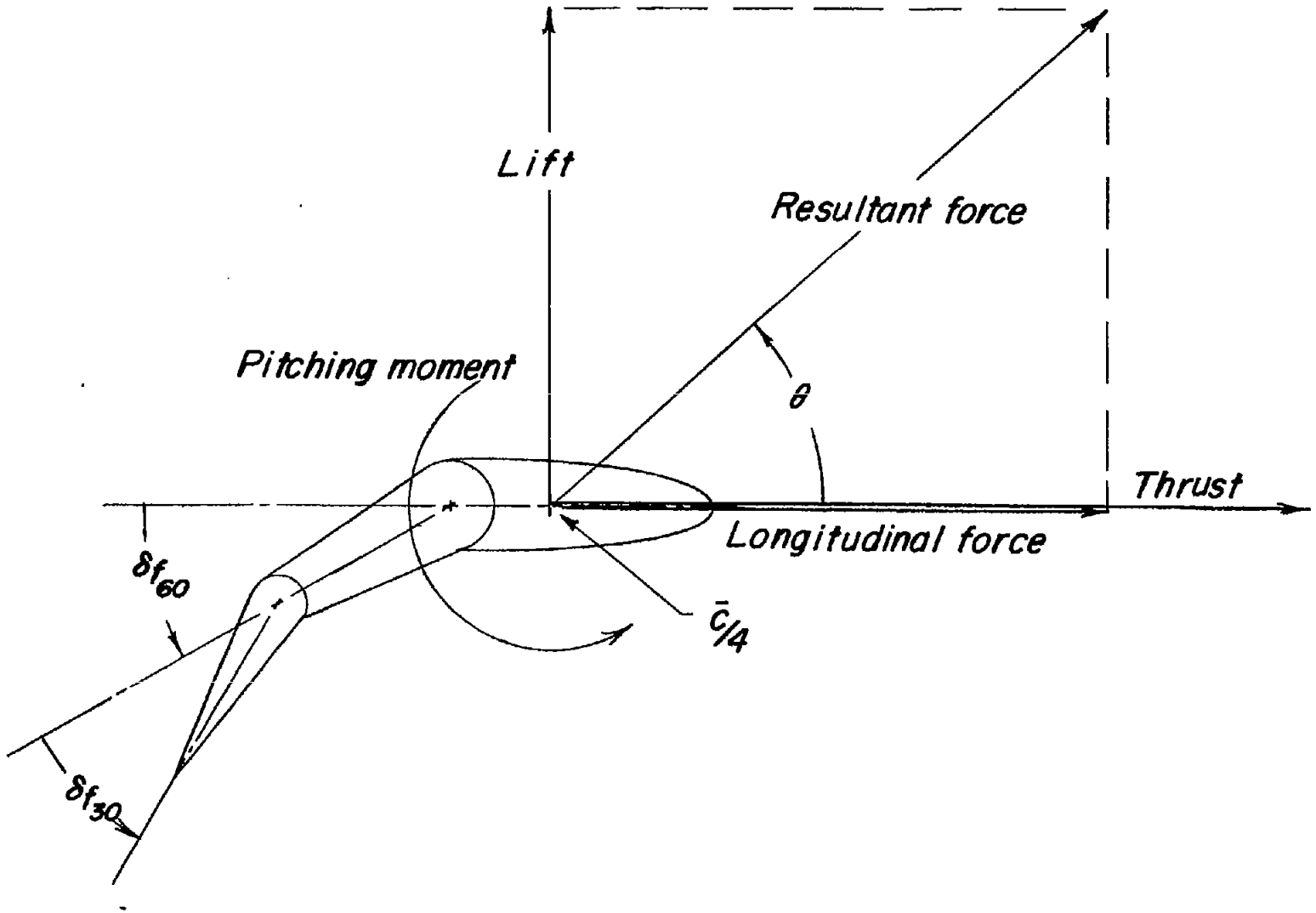

Figure 1.- Sketch of convention used to define positive sense of forces, moments, and angles.

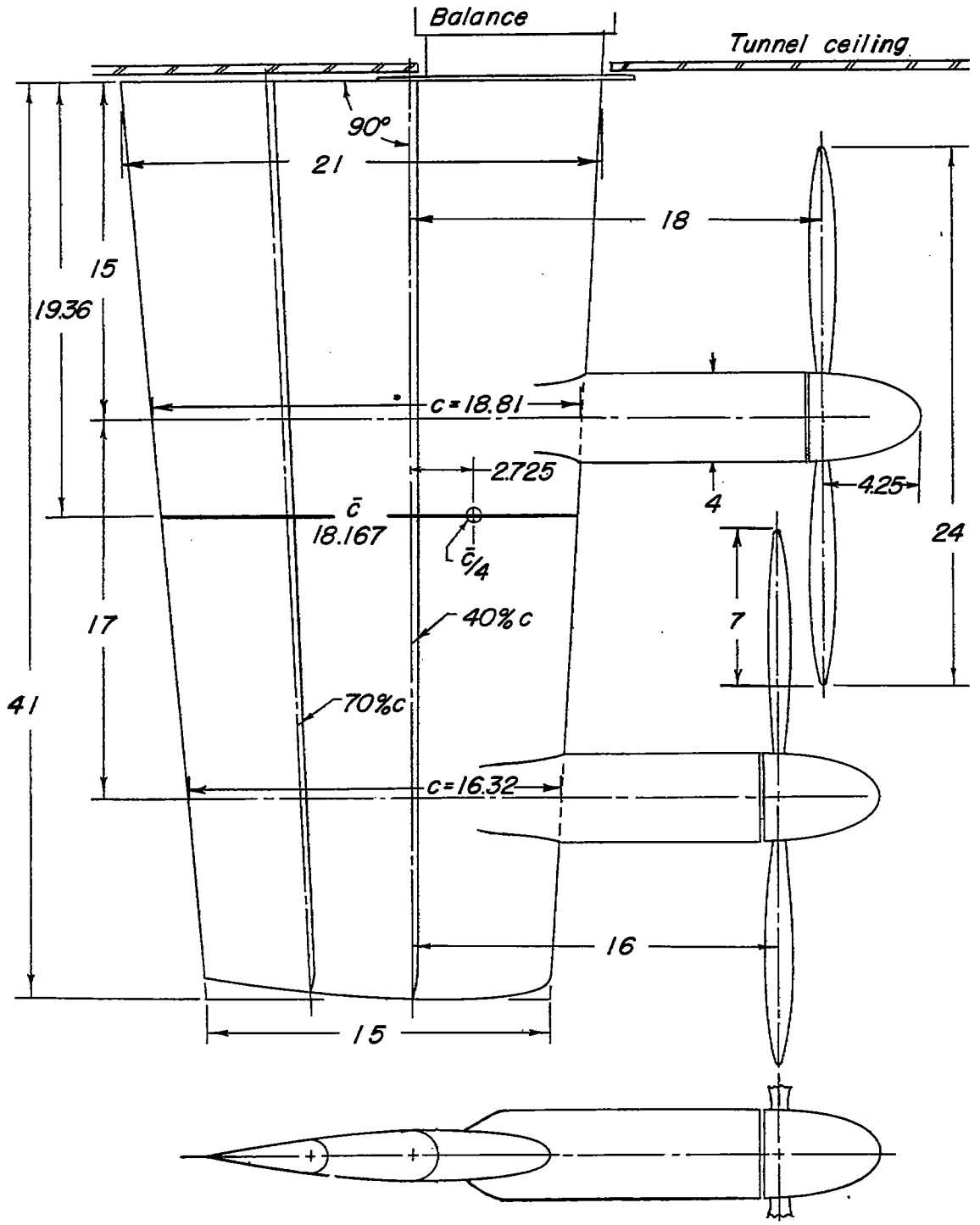

Figure 2.- Drawing of model. (All dimensions in inches.)

L-82207

Figure 3.- Photograph of model installed in the test section of the Langley 300 MPH 7- by 10-foot tunnel. $\alpha = 0^\circ$; $\delta_{f_{60}} = 0^\circ$; $\delta_{f_{30}} = 30^\circ$.

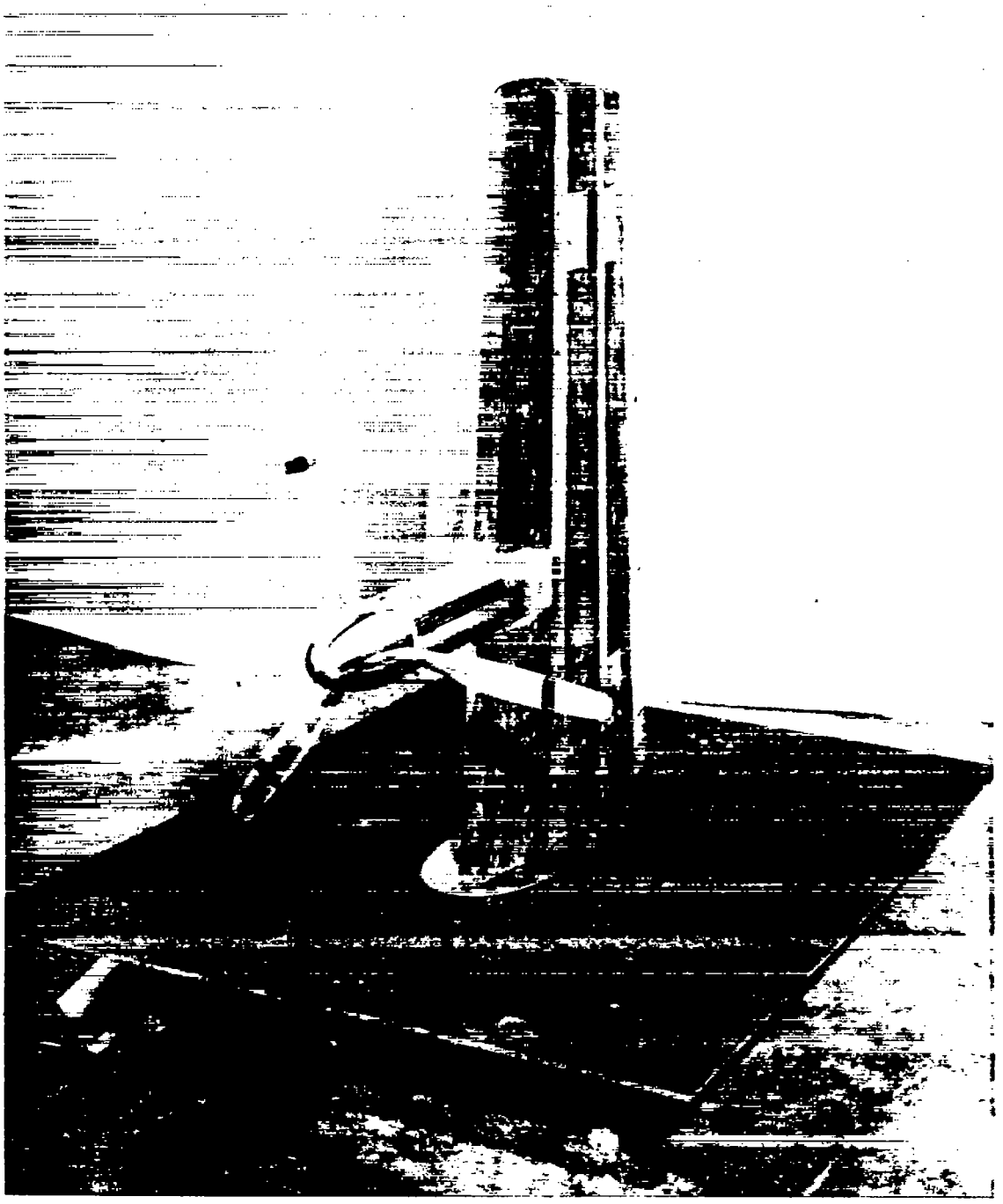

L-80958

Figure 4.- Photograph of model installed on the static-thrust test stand for single propeller test. $\alpha = 0^{\circ}$; $\delta_{f_{60}} = 0^{\circ}$; $\delta_{f_{30}} = 0^{\circ}$.

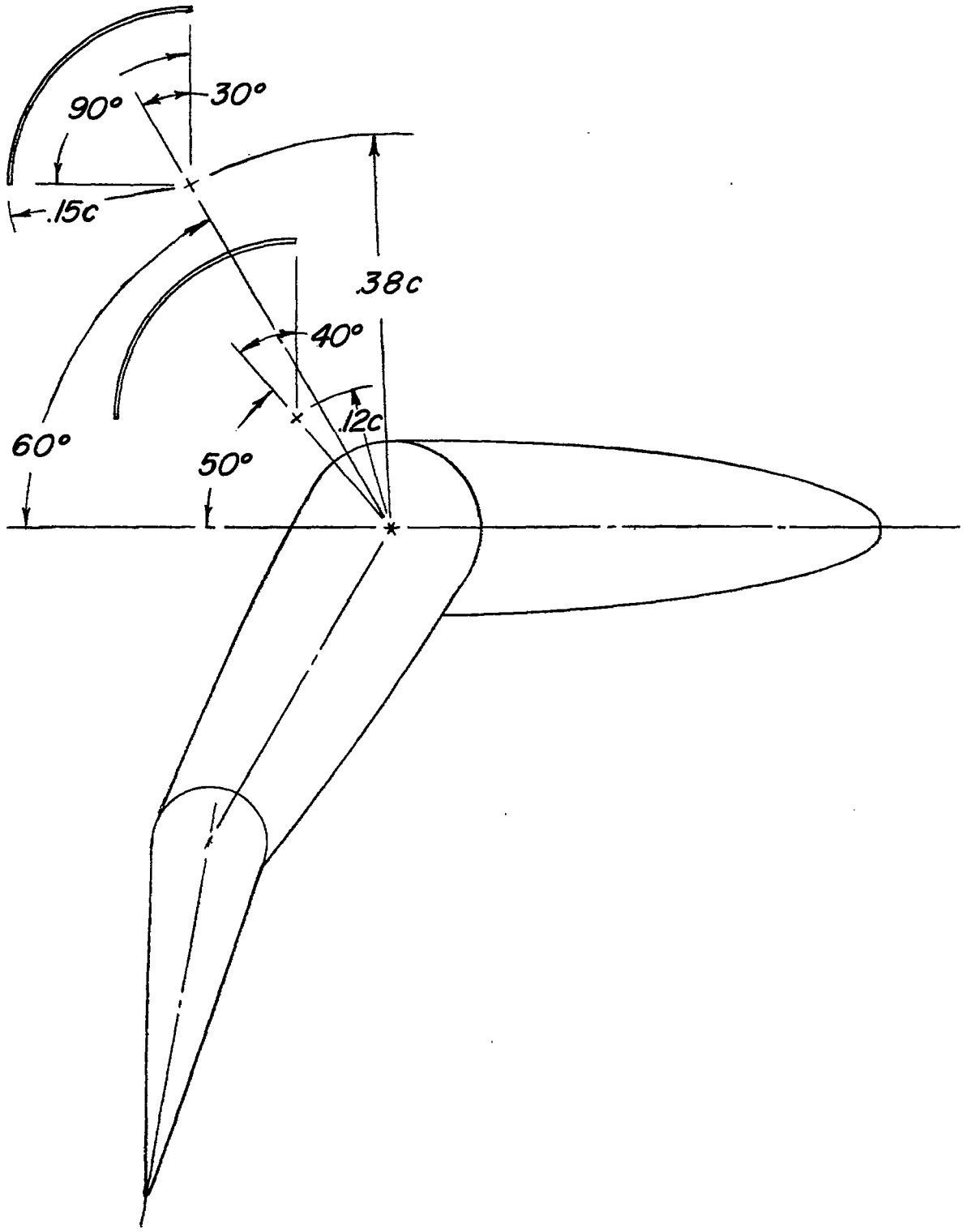

Figure 5.- Sketch of auxiliary-vane configuration. 1/8-inch sheet metal vanes. Both vanes identical.

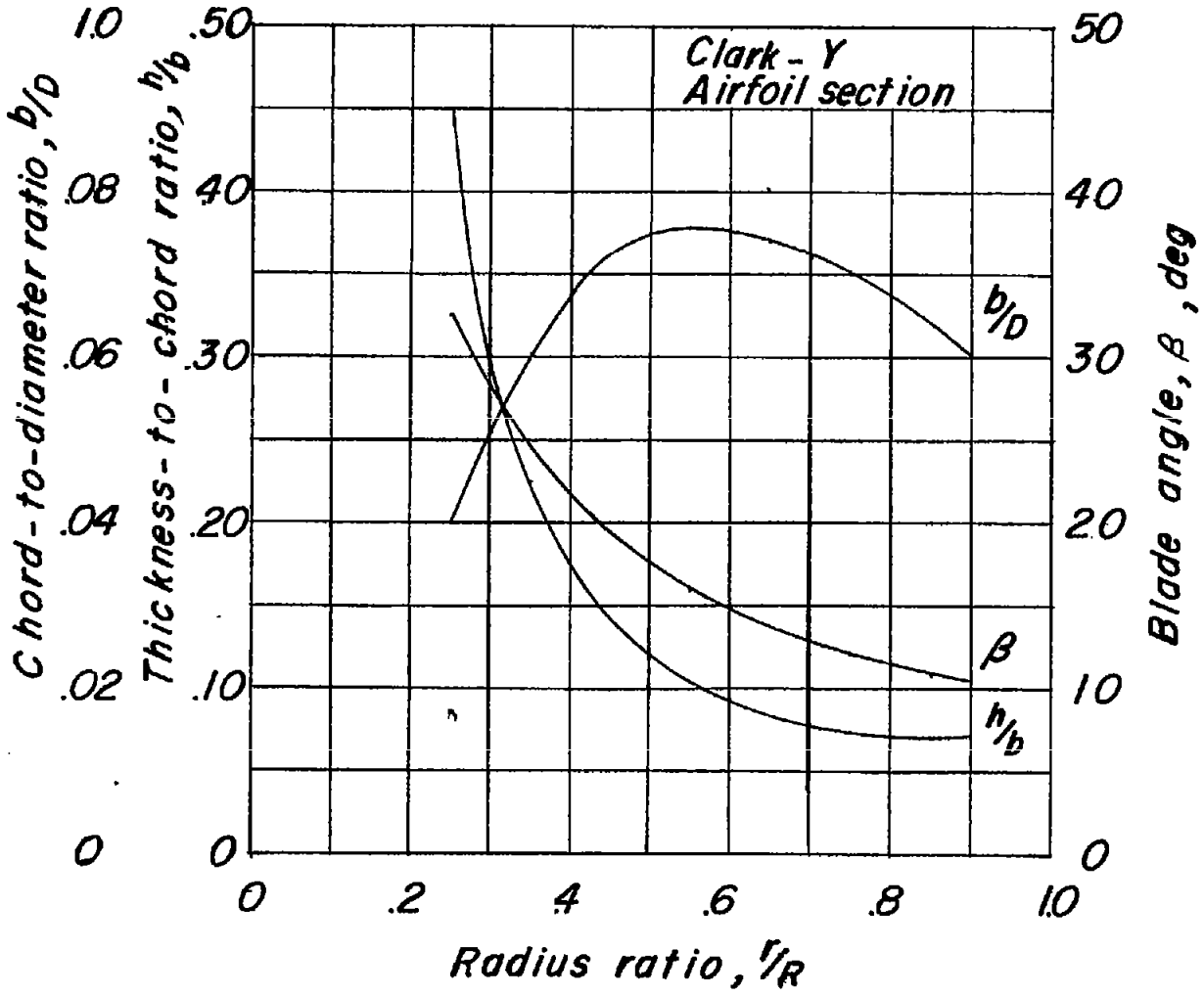

Figure 6.- Propeller-blade geometric characteristics.

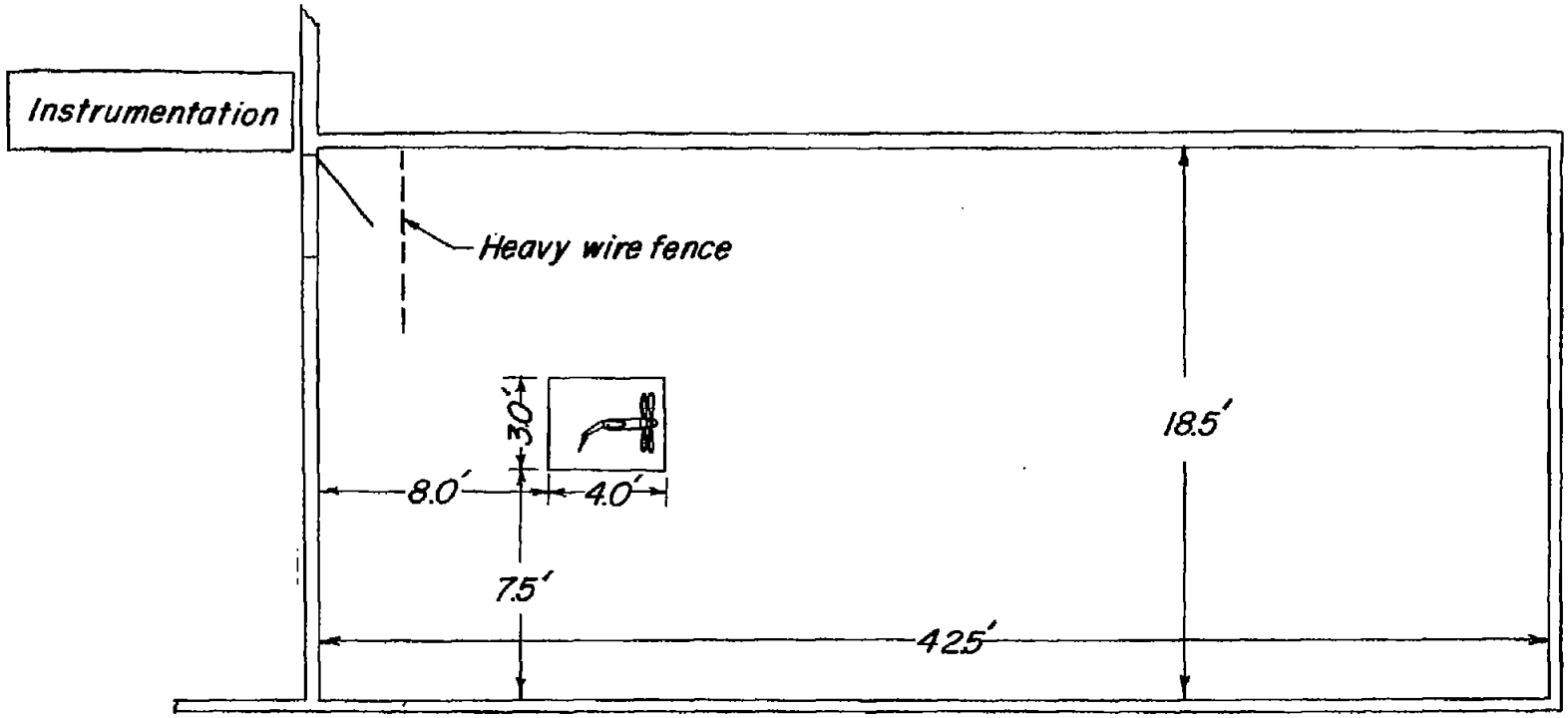

Figure 7.- View of the test setup used for tests at zero forward speed.

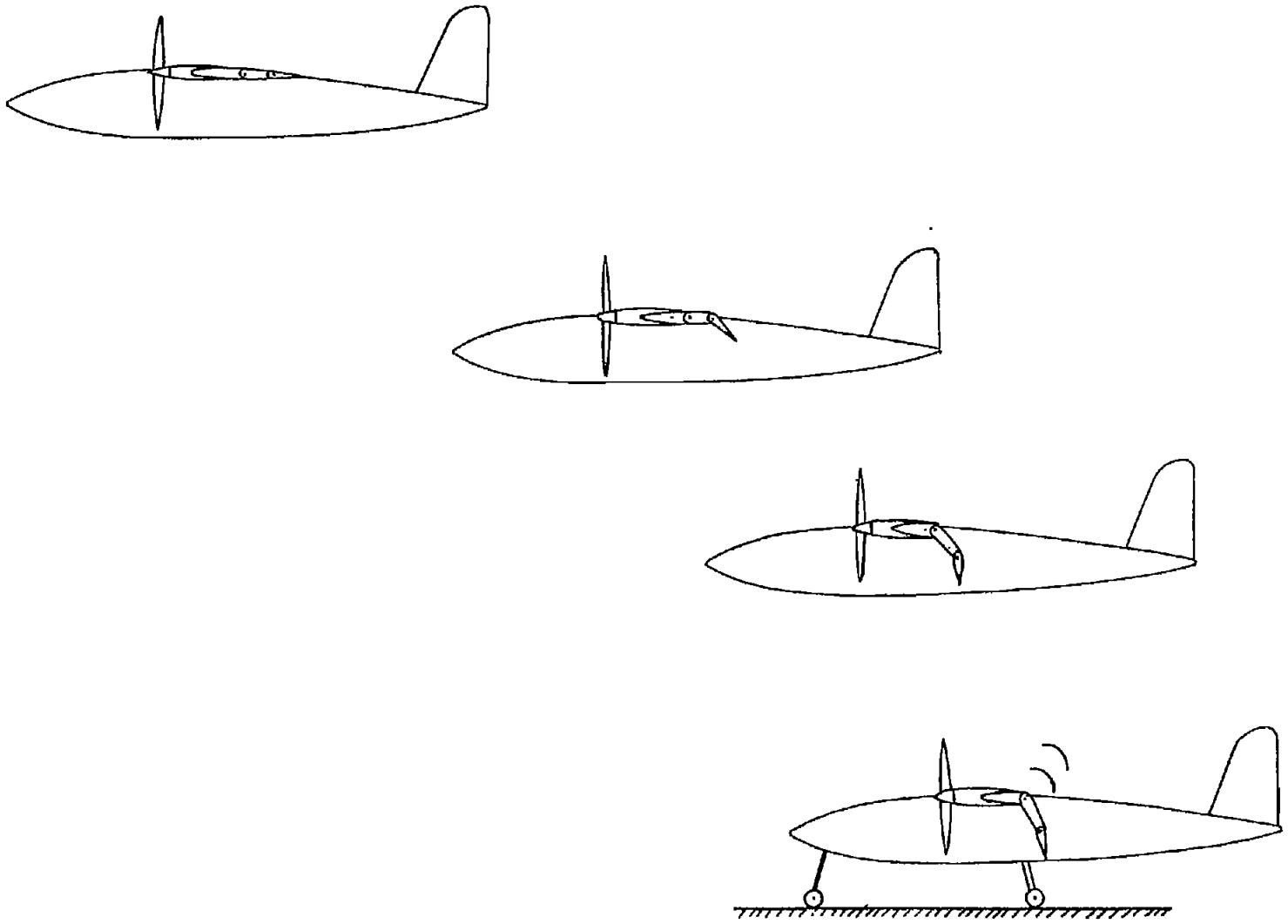

Figure 8.- Sketch of typical vertical take-off for airplane equipped with flaps and vanes to deflect the slipstream. Note progression of controls.

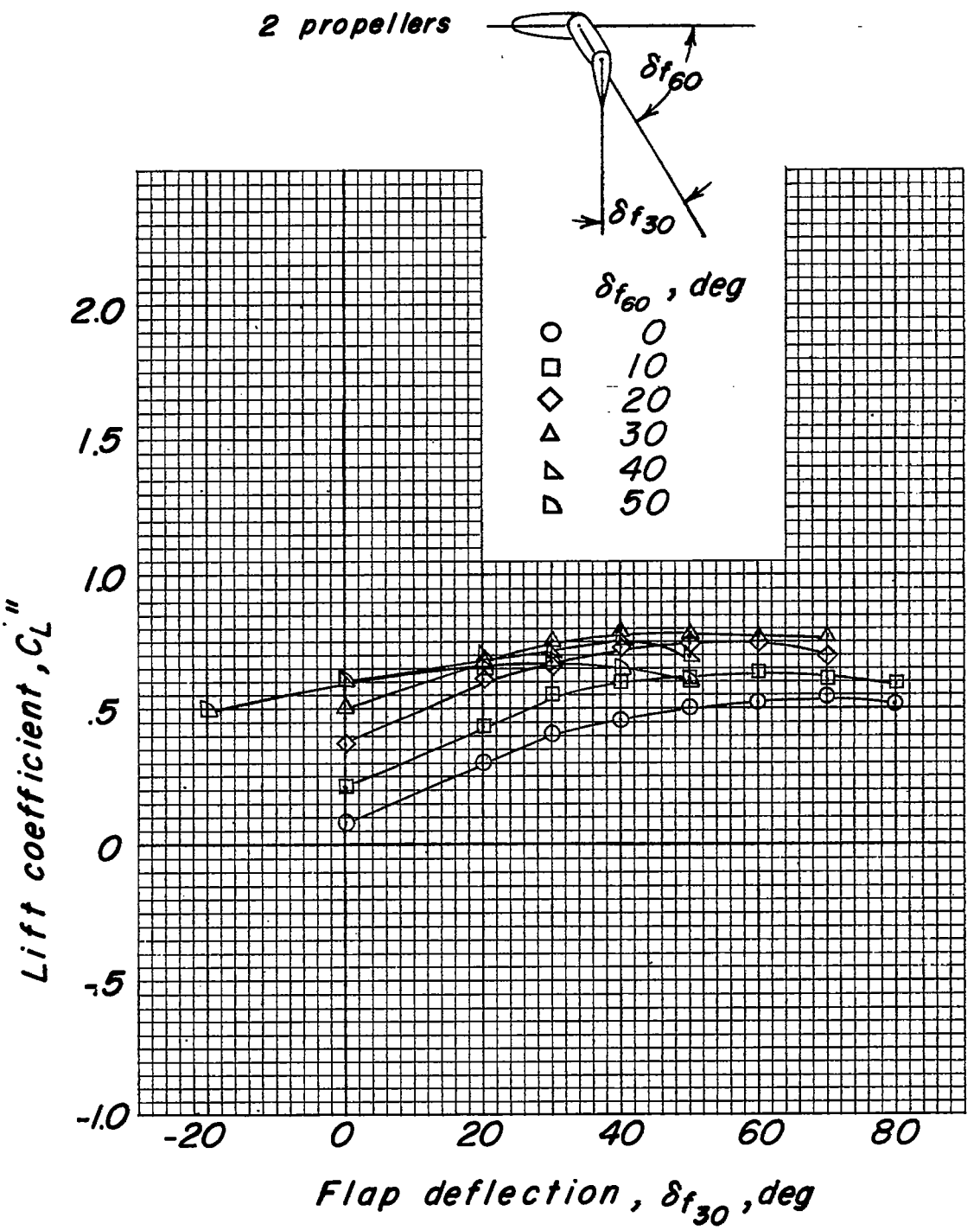

(a) Lift coefficient.

Figure 9.- Effect of flap deflection on aerodynamic characteristics of wing in slipstream at zero forward velocity. Two propellers; $T_e'' = 1$; $\beta = 8^\circ$.

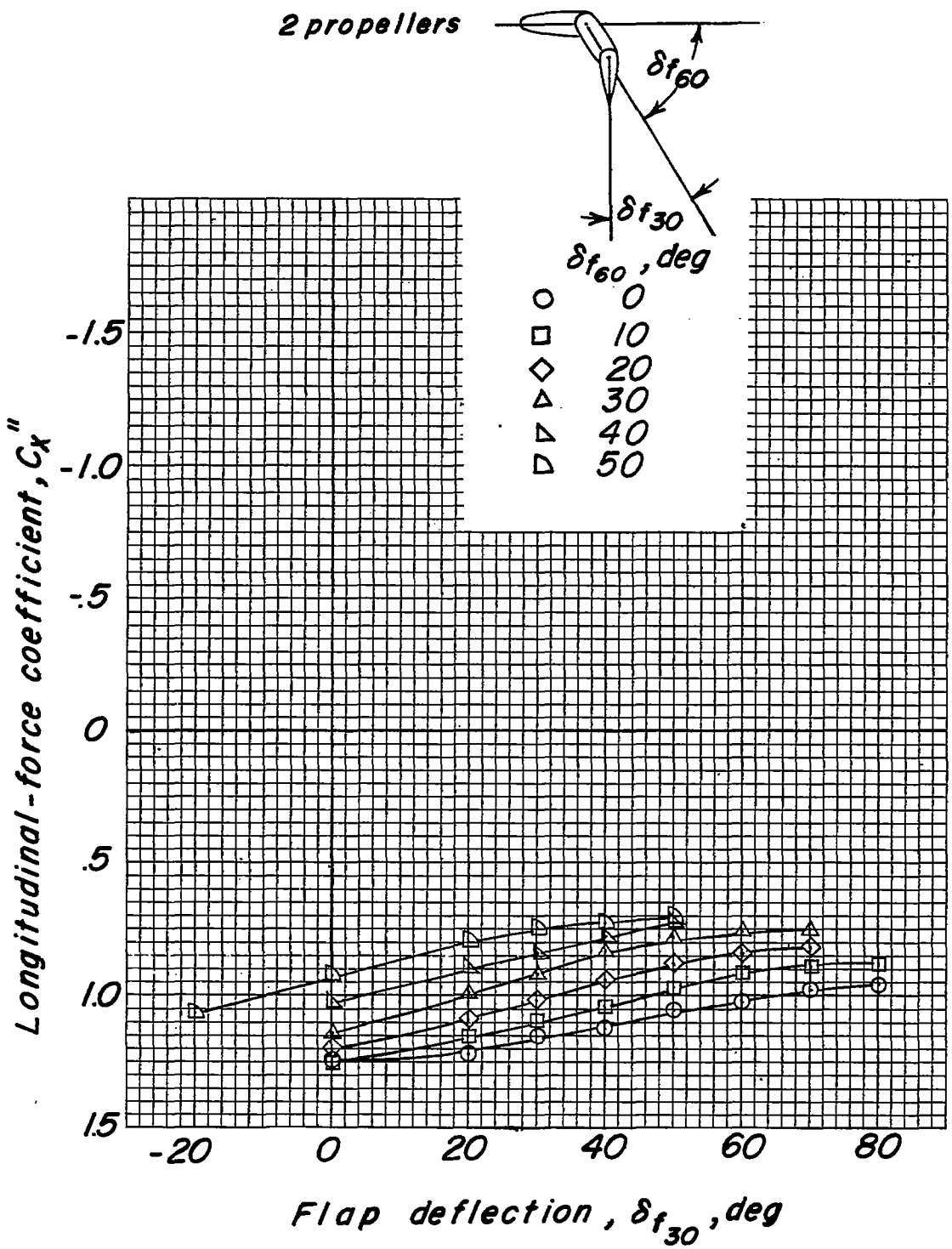

(b) Longitudinal-force coefficient.

Figure 9.- Continued.

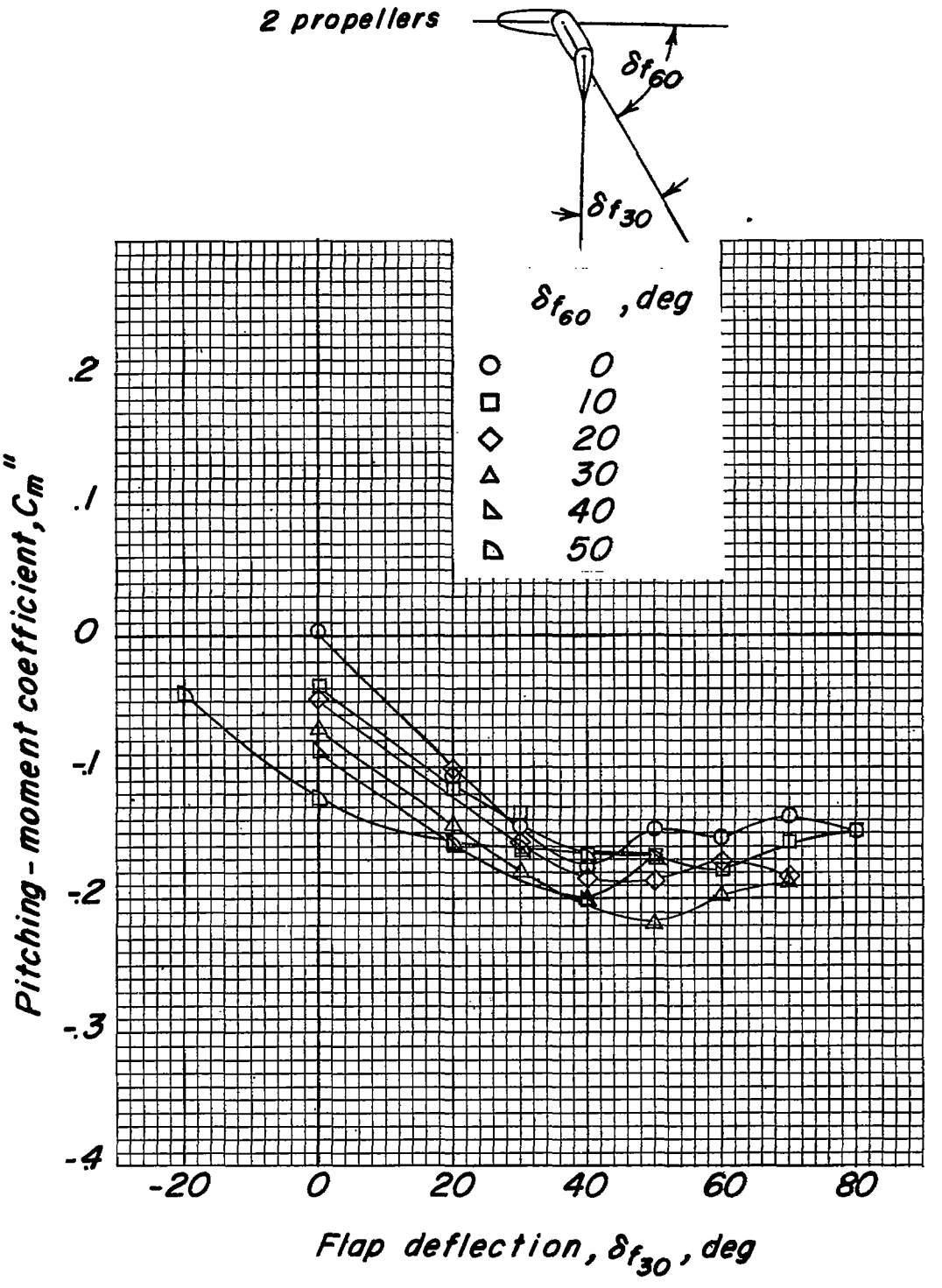

(c) Pitching-moment coefficient.

Figure 9.- Continued.

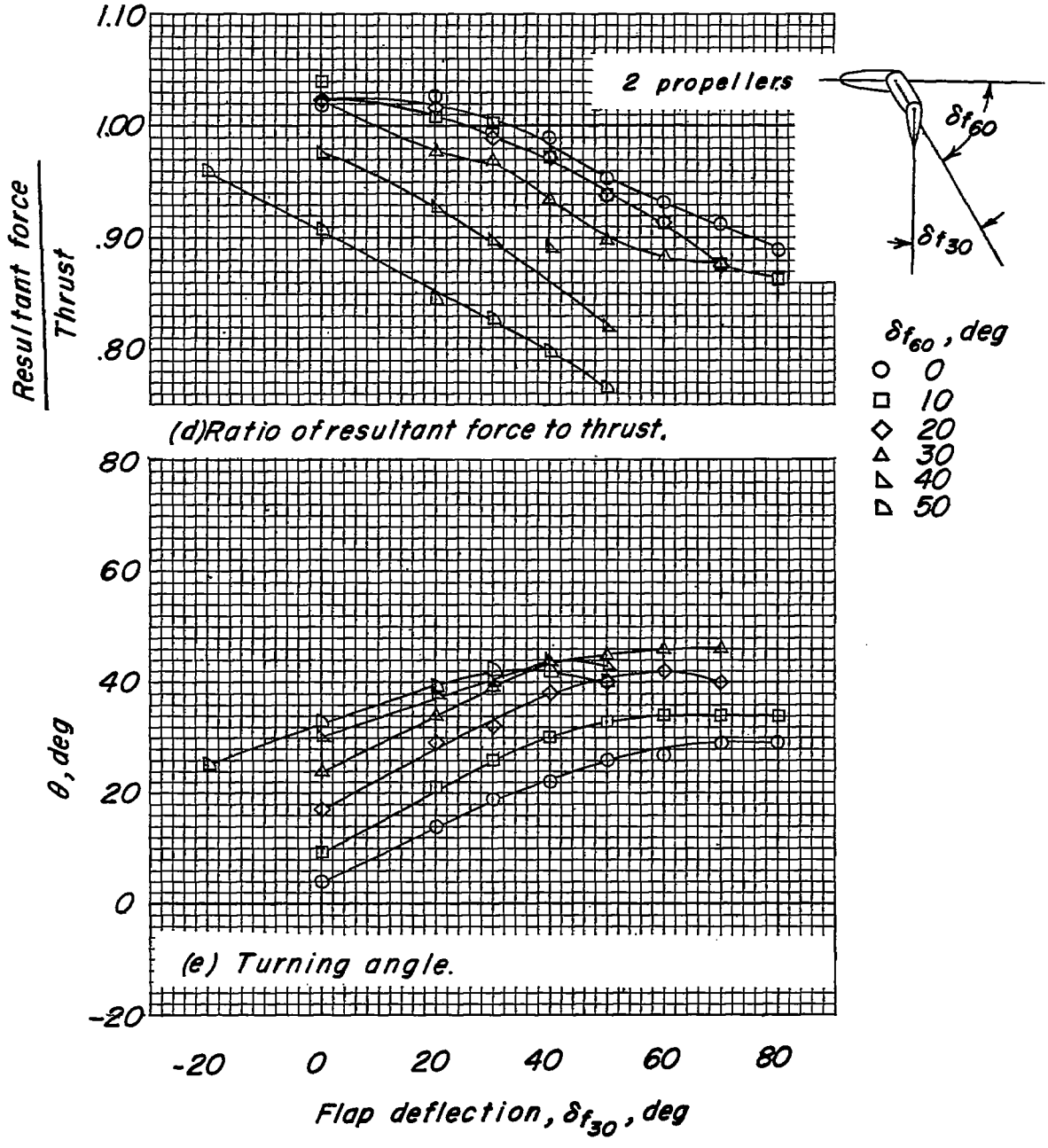

Figure 9.- Continued.

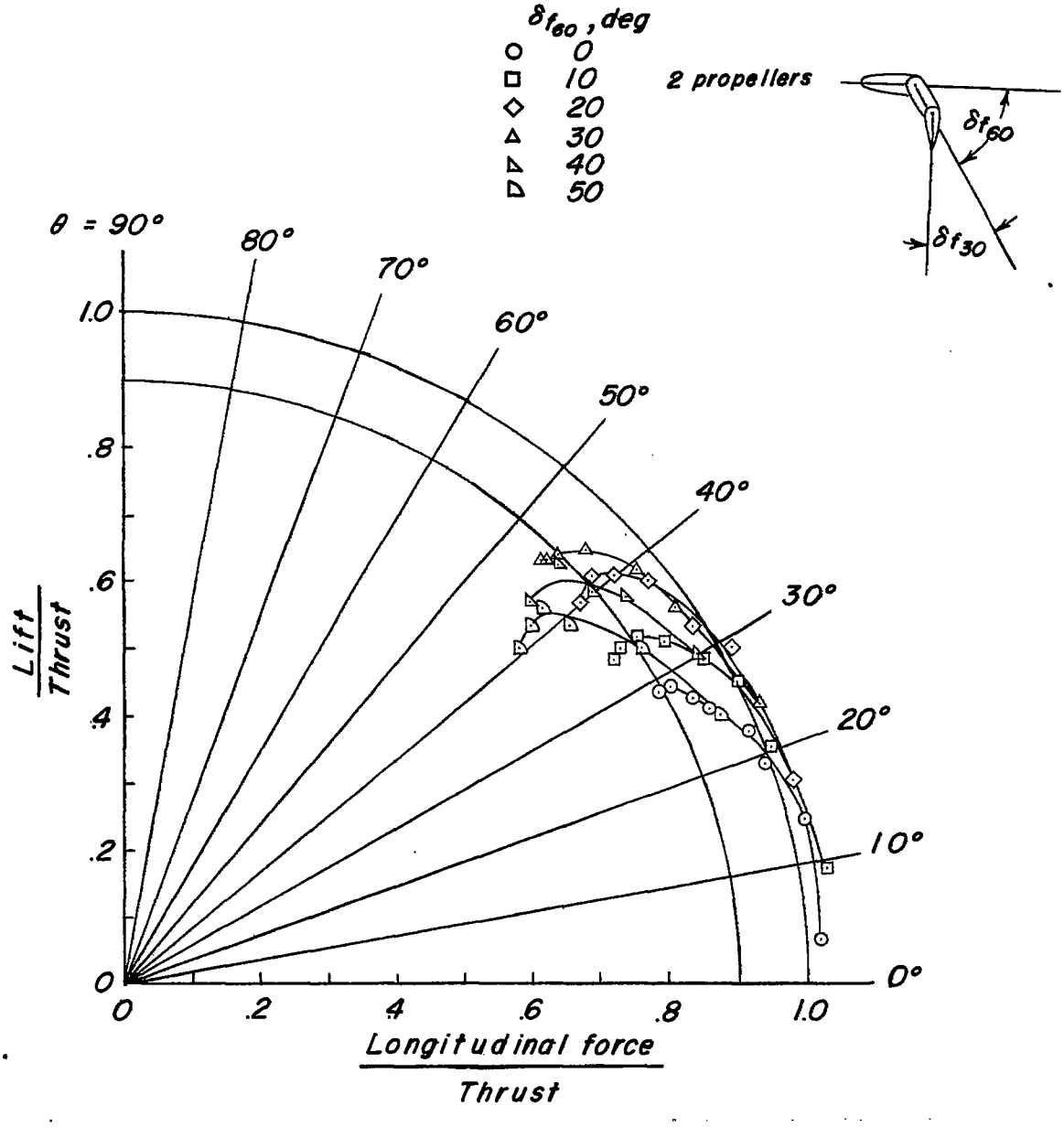

(f) Summary of turning effectiveness and turning angle.

Figure 9.- Concluded.

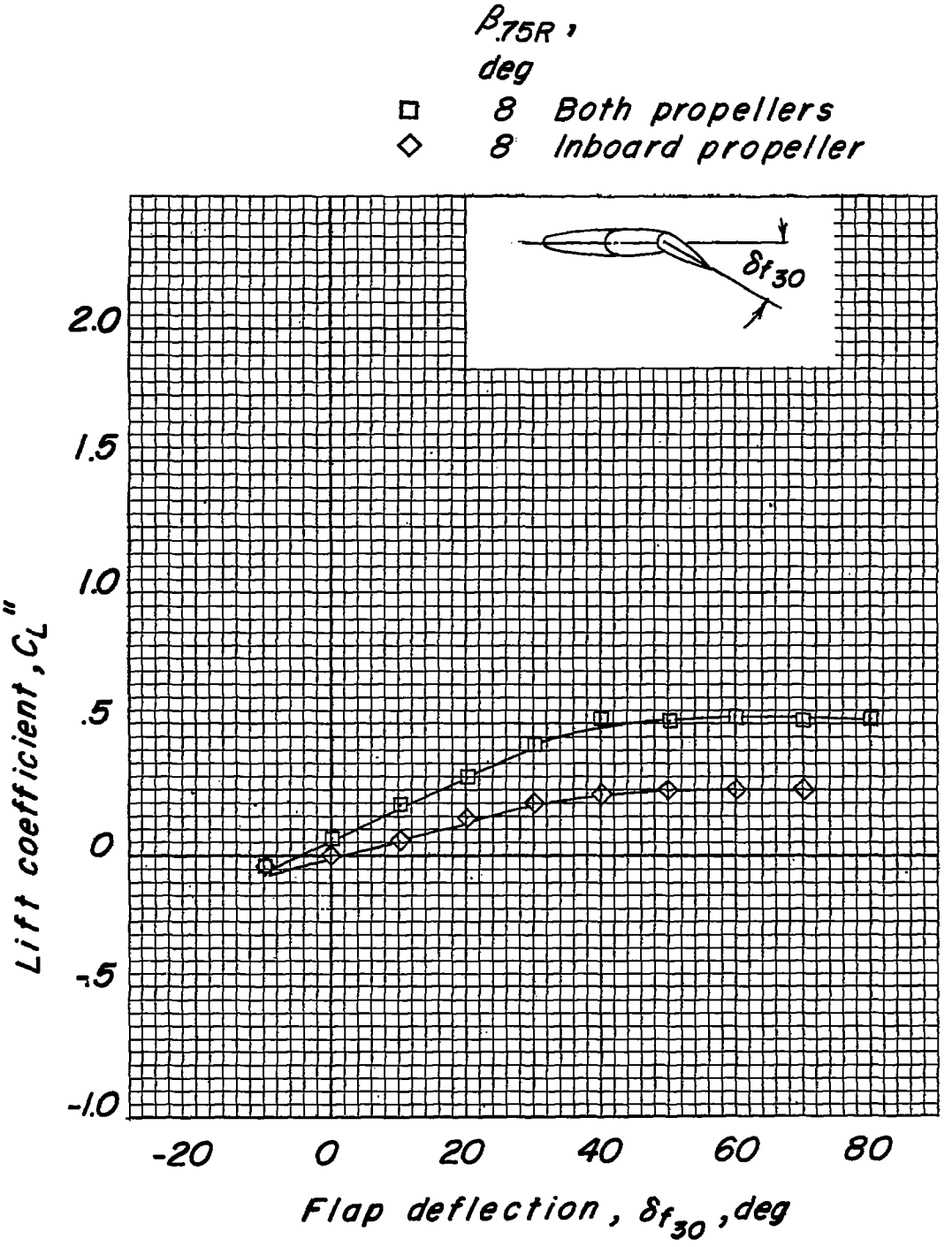

(a) Lift coefficient.

Figure 10.- Effect of number of propellers on aerodynamic characteristics of model. T_c" = 1.0; $\delta_{f_{60}} = 0^o$.

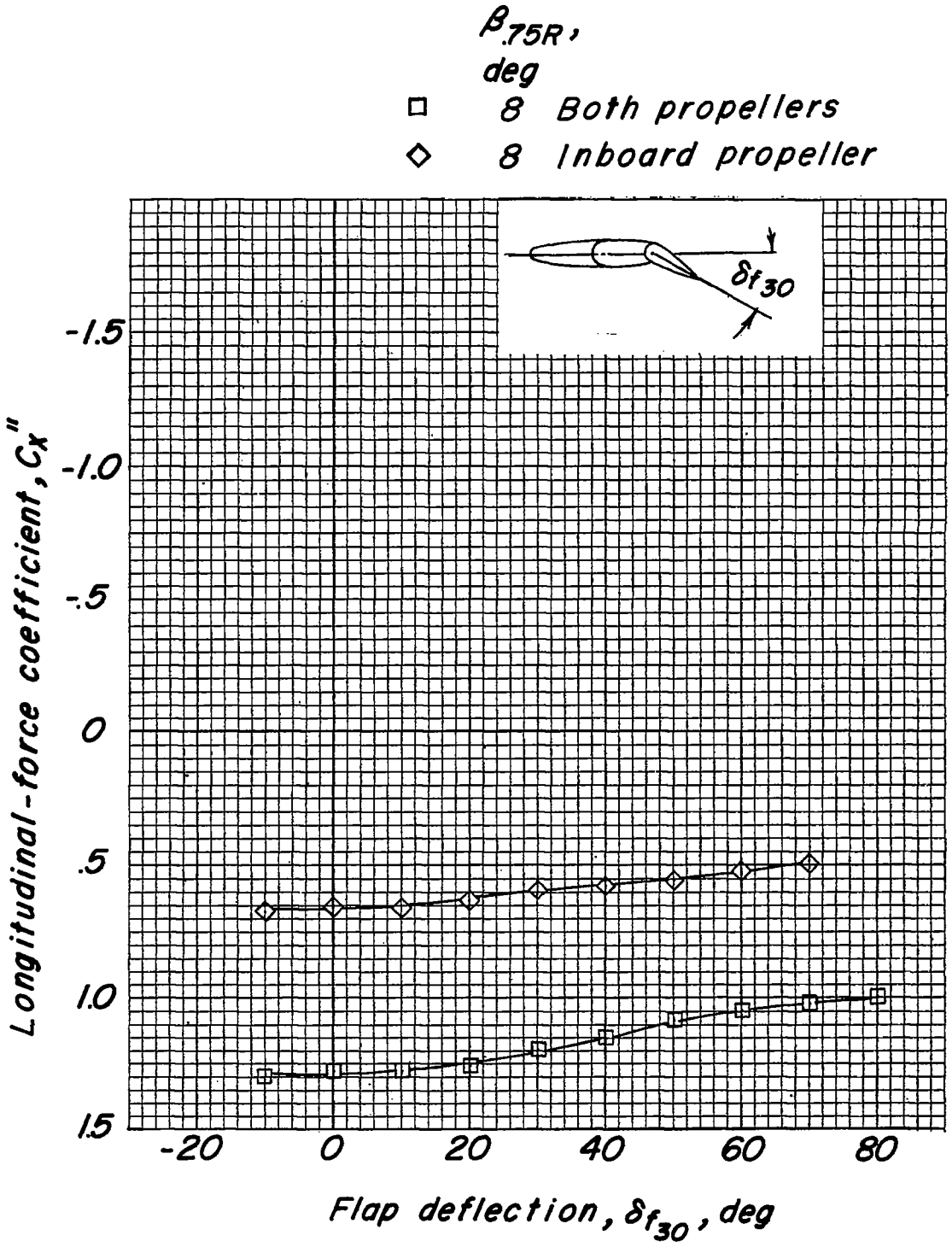

(b) Longitudinal-force coefficient.

Figure 10.- Continued.

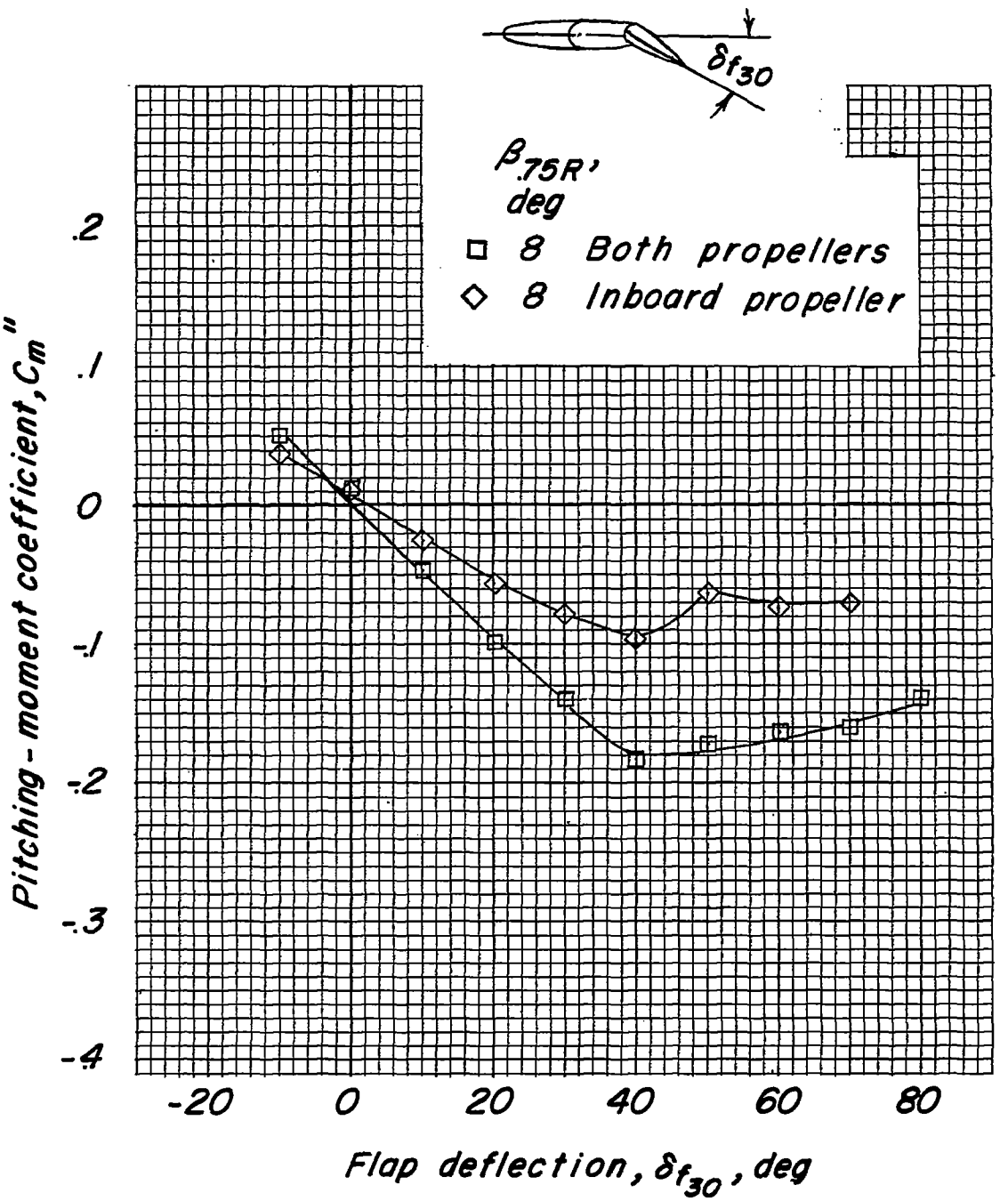

(c) Pitching-moment coefficient.

Figure 10.- Continued.

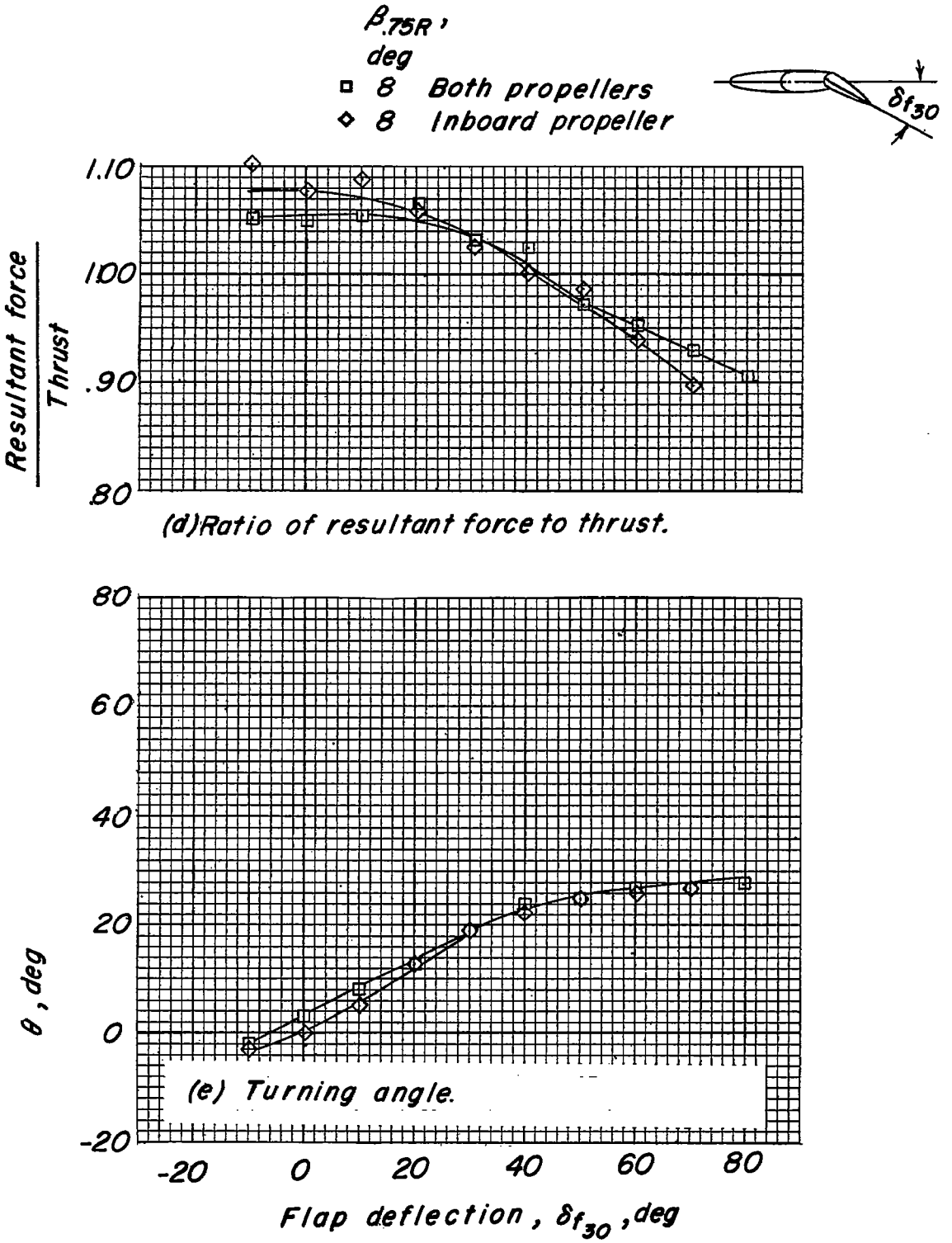

Figure 10.- Continued.

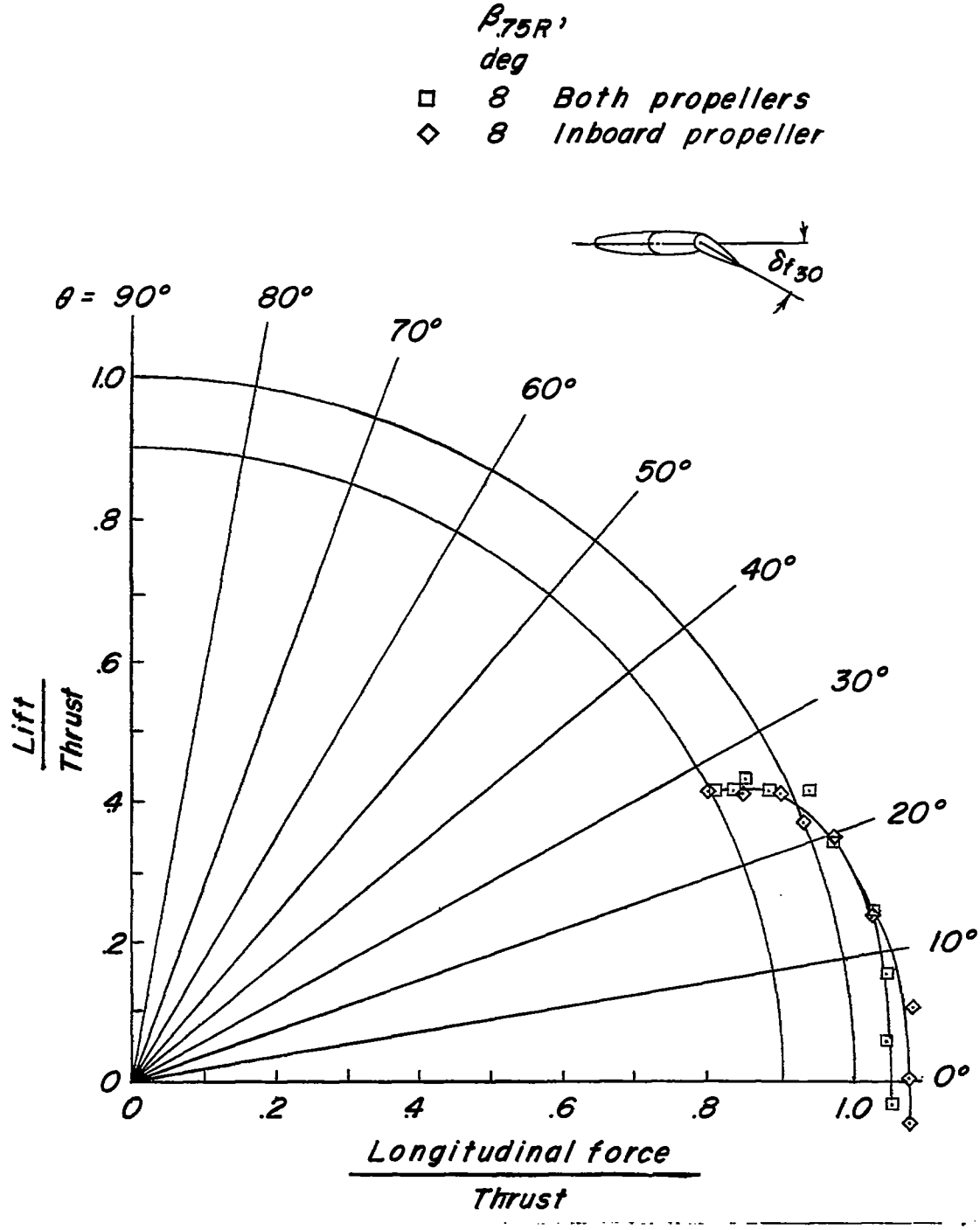

(f) Summary of turning effectiveness and turning angle.

Figure 10.- Concluded.

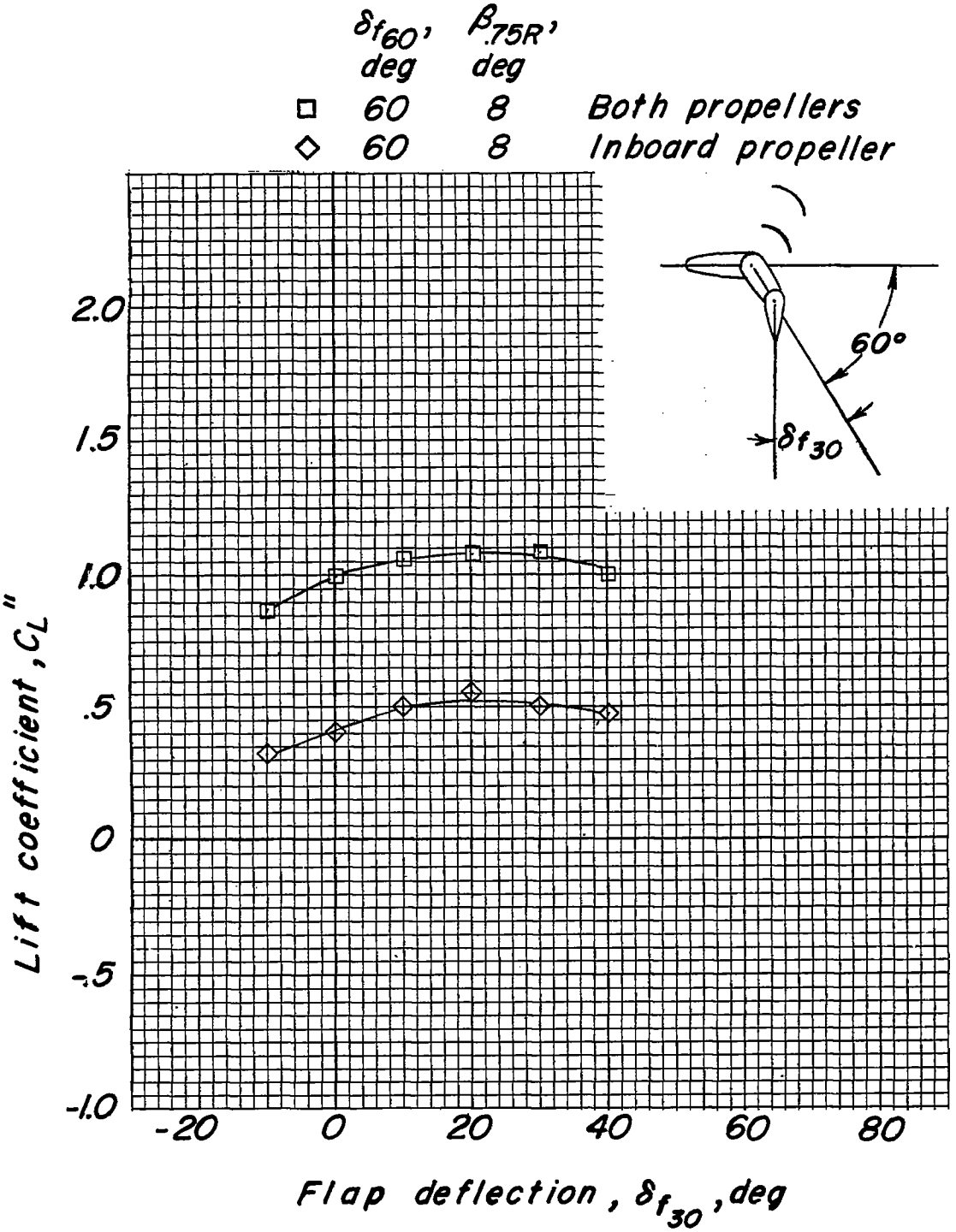

(a) Lift coefficient.

Figure 11.- Aerodynamic characteristics of model with two auxilary vanes added. $T_c'' = 1$; $\delta_{f_{60}} = 60^\circ$.

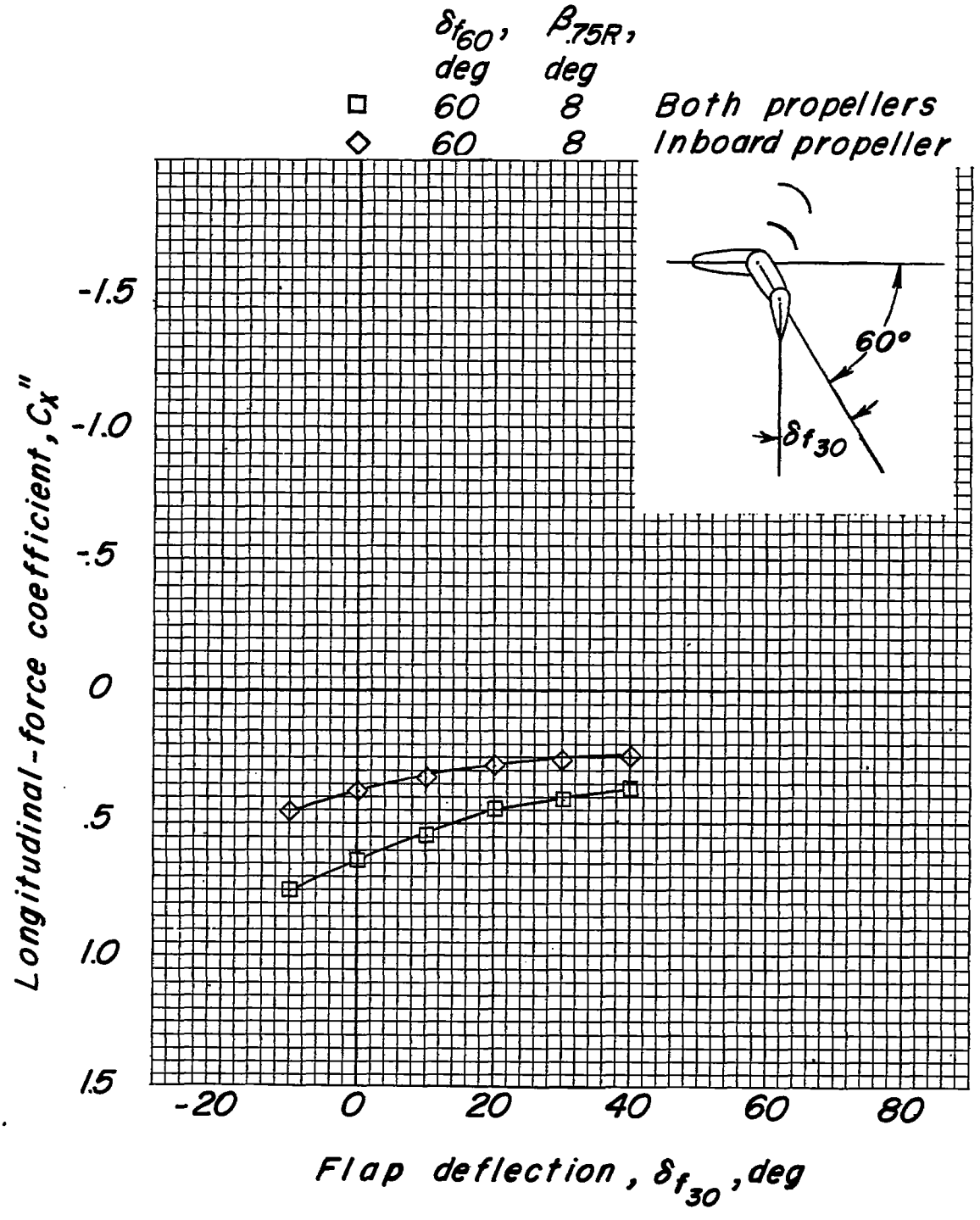

(b) Longitudinal-force coefficient.

Figure 11.- Continued.

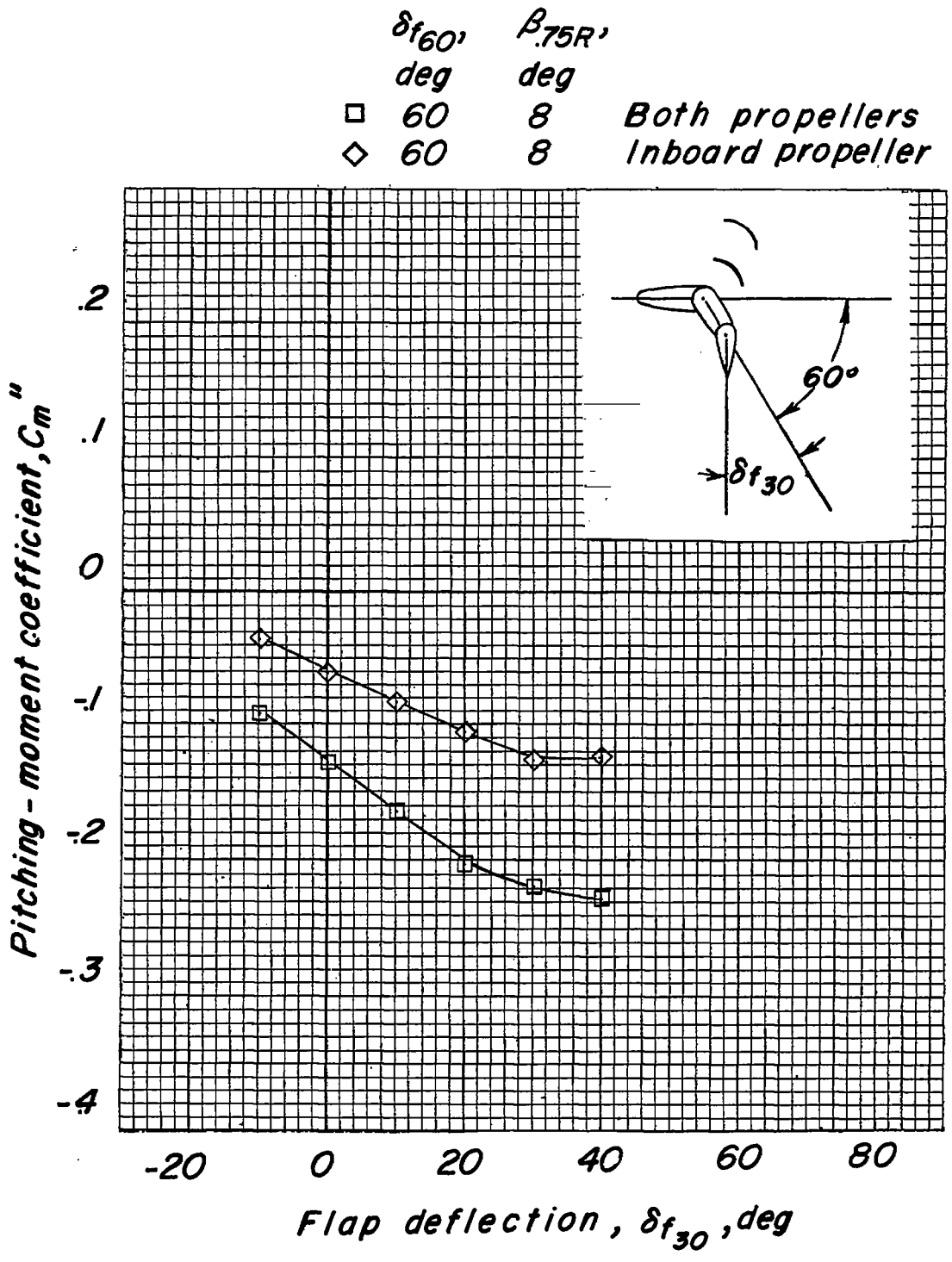

(c) Pitching-moment coefficient.

Figure 11.- Continued.

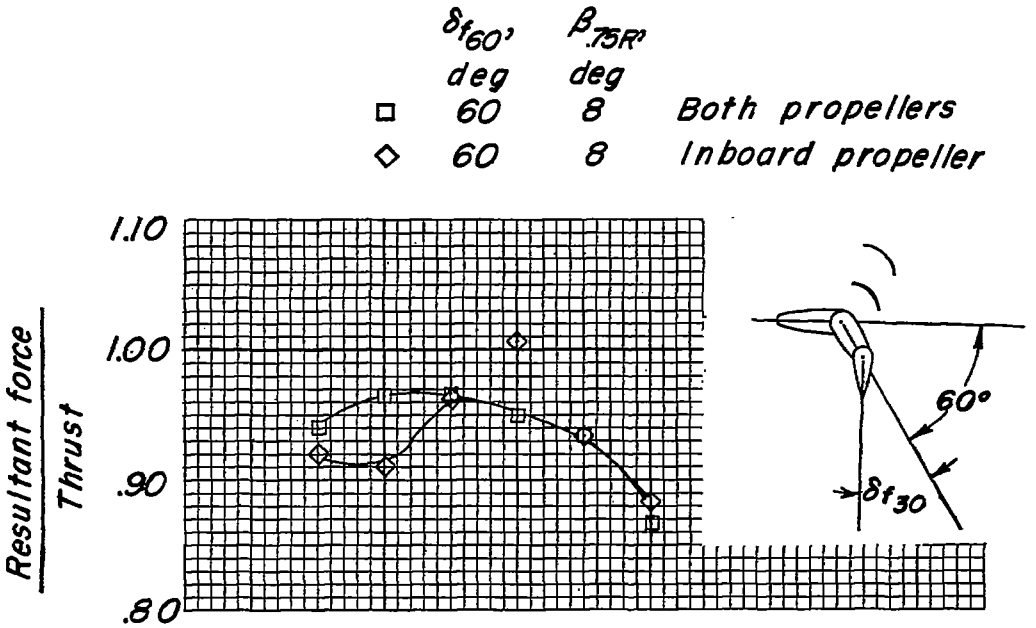

(d) Ratio of resultant force to thrust.

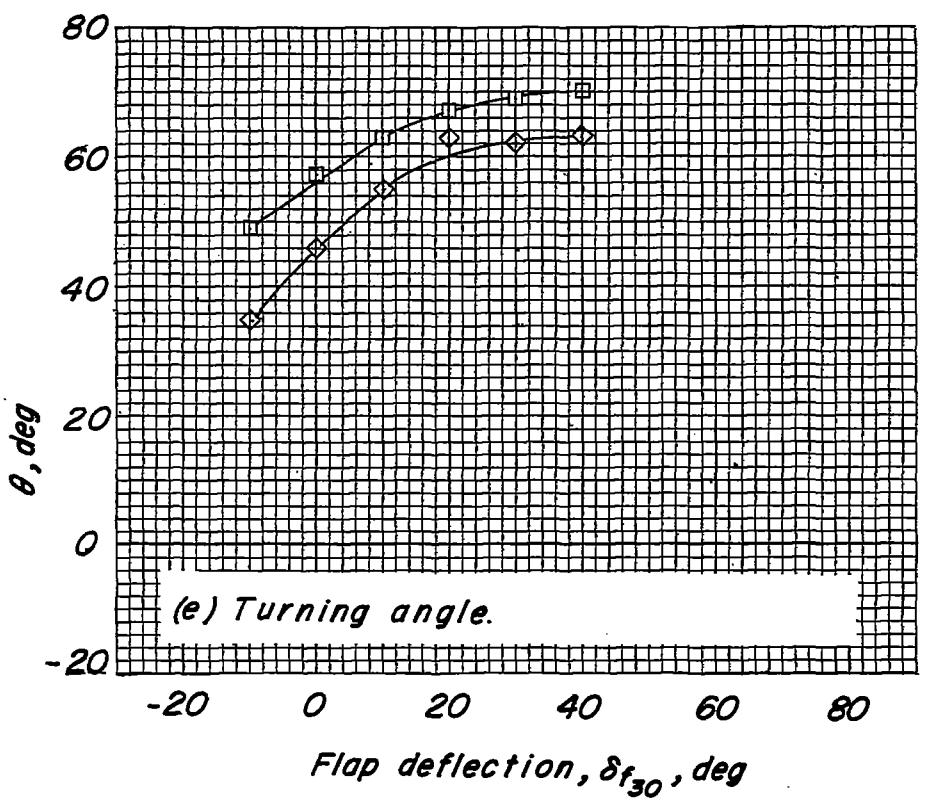

Figure 11.- Continued.

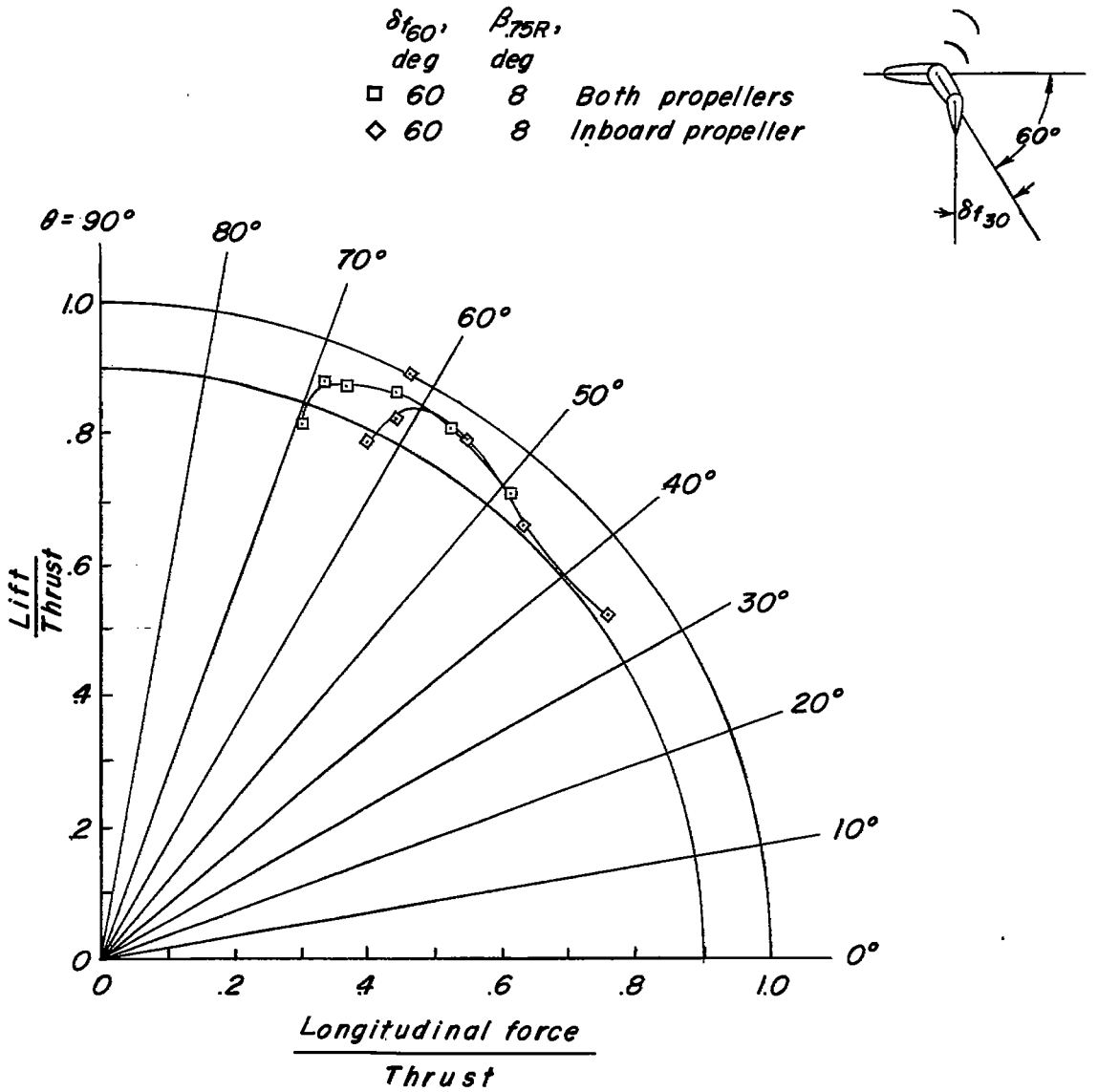

(f) Summary of turning effectiveness and turning angle.

Figure 11.- Concluded.

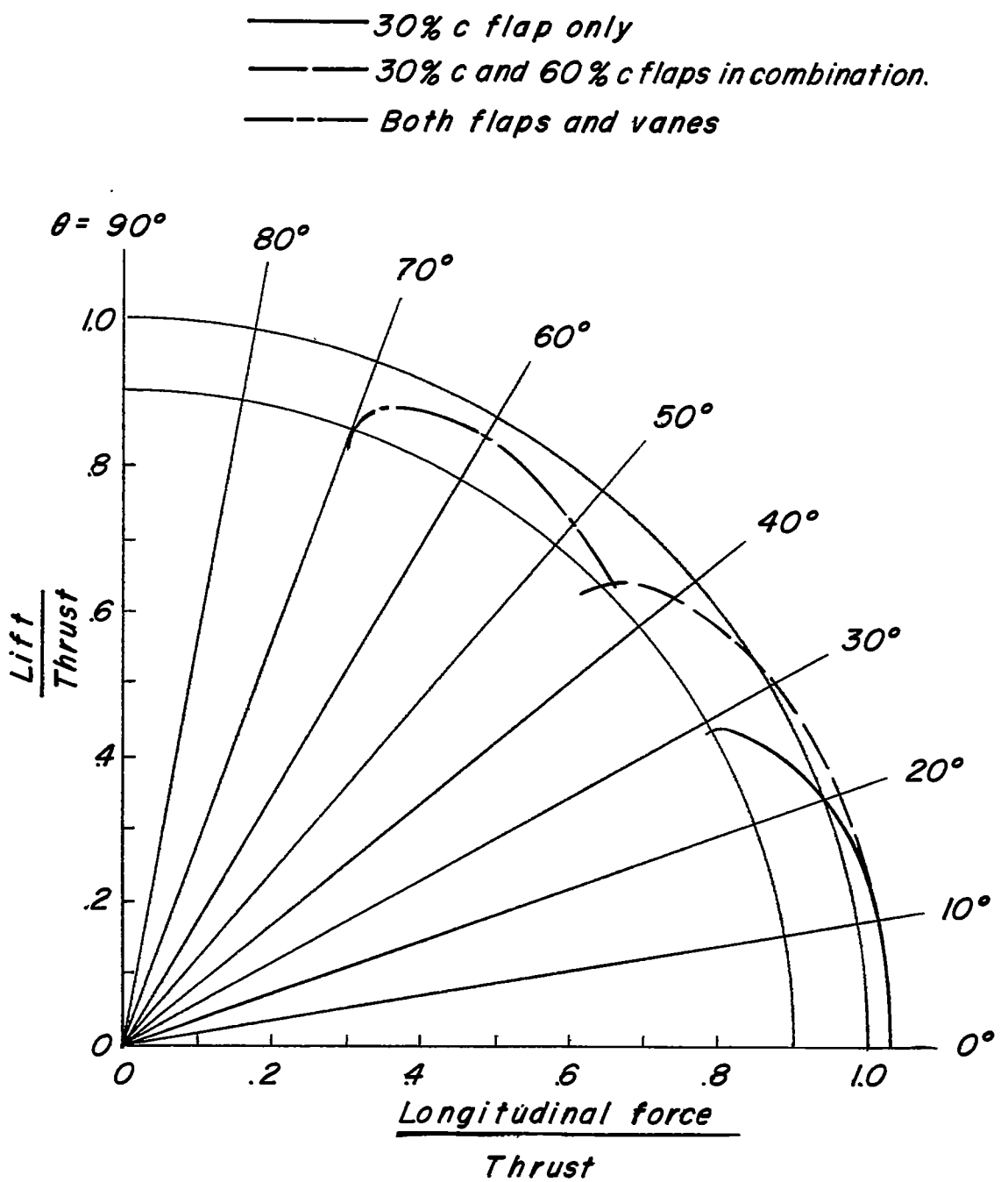

Figure 12.- Summary of turning effectiveness of wing with plain flaps and vanes. $\beta_{.75R} = 8^{\circ}$.

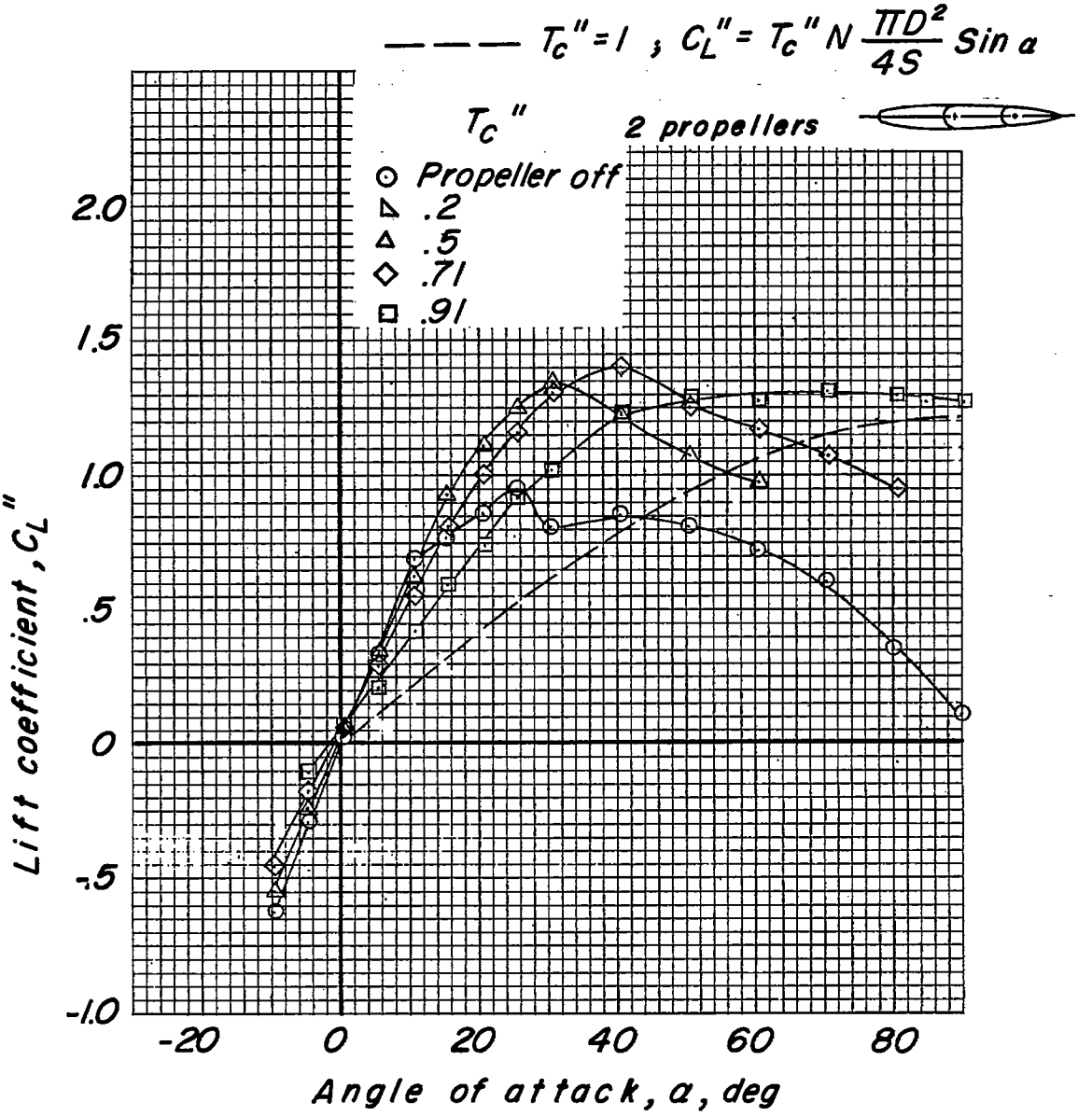

(a) Lift coefficient.

Figure 13.- Effect of thrust coefficient on aerodynamic characteristics of model with two propellers operating. $\delta_{f_{30}} = 0^\circ$; $\delta_{f_{60}} = 0^\circ$.

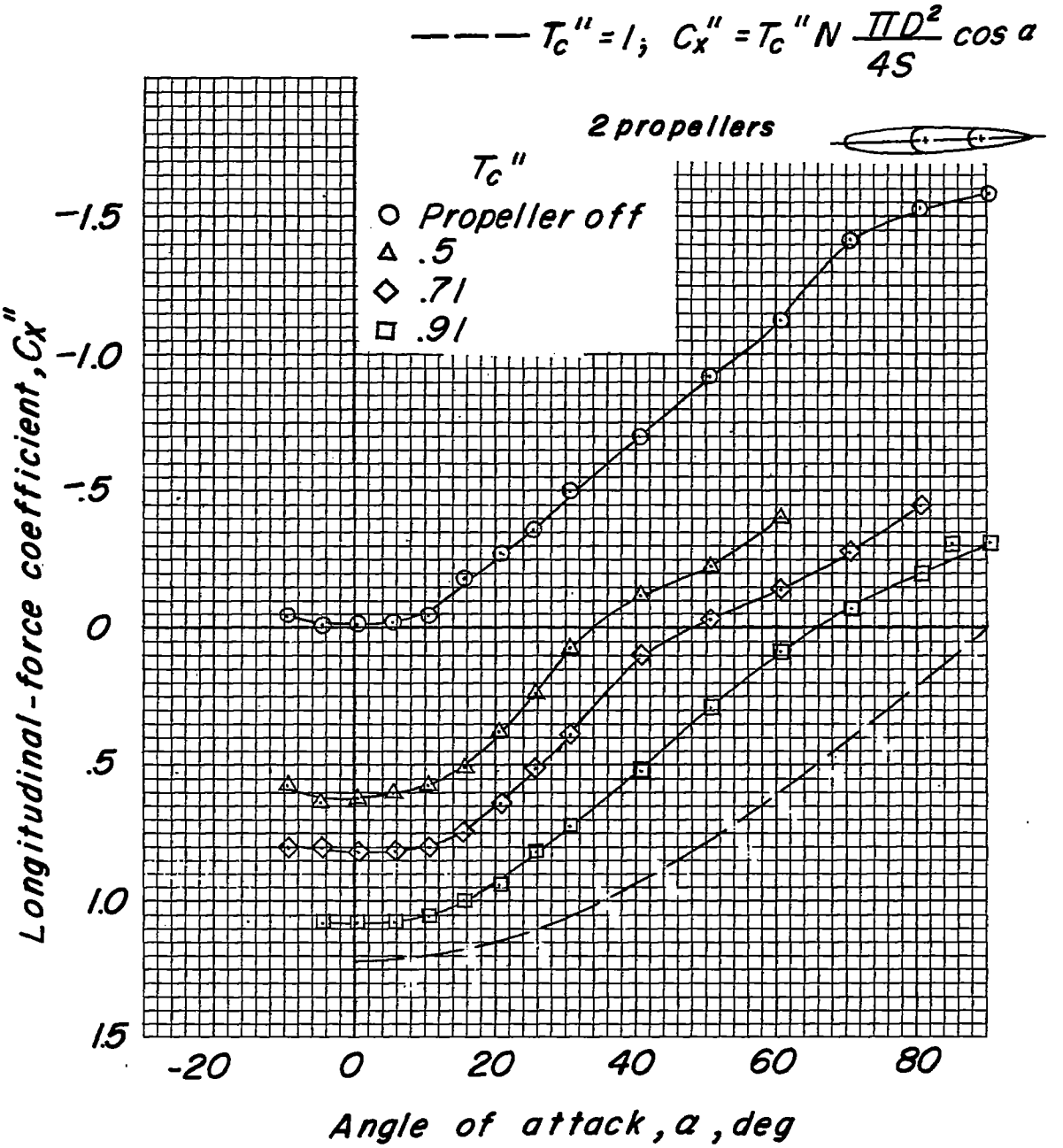

(b) Longitudinal-force coefficient.

Figure 13.- Continued.

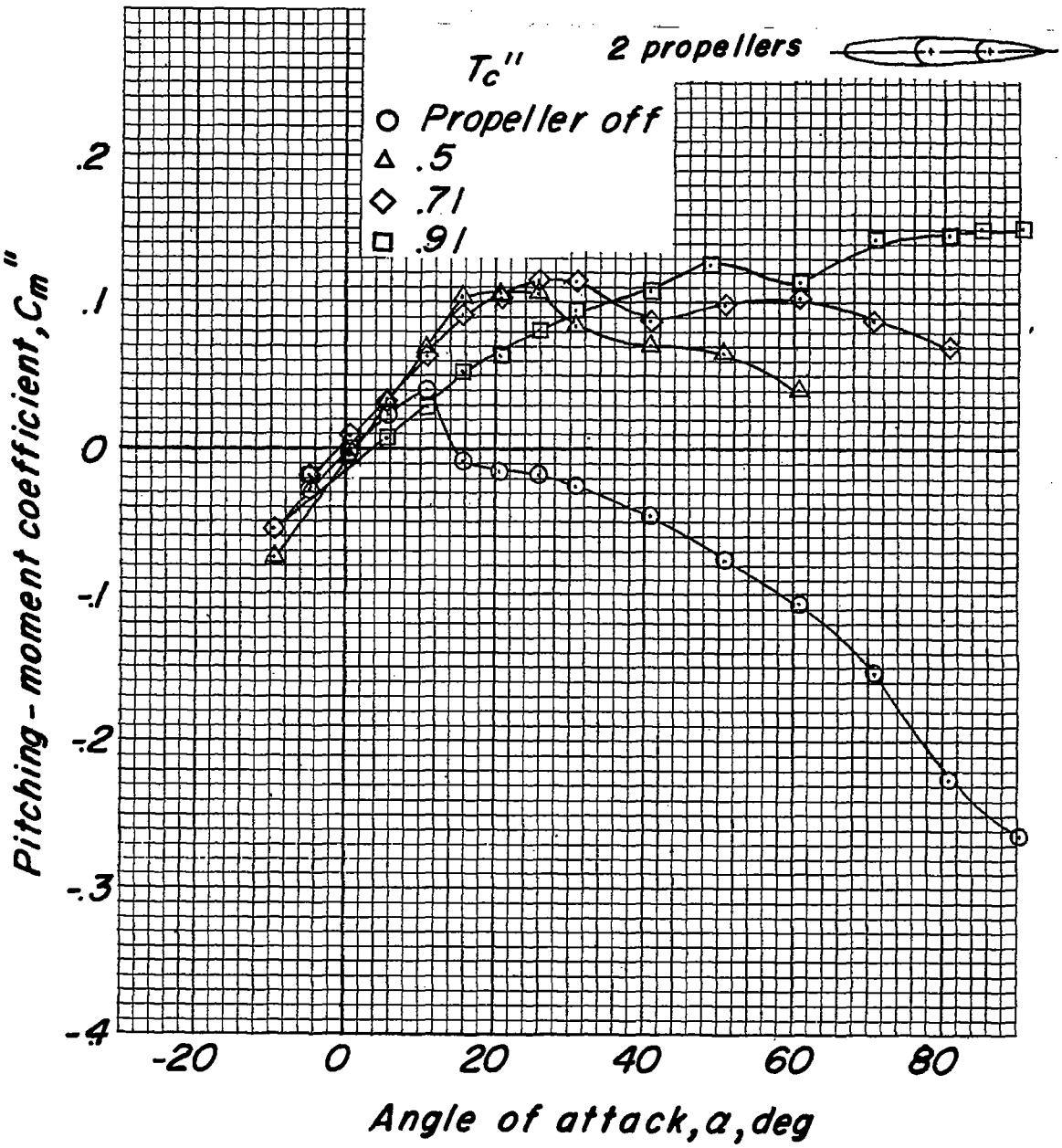

(c) Pitching-moment coefficient.

Figure 13.- Concluded.

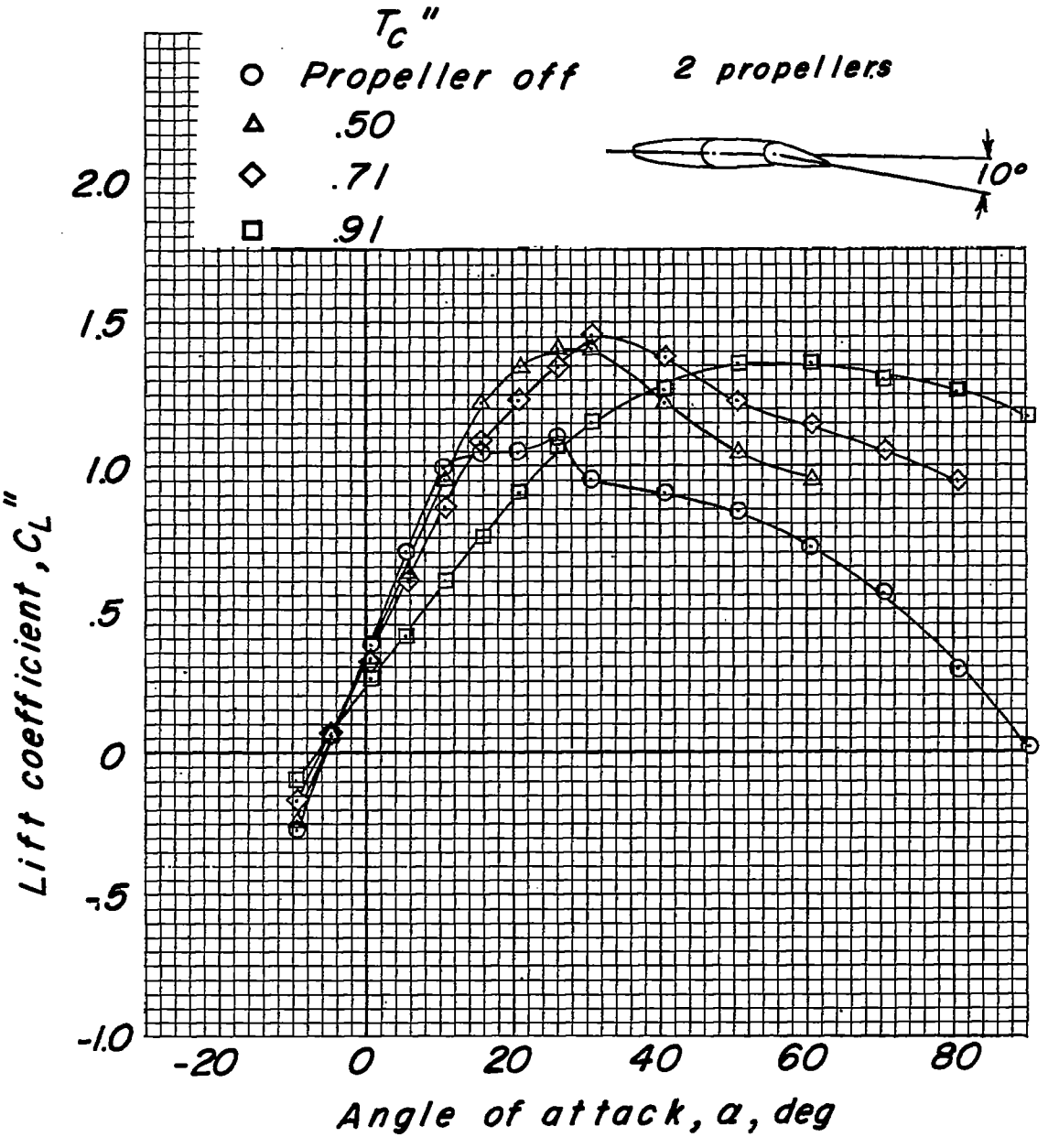

(a) Lift coefficient.

Figure 14.- Effect of thrust coefficient on aerodynamic characteristics of model. $\delta_{f_{30}} = 10^\circ$; $\delta_{f_{60}} = 0^\circ$.

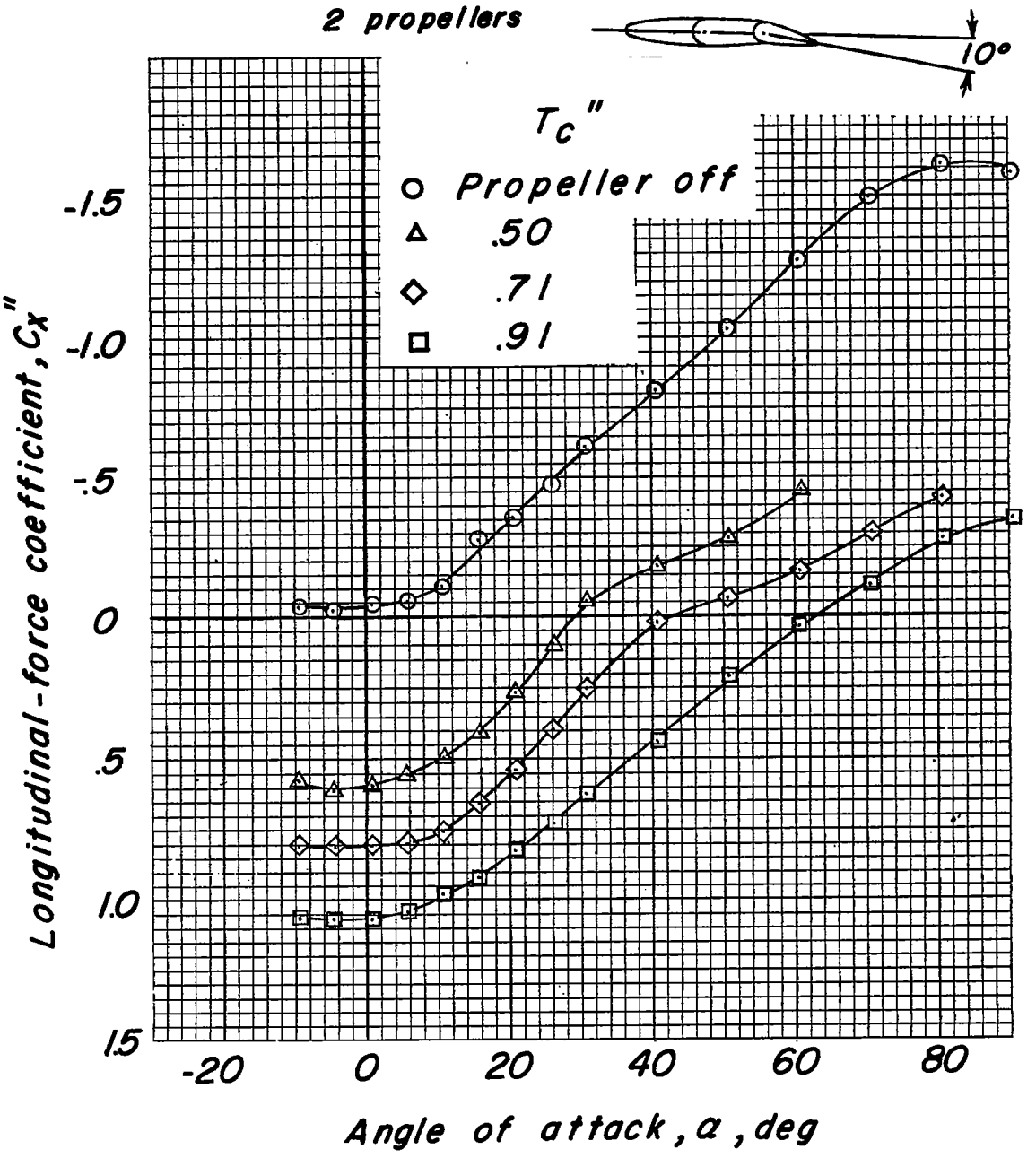

(b) Longitudinal-force coefficient.

Figure 14.- Continued.

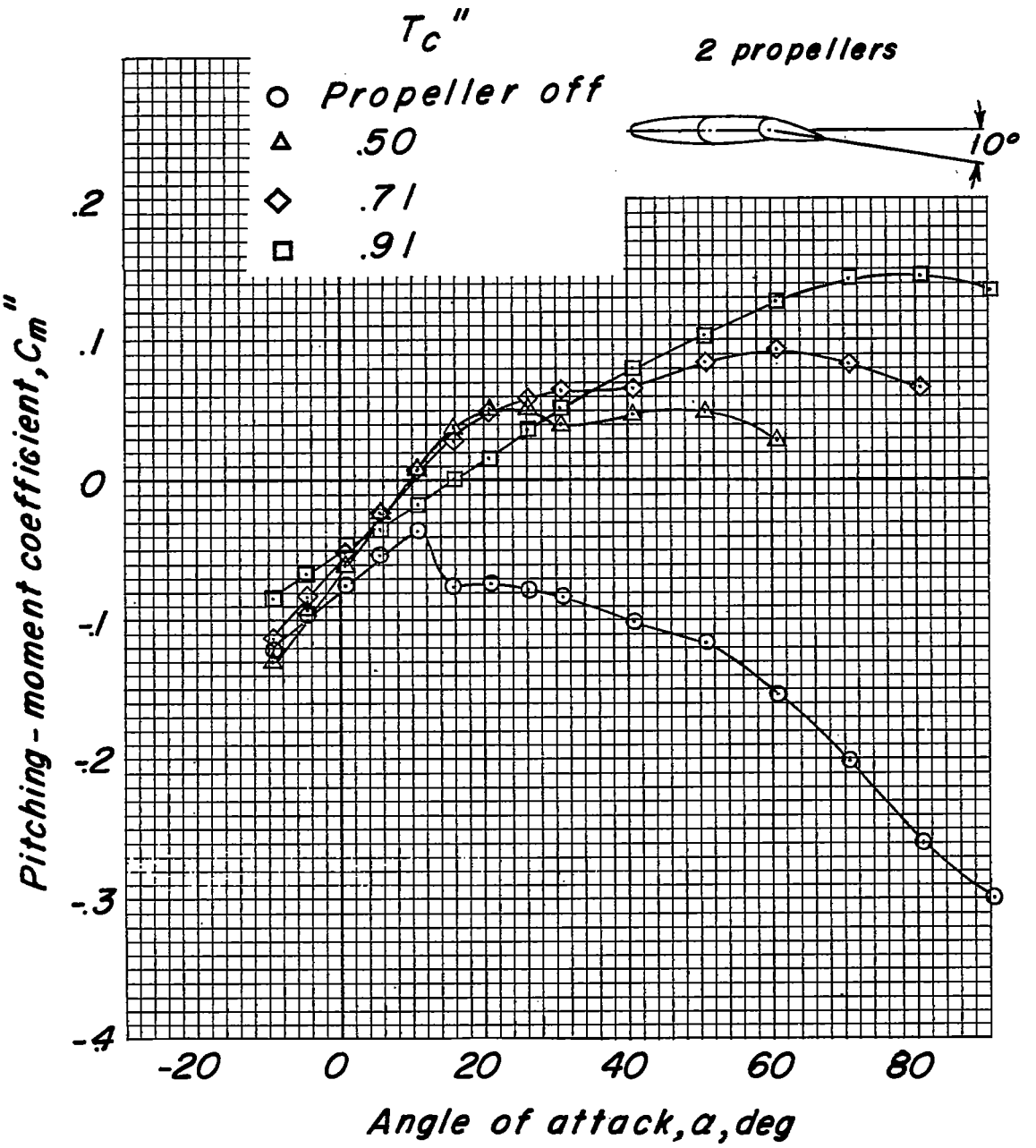

(c) Pitching-moment coefficient.

Figure 14.- Concluded.

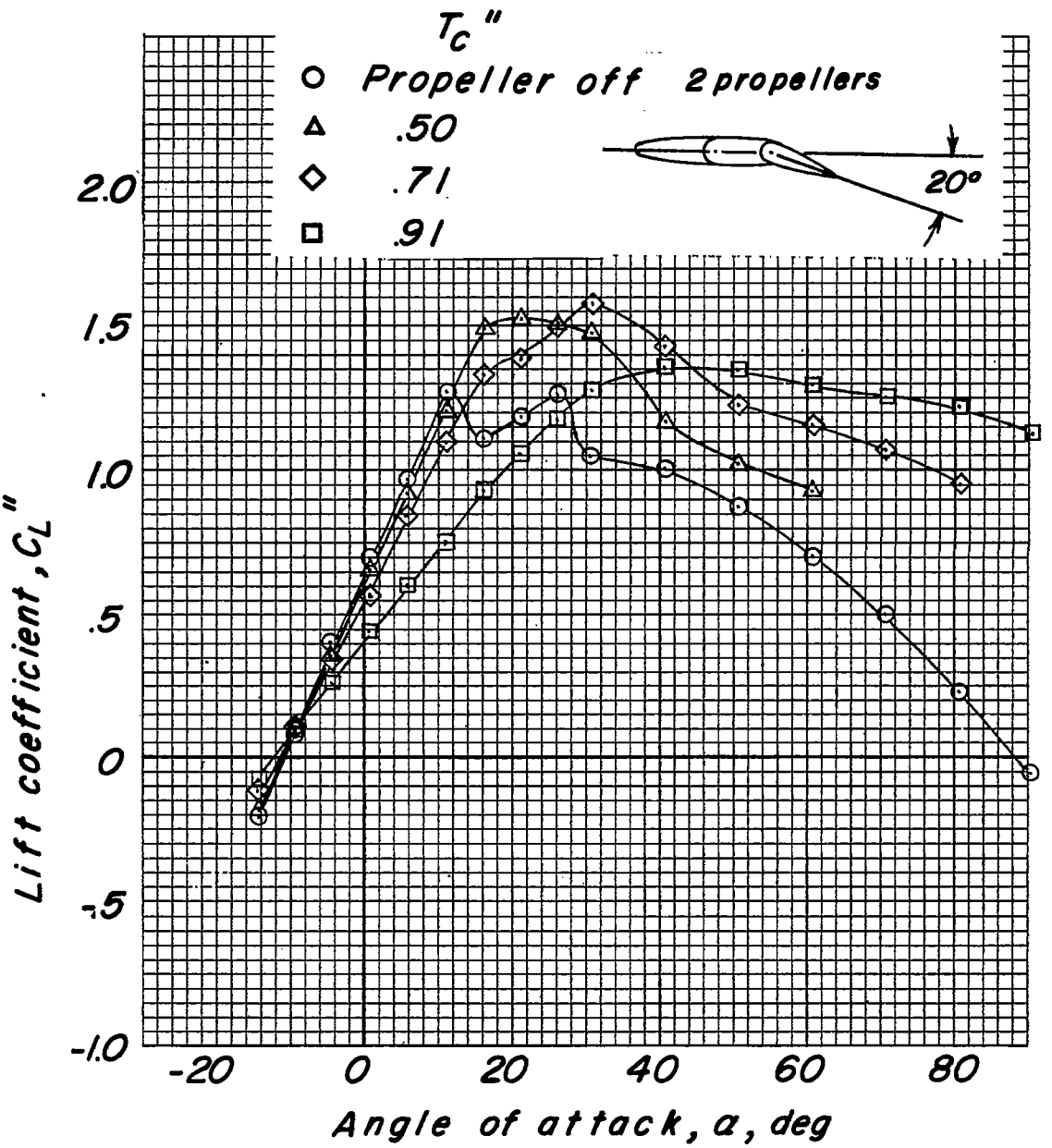

(a) Lift coefficient.

Figure 15.- Effect of thrust coefficient on aerodynamic characteristics of model. $\delta_{f_{30}} = 20^\circ$; $\delta_{f_{60}} = 0^\circ$.

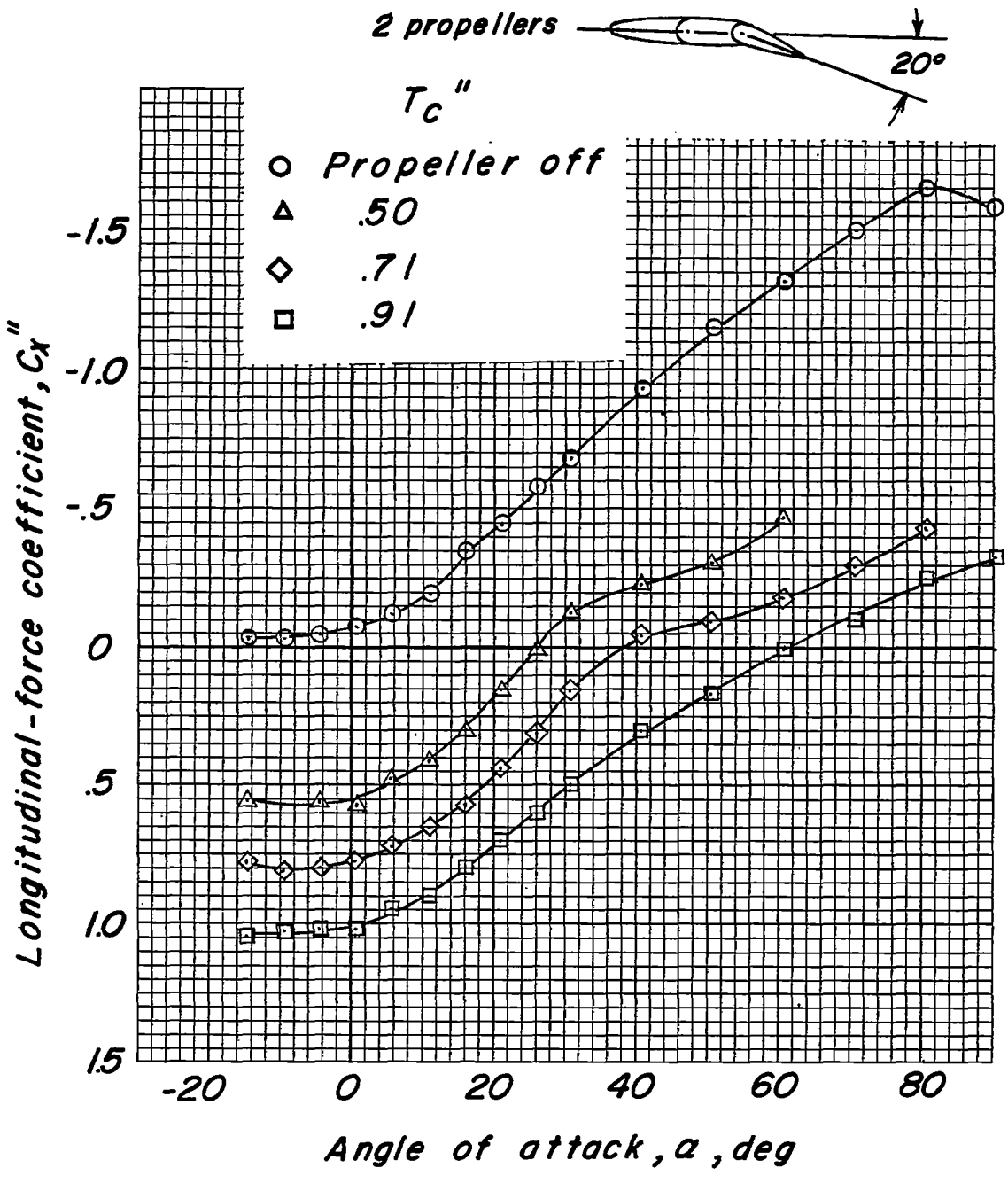

(b) Longitudinal-force coefficient.

Figure 15.- Continued.

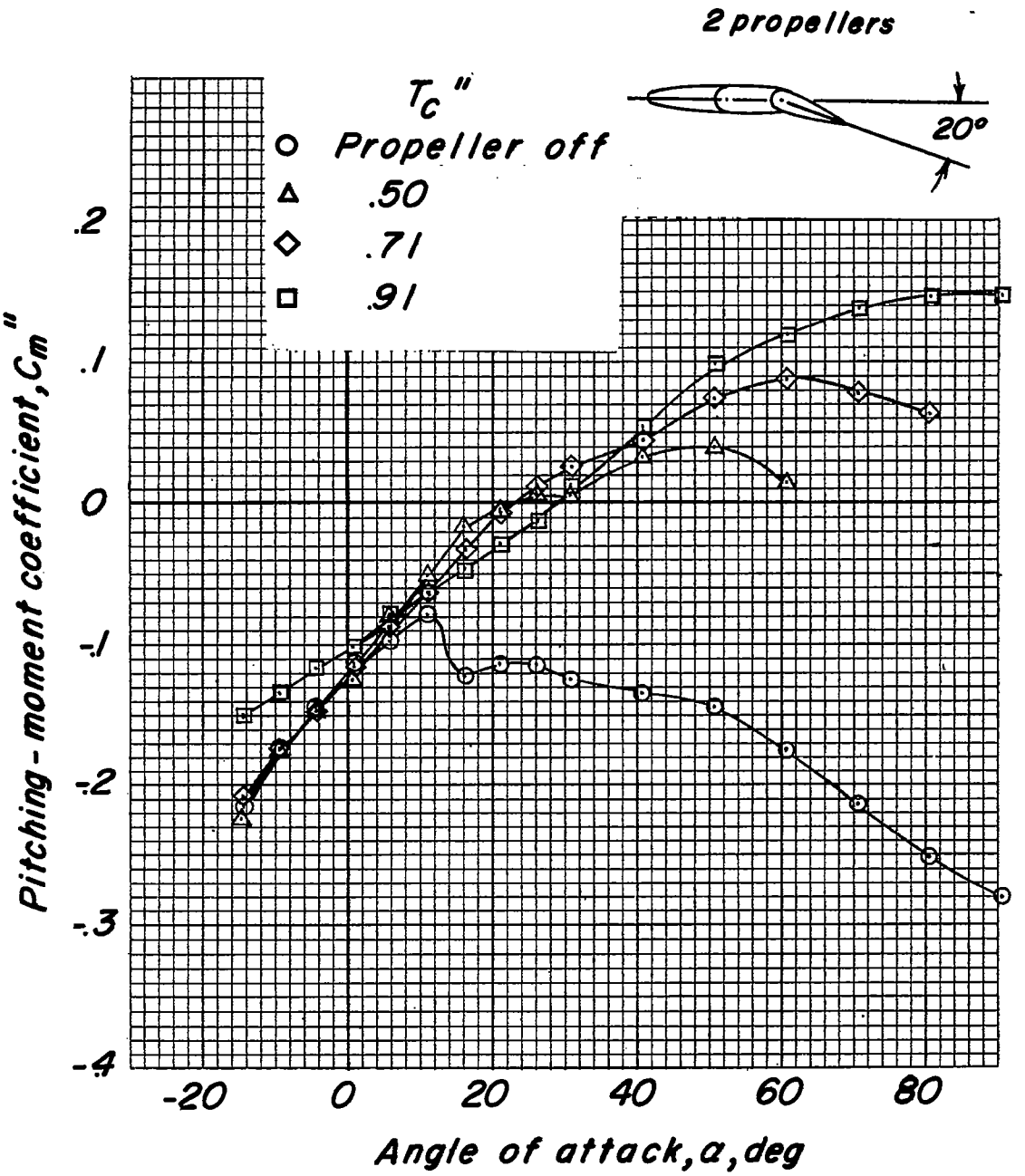

(c) Pitching-moment coefficient.

Figure 15.- Concluded.

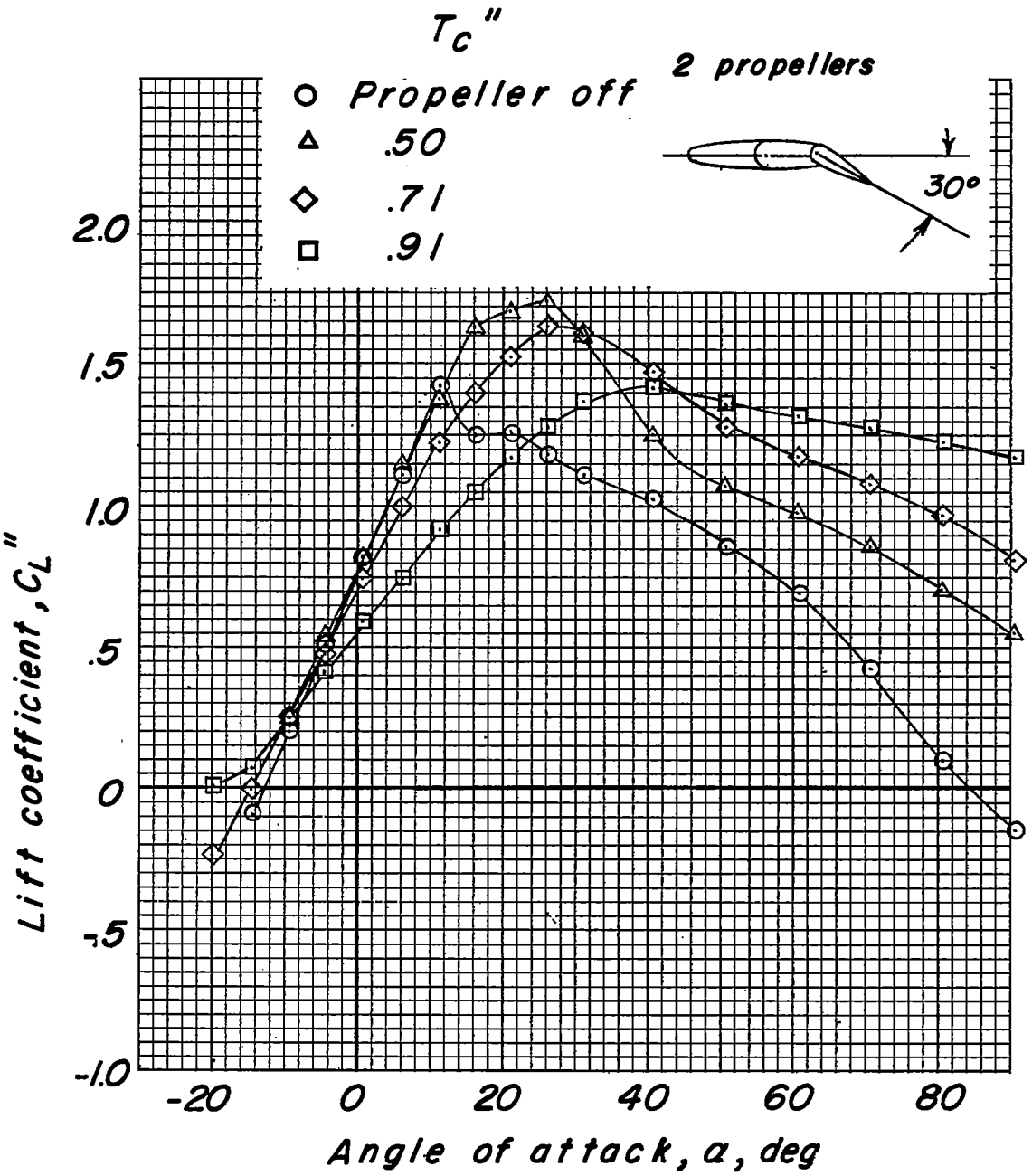

(a) Lift coefficient.

Figure 16.- Effect of thrust coefficient on aerodynamic characteristics of model. $\delta_{f_{30}} = 30^\circ$; $\delta_{f_{60}} = 0^\circ$.

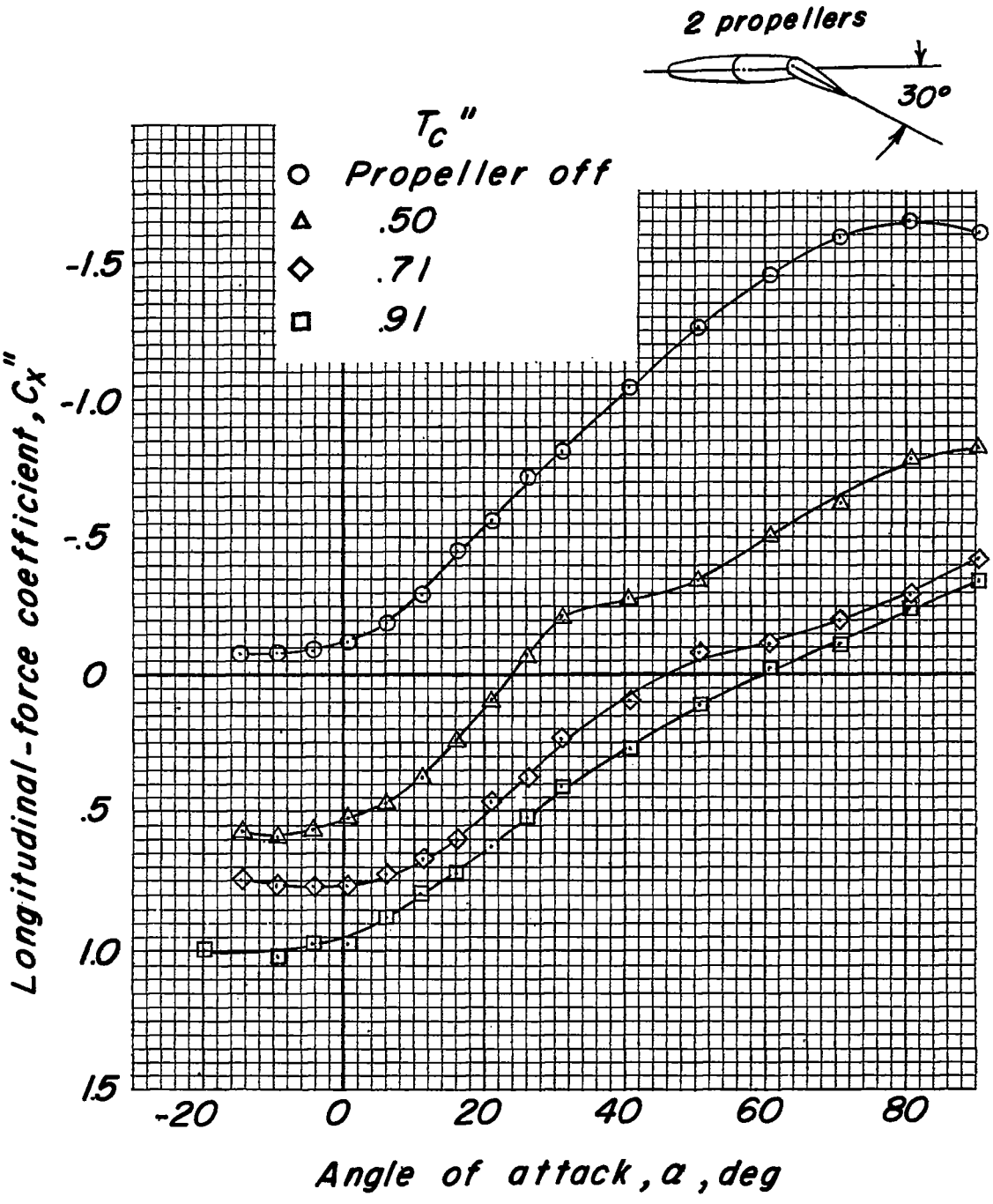

(b) Longitudinal-force coefficient.

Figure 16.- Continued.

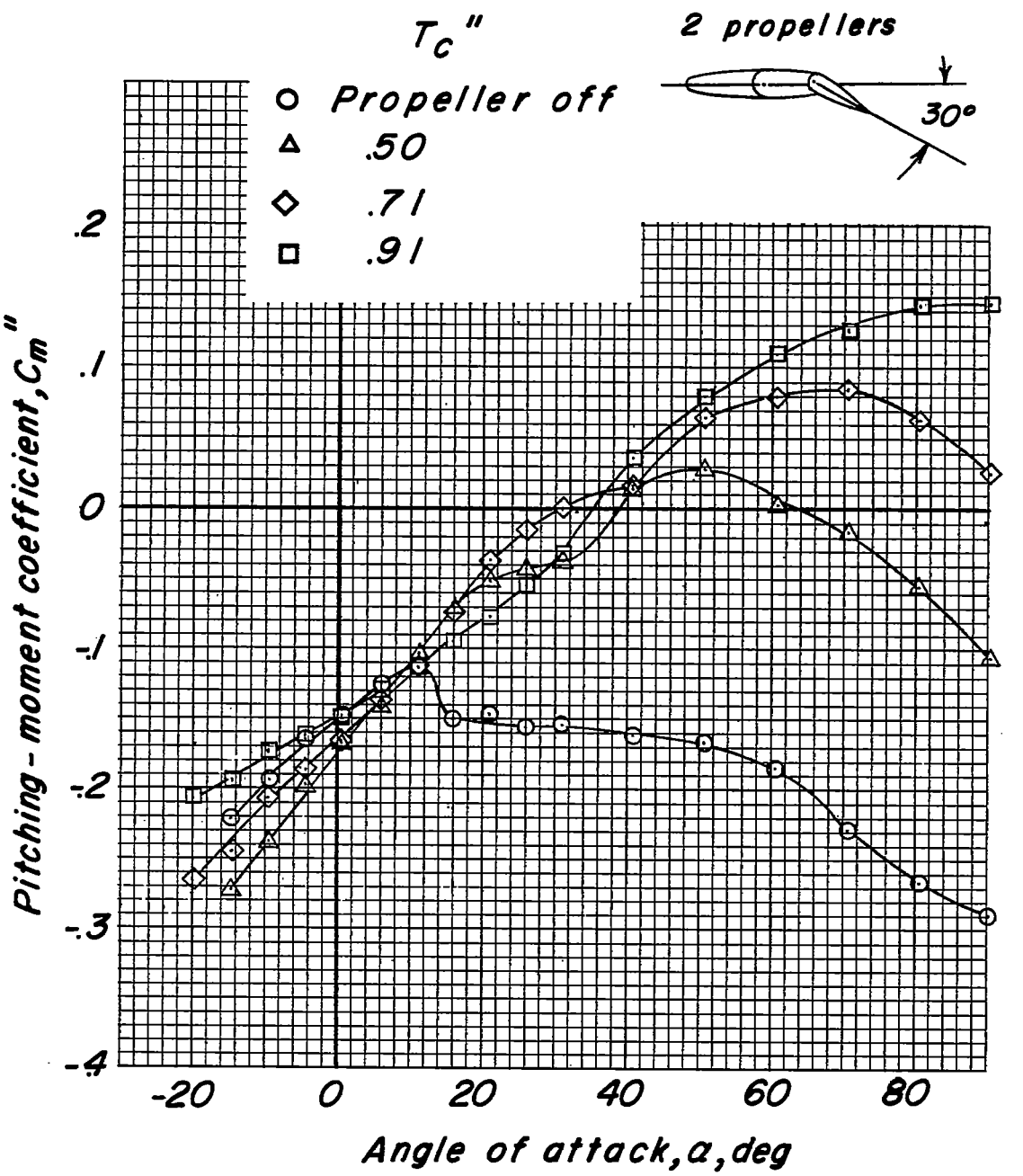

(c) Pitching-moment coefficient.

Figure 16.- Concluded.

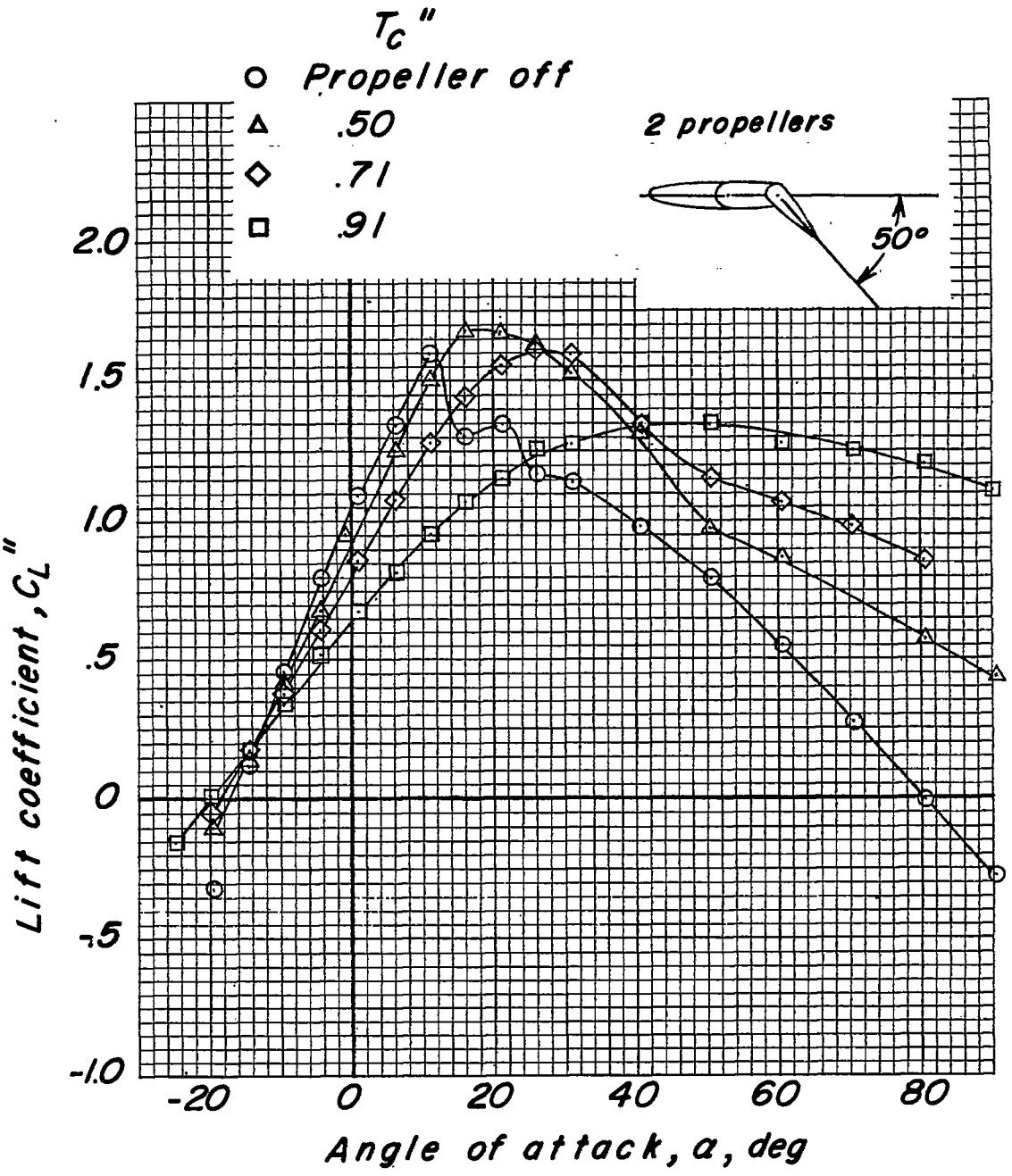

(a) Lift coefficient.

Figure 17.- Effect of thrust coefficient on aerodynamic characteristics of model. $\delta_{f_{30}} = 50°$; $\delta_{f_{60}} = 0°$.

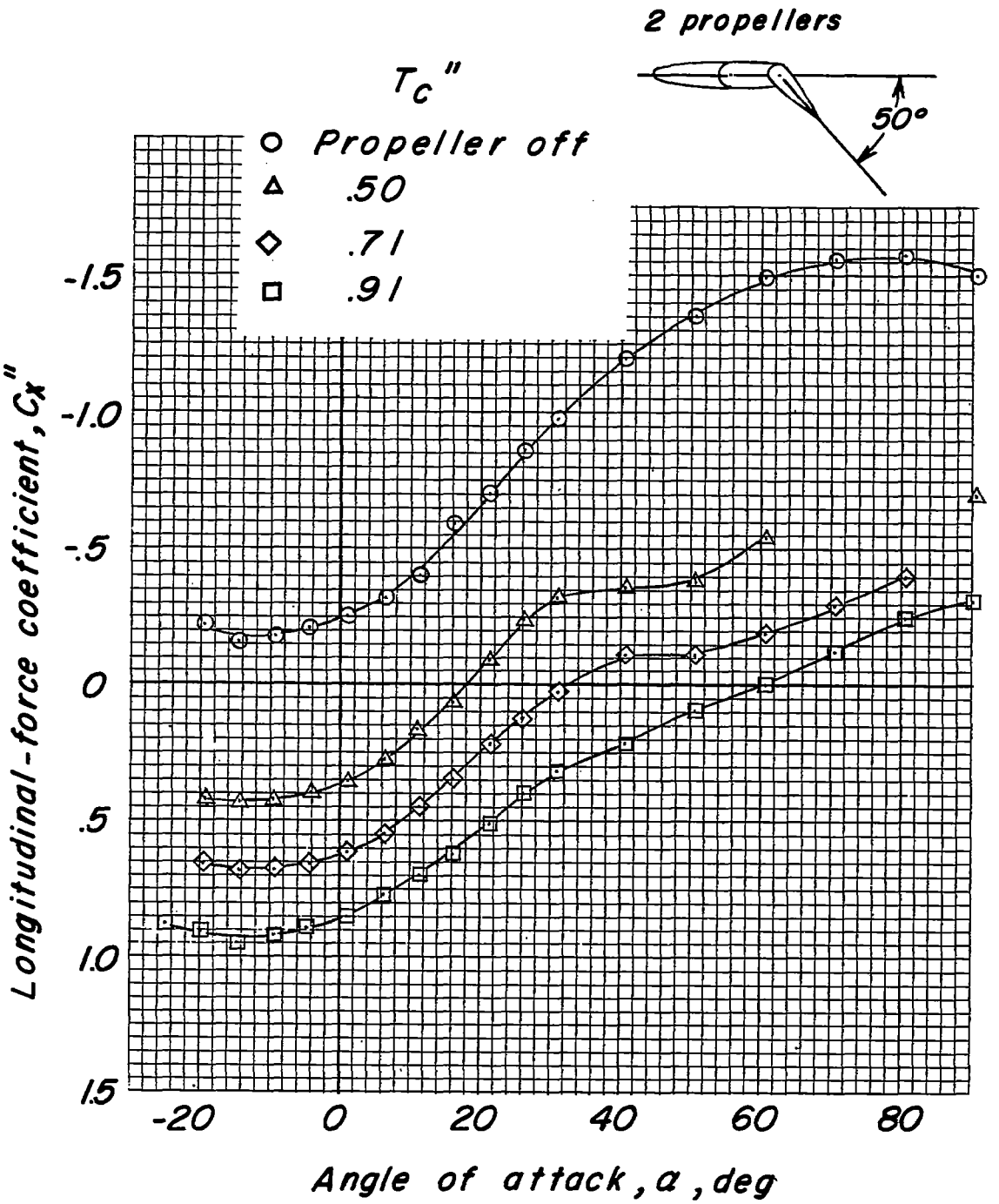

(b) Longitudinal-force coefficient.

Figure 17.- Continued.

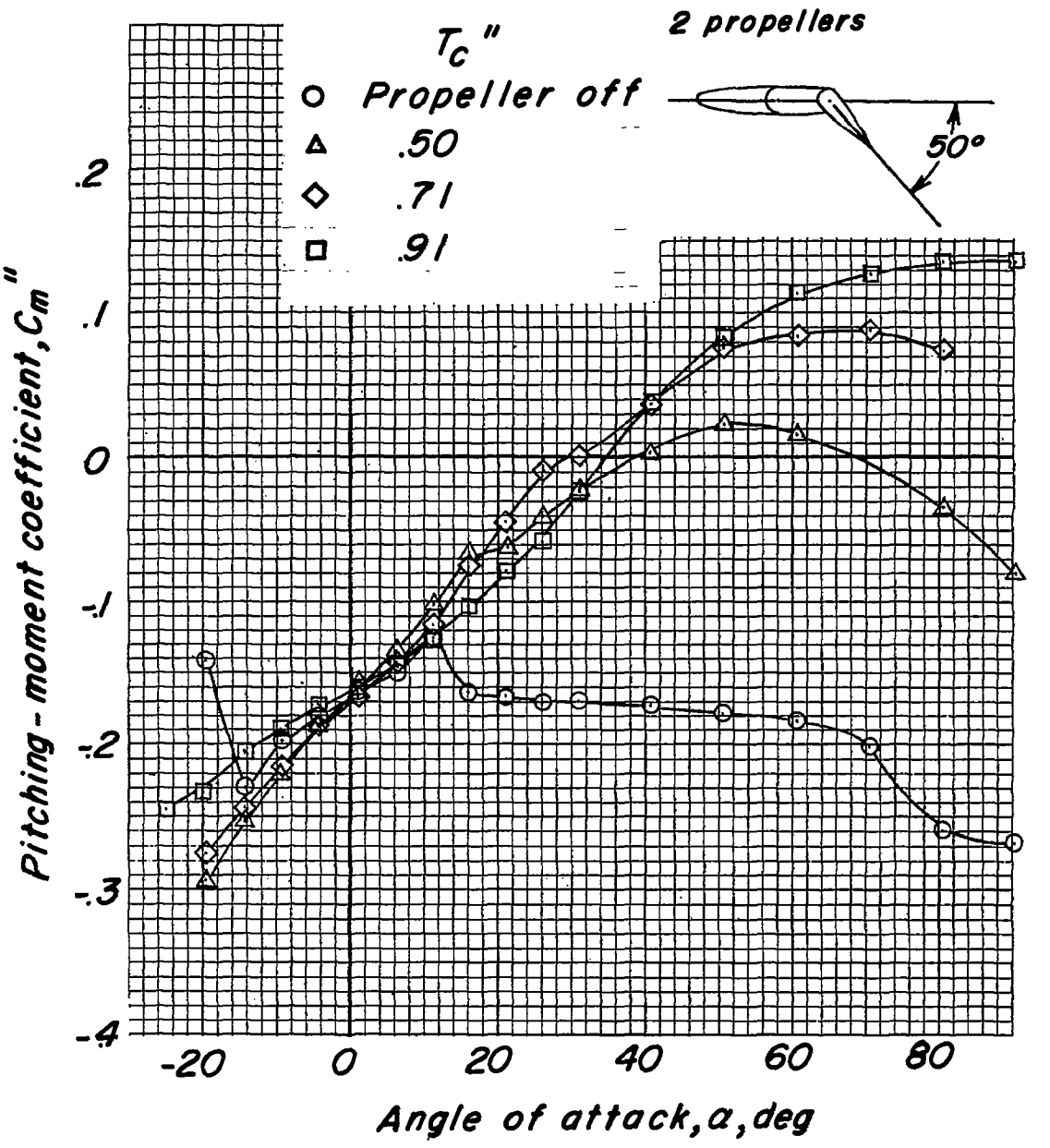

(c) Pitching-moment coefficient.

Figure 17.- Concluded.

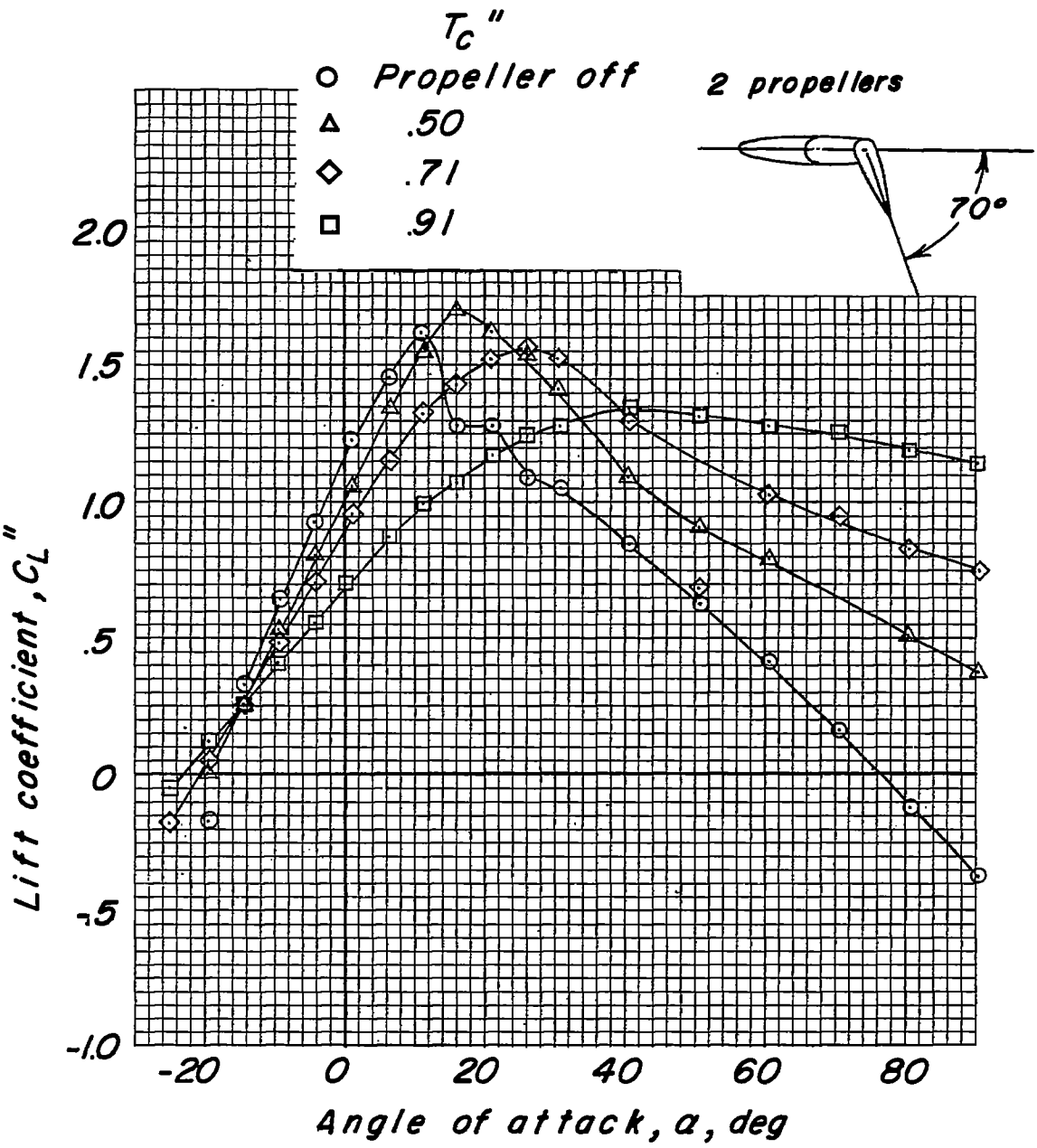

(a) Lift coefficient.

Figure 18.- Effects of thrust coefficient on aerodynamic characteristics of model. $\delta_{f_{30}} = 70^\circ$; $\delta_{f_{60}} = 0^\circ$.

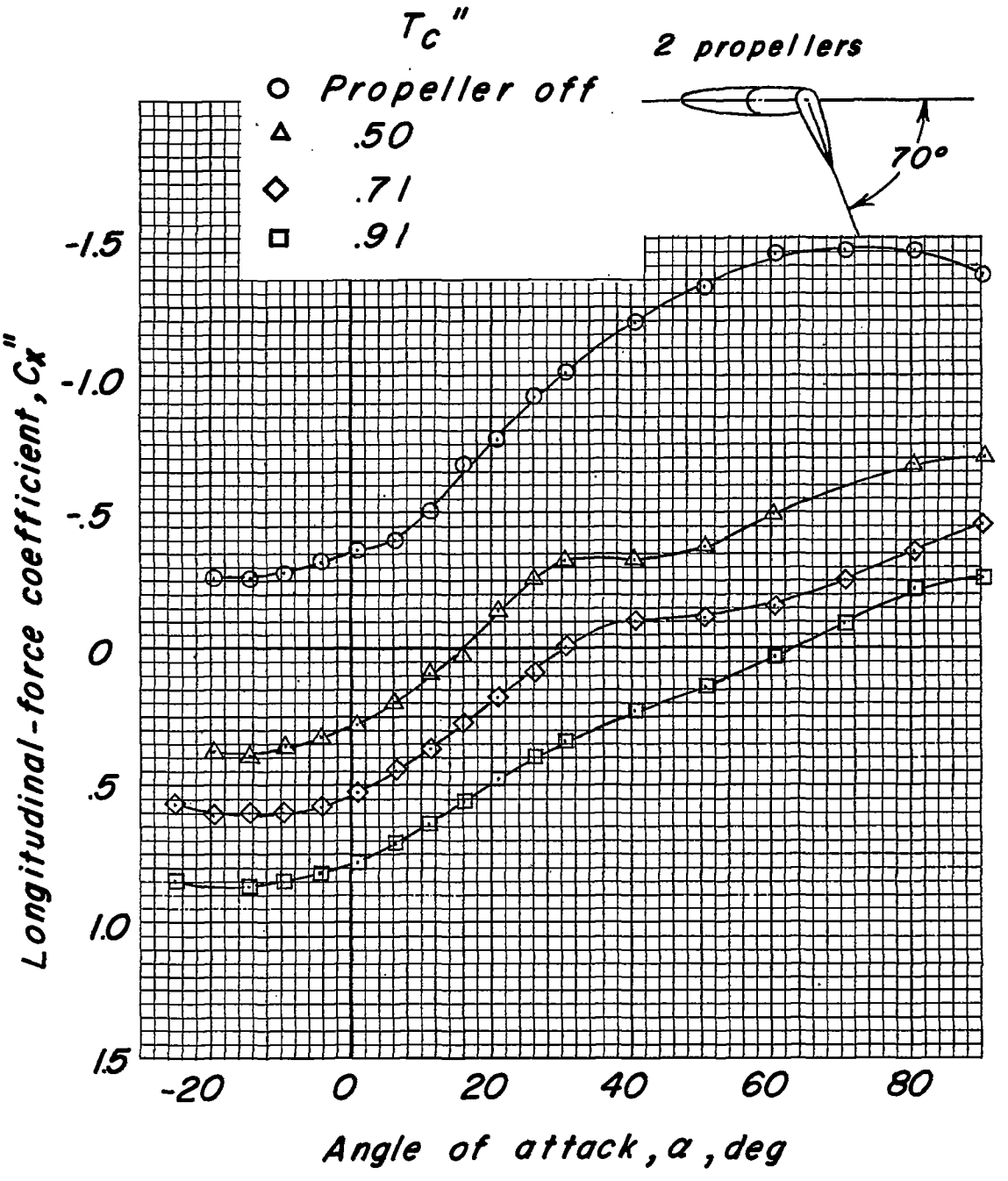

(b) Longitudinal-force coefficient.

Figure 18.- Continued.

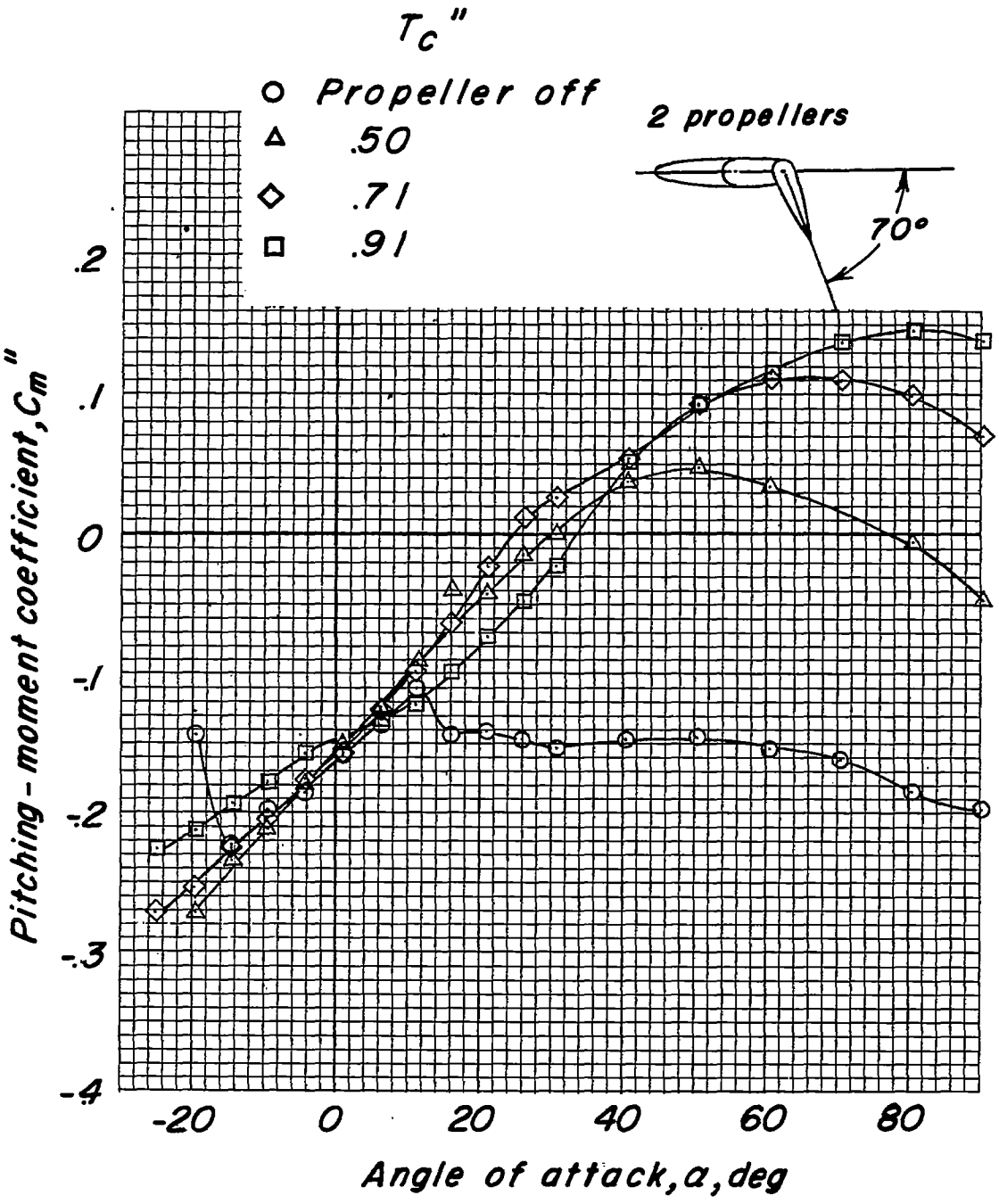

(c) Pitching-moment coefficient.

Figure 18.- Concluded.

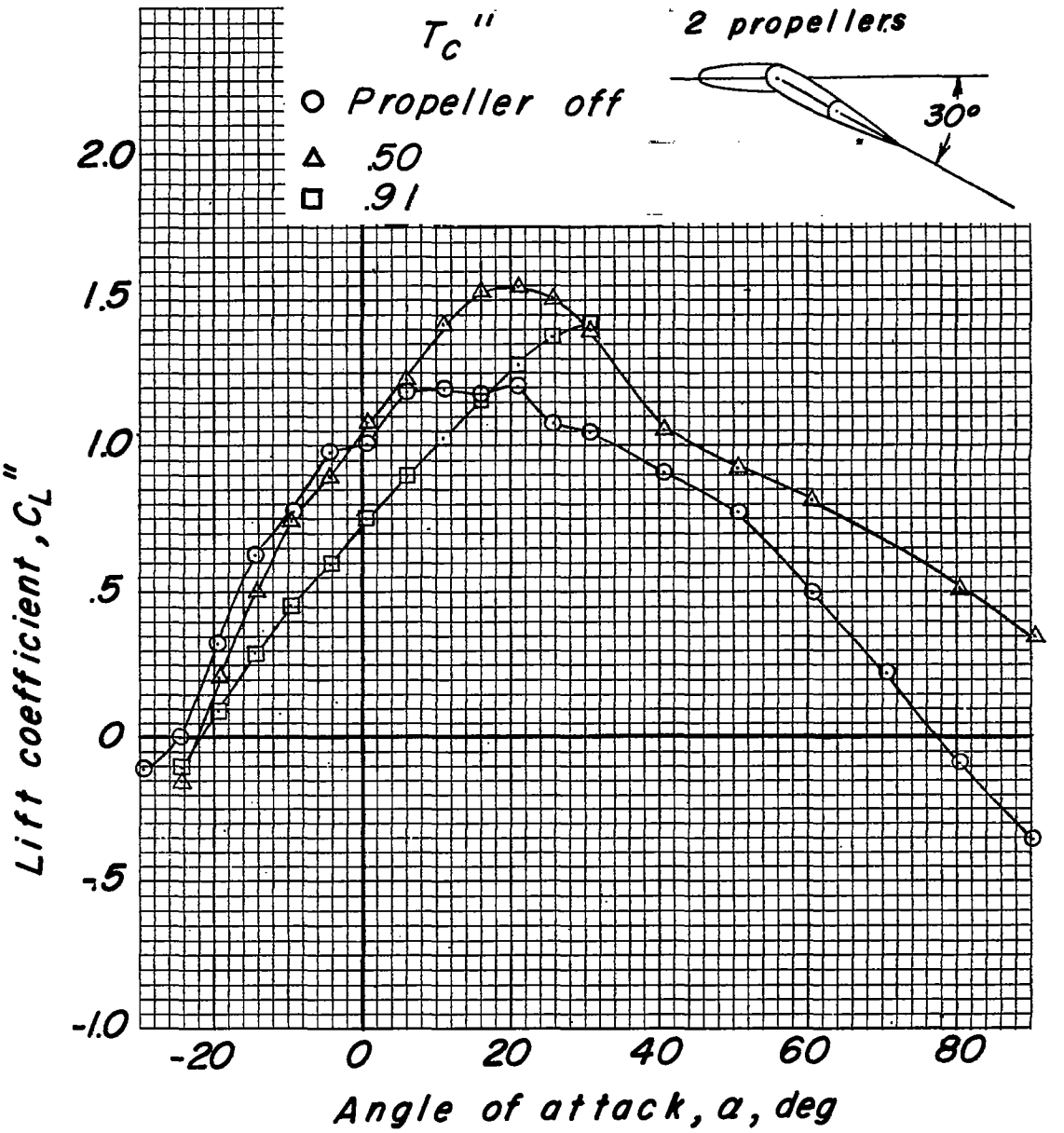

(a) Lift coefficient.

Figure 19.- Effects of thrust coefficient on aerodynamic characteristics of model. $\delta_{f_{30}} = 0^\circ$; $\delta_{f_{60}} = 30^\circ$.

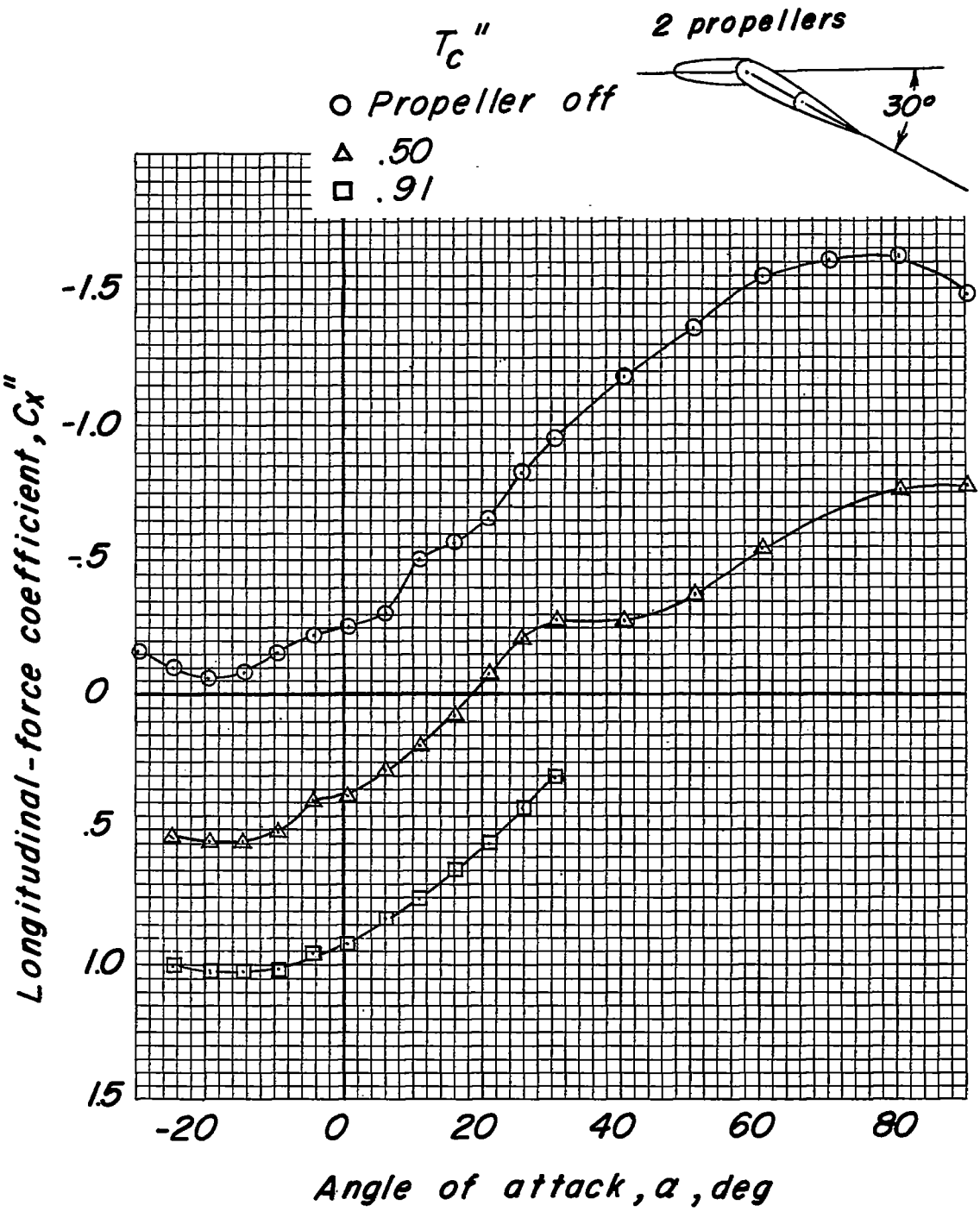

(b) Longitudinal-force coefficient.

Figure 19.- Continued.

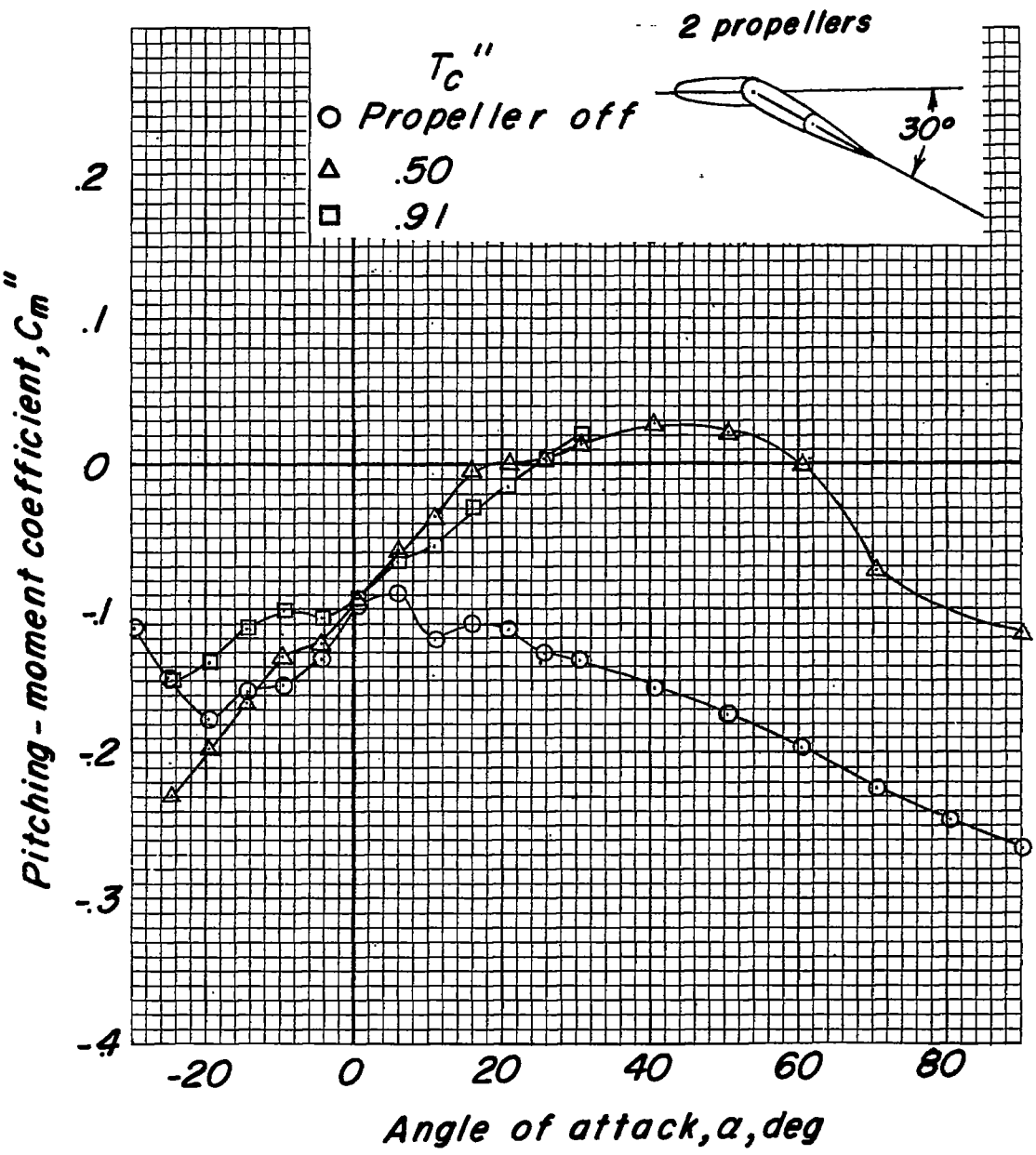

(c) Pitching-moment coefficient.

Figure 19.- Concluded.

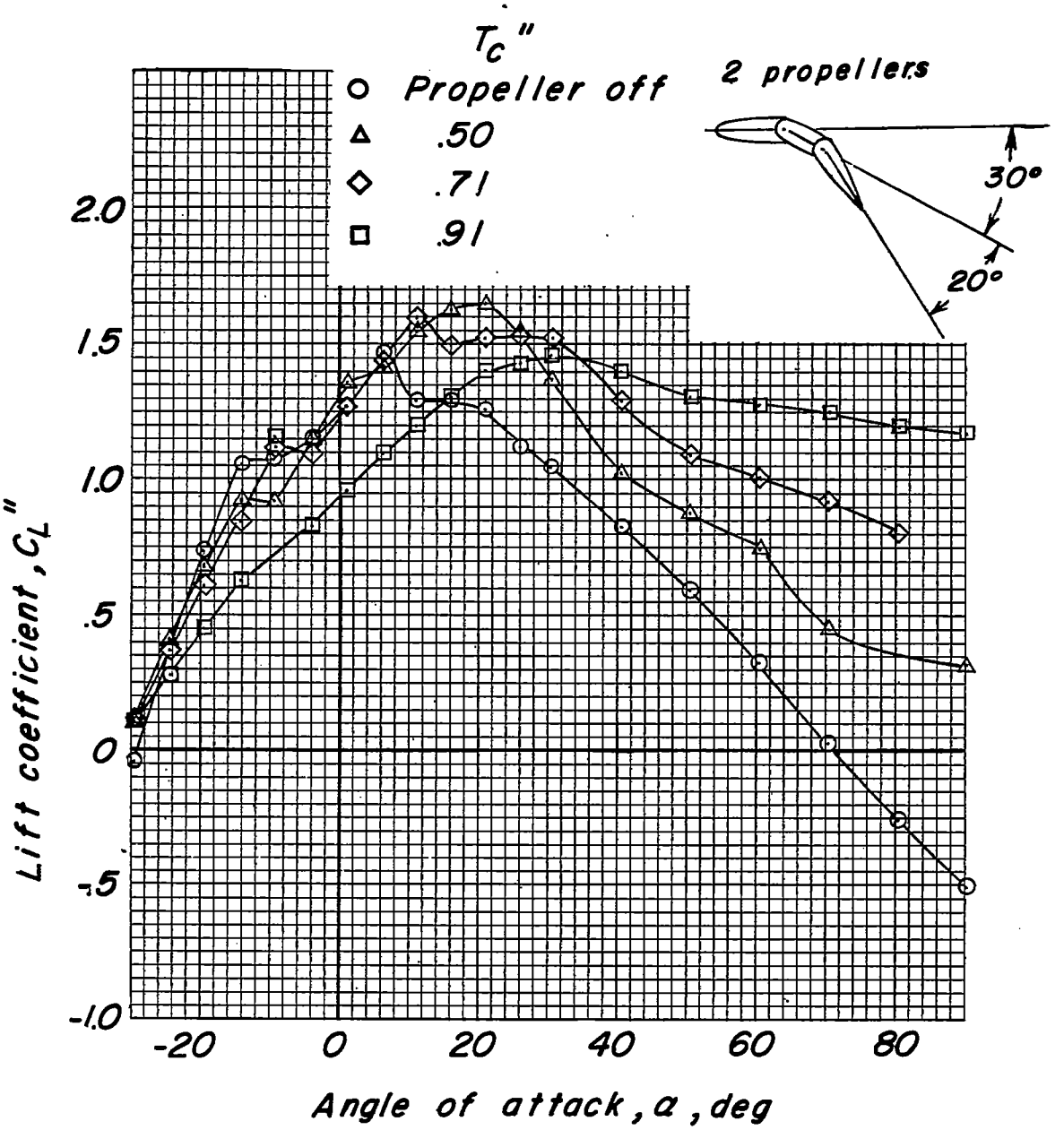

(a) Lift coefficient.

Figure 20.- Effects of thrust coefficient on aerodynamic characteristics of model. $\delta_{f_{30}} = 20^\circ$; $\delta_{f_{60}} = 30^\circ$.

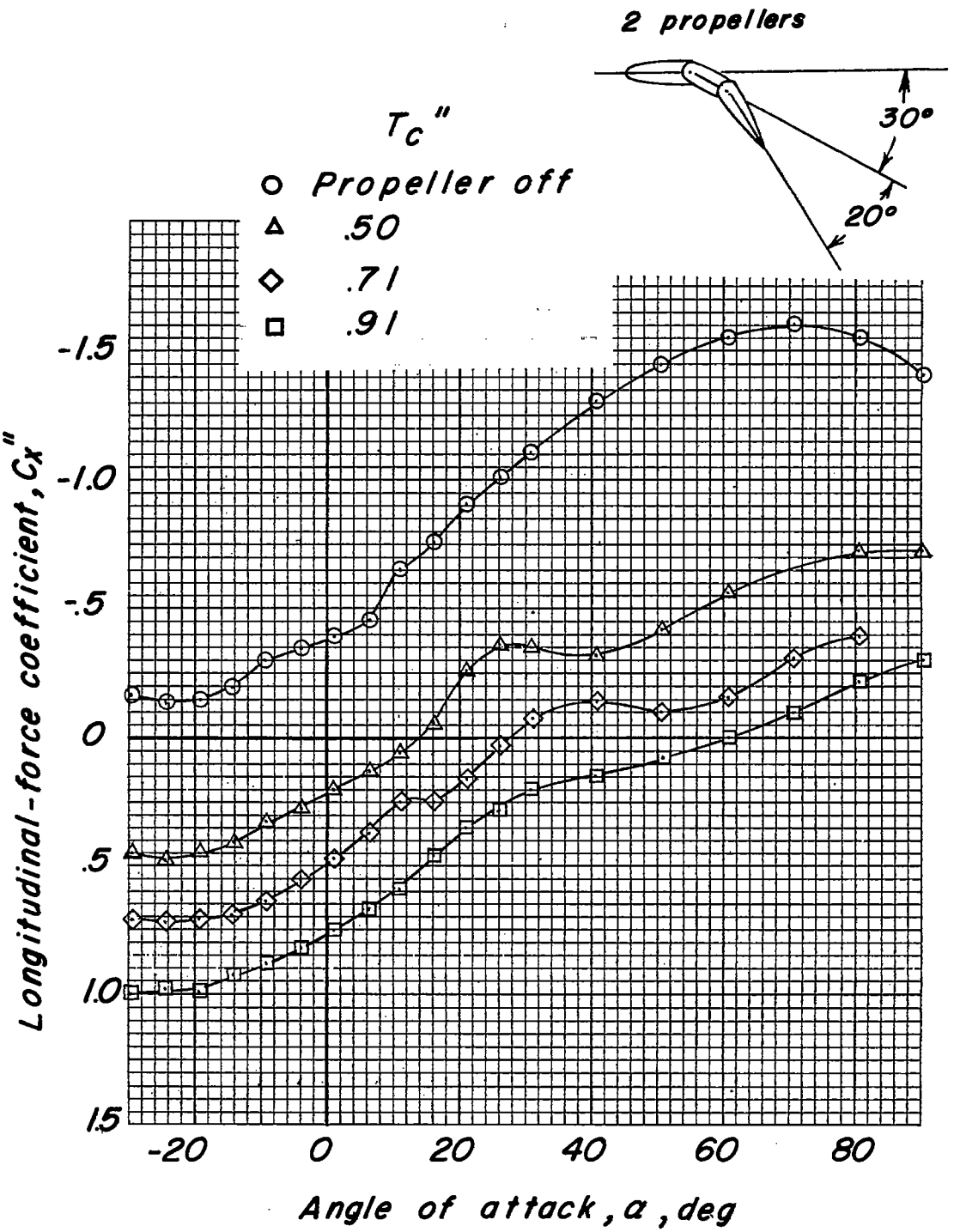

(b) Longitudinal-force coefficient.

Figure 20.- Continued.

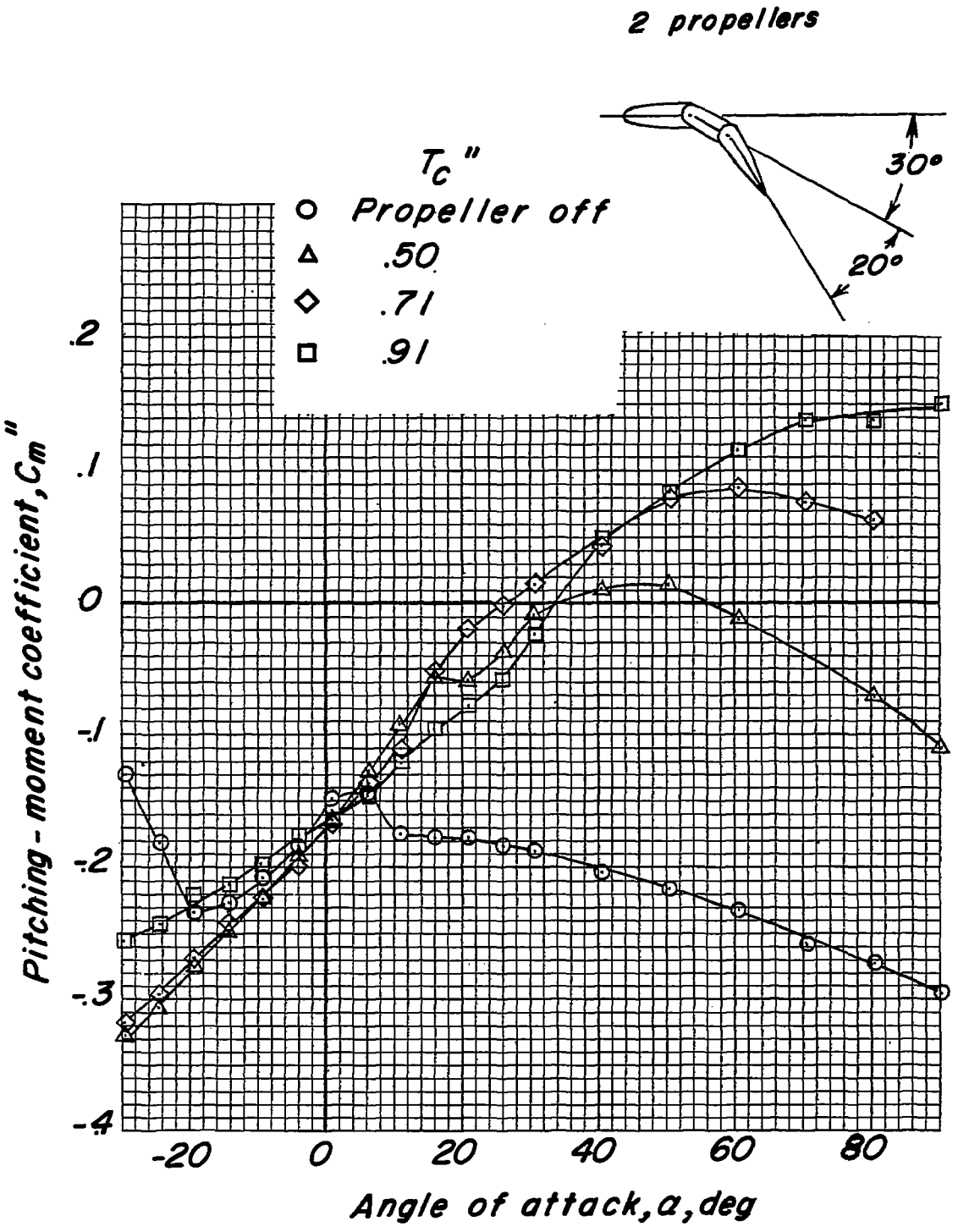

(c) Pitching-moment coefficient.

Figure 20.- Concluded.

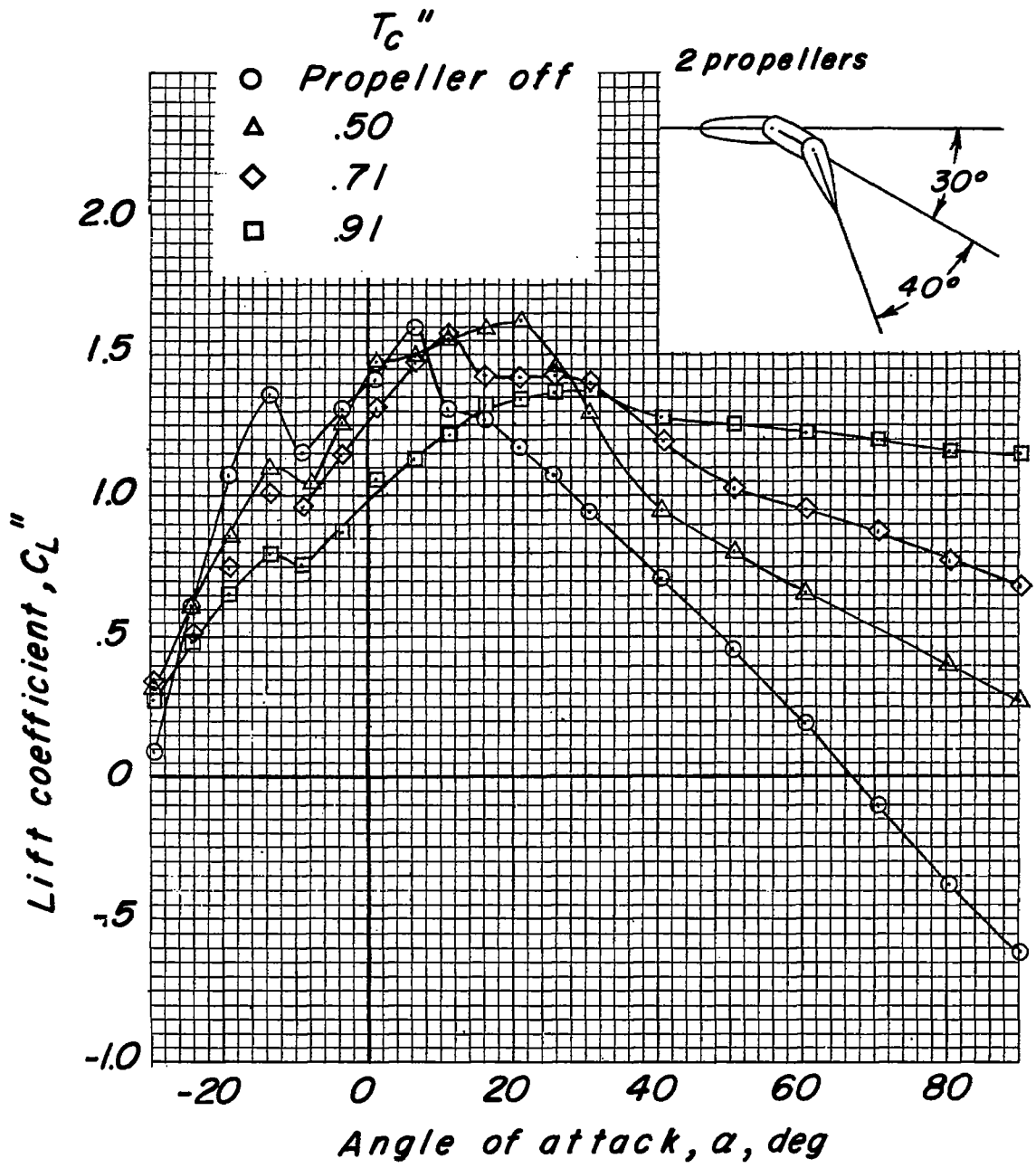

(a) Lift coefficient.

Figure 21.- Effect of thrust coefficient on aerodynamic characteristics of model. $\delta_{f_{30}} = 40^\circ$; $\delta_{f_{60}} = 30^\circ$.

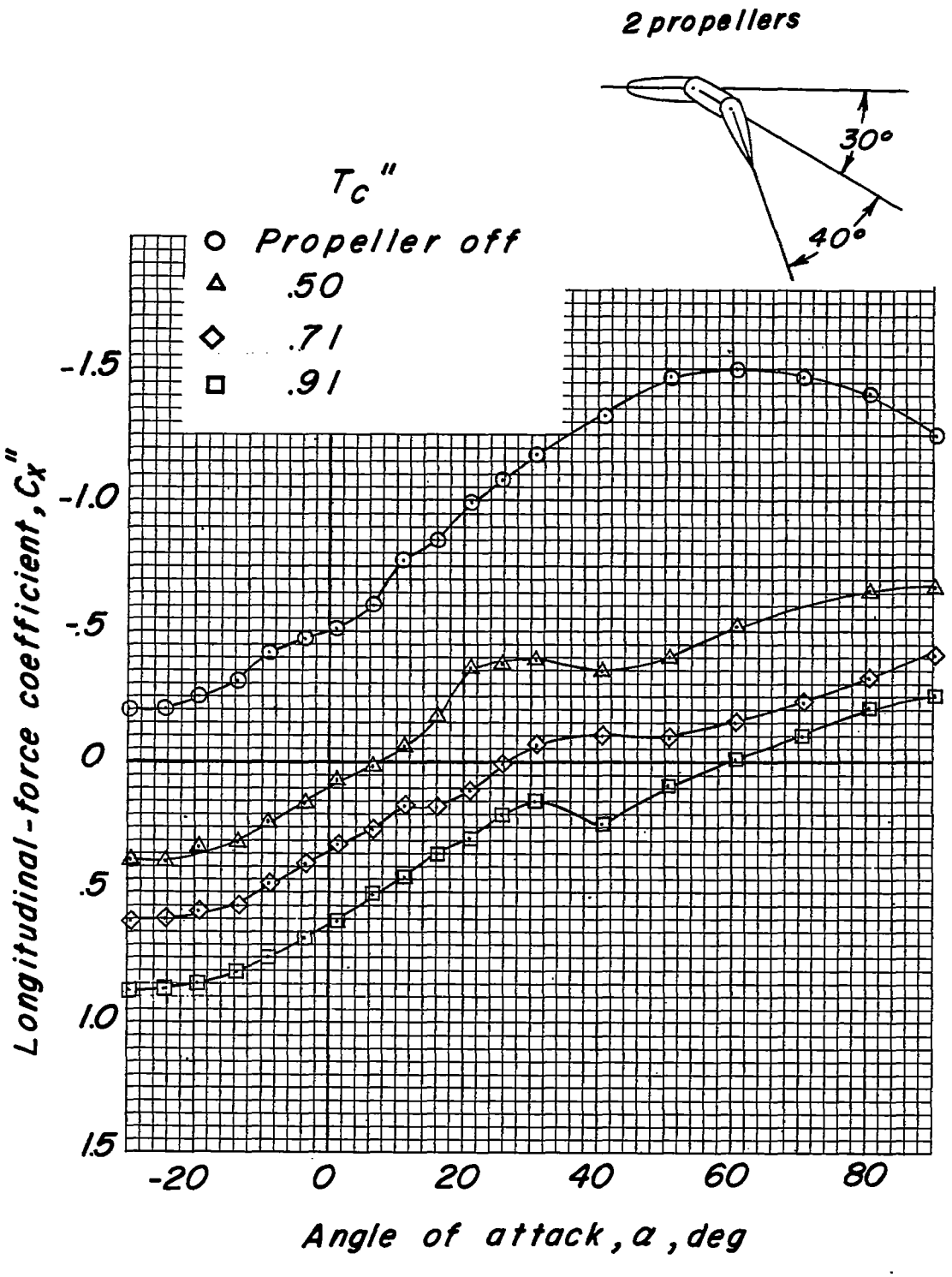

(b) Longitudinal-force coefficient.

Figure 21.- Continued.

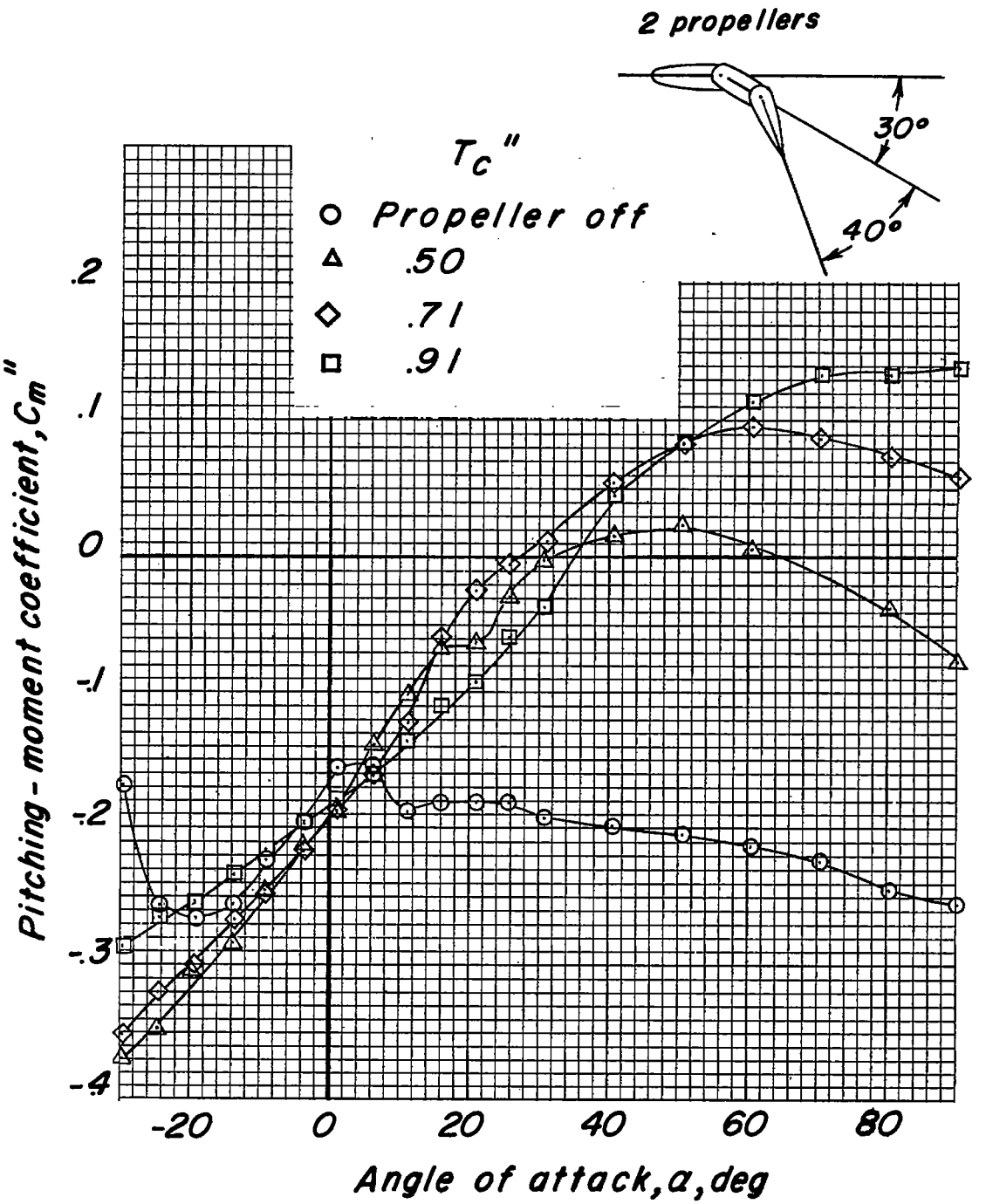

(c) Pitching-moment coefficient.

Figure 21.- Concluded.

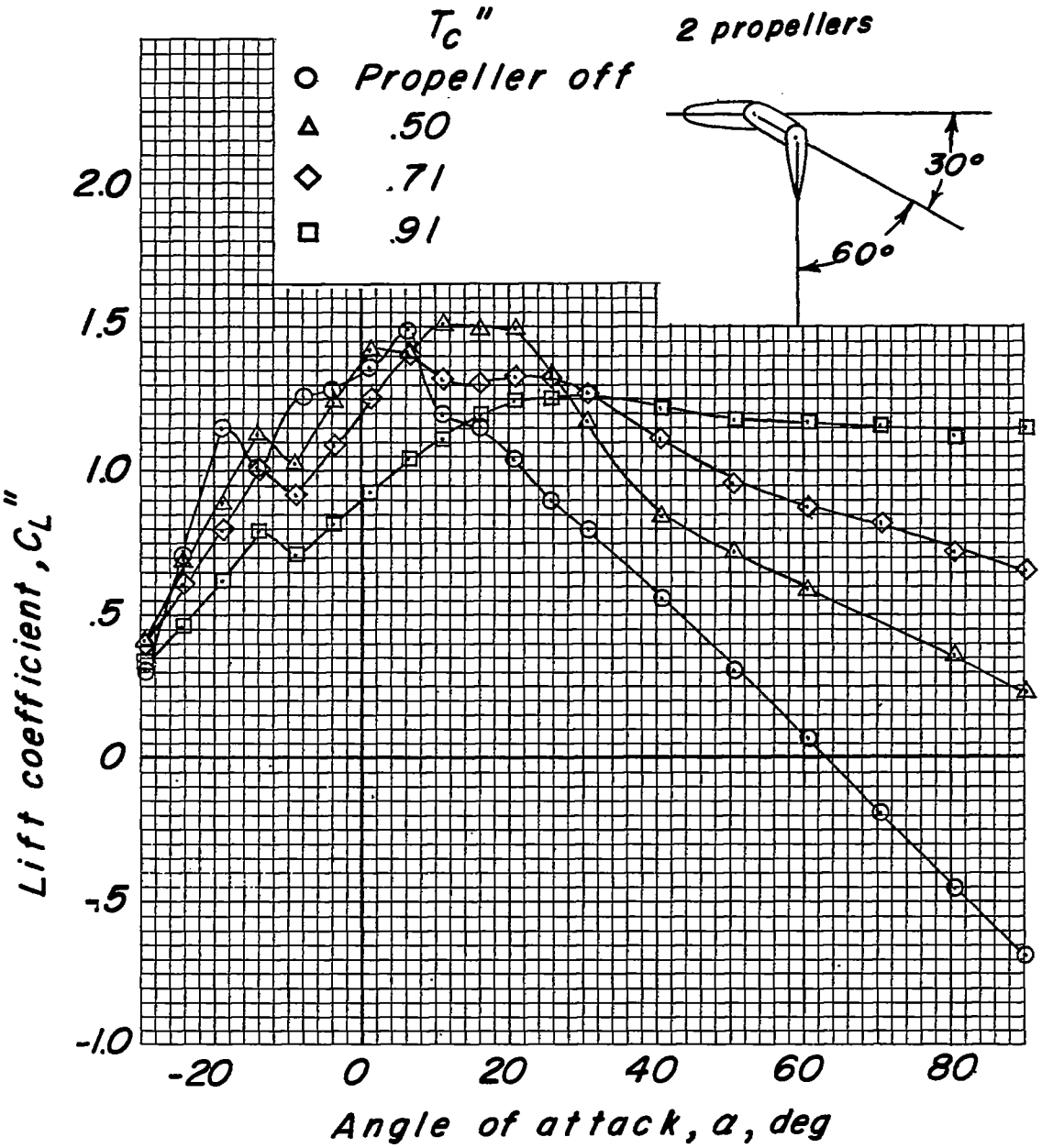

(a) Lift coefficient.

Figure 22.- Effect of thrust coefficient on aerodynamic characteristics of model. $\delta_{f_{30}} = 60^\circ$; $\delta_{f_{60}} = 30^\circ$.

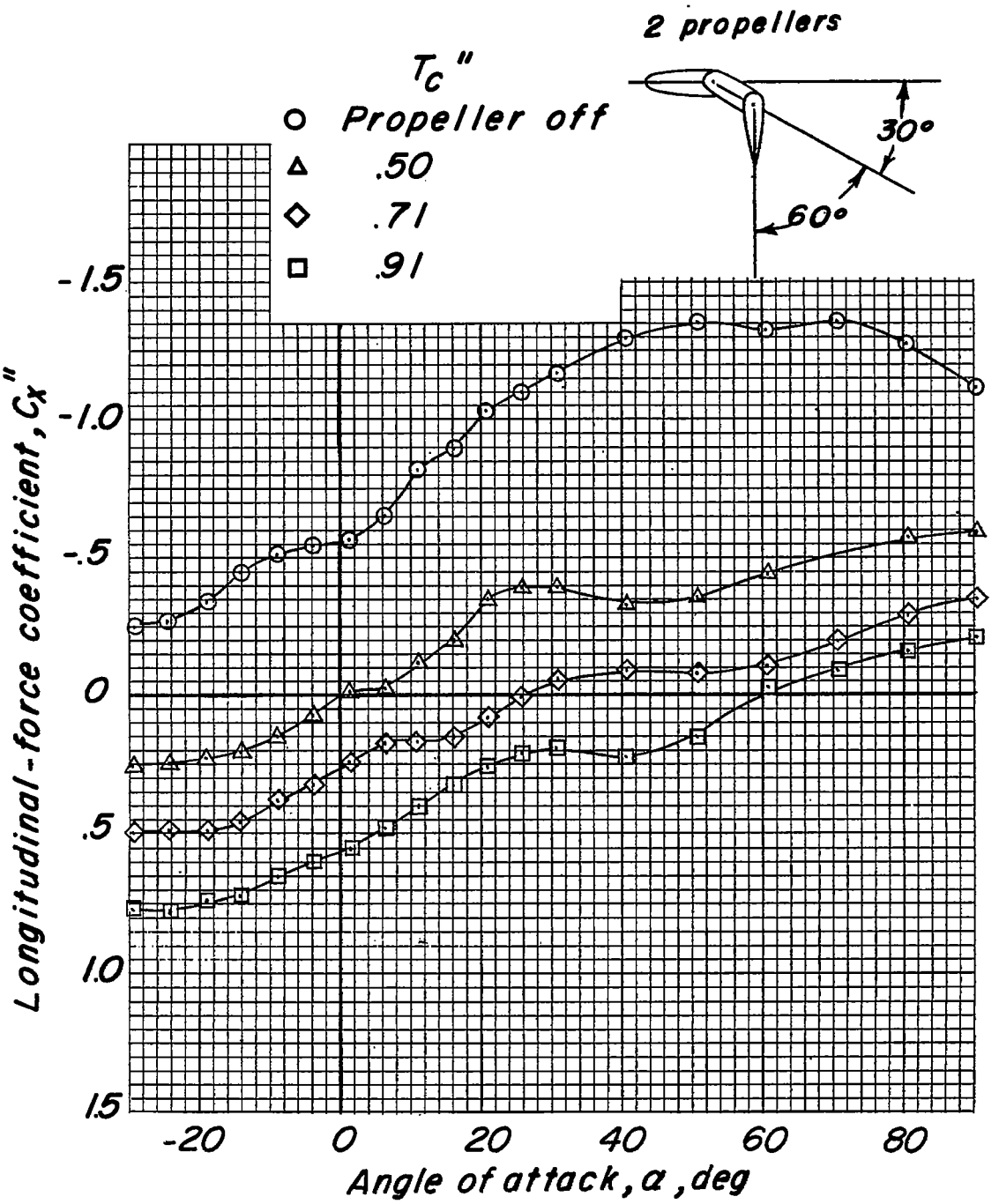

(b) Longitudinal-force coefficient.

Figure 22.- Continued.

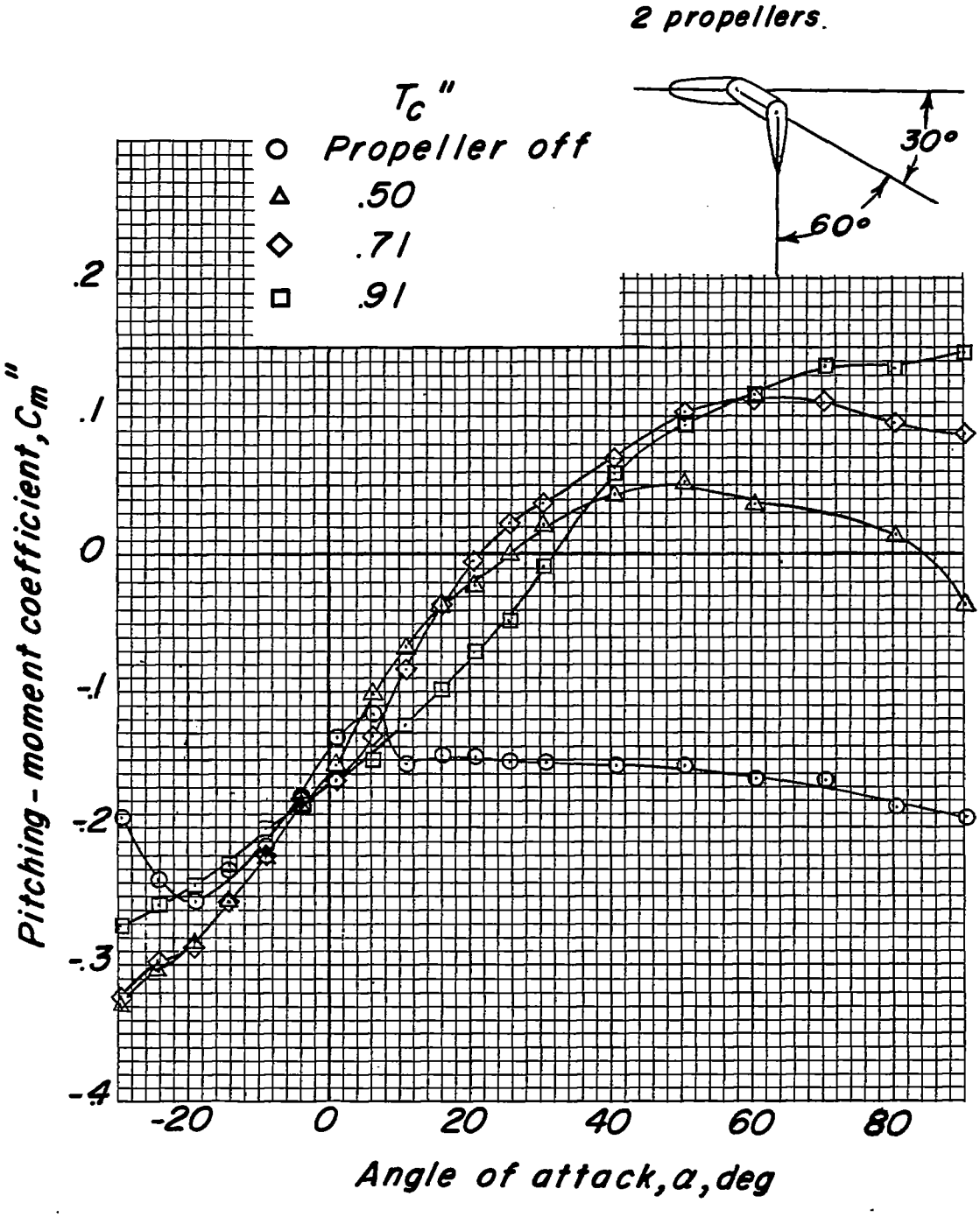

(c) Pitching-moment coefficient.

Figure 22.- Concluded.

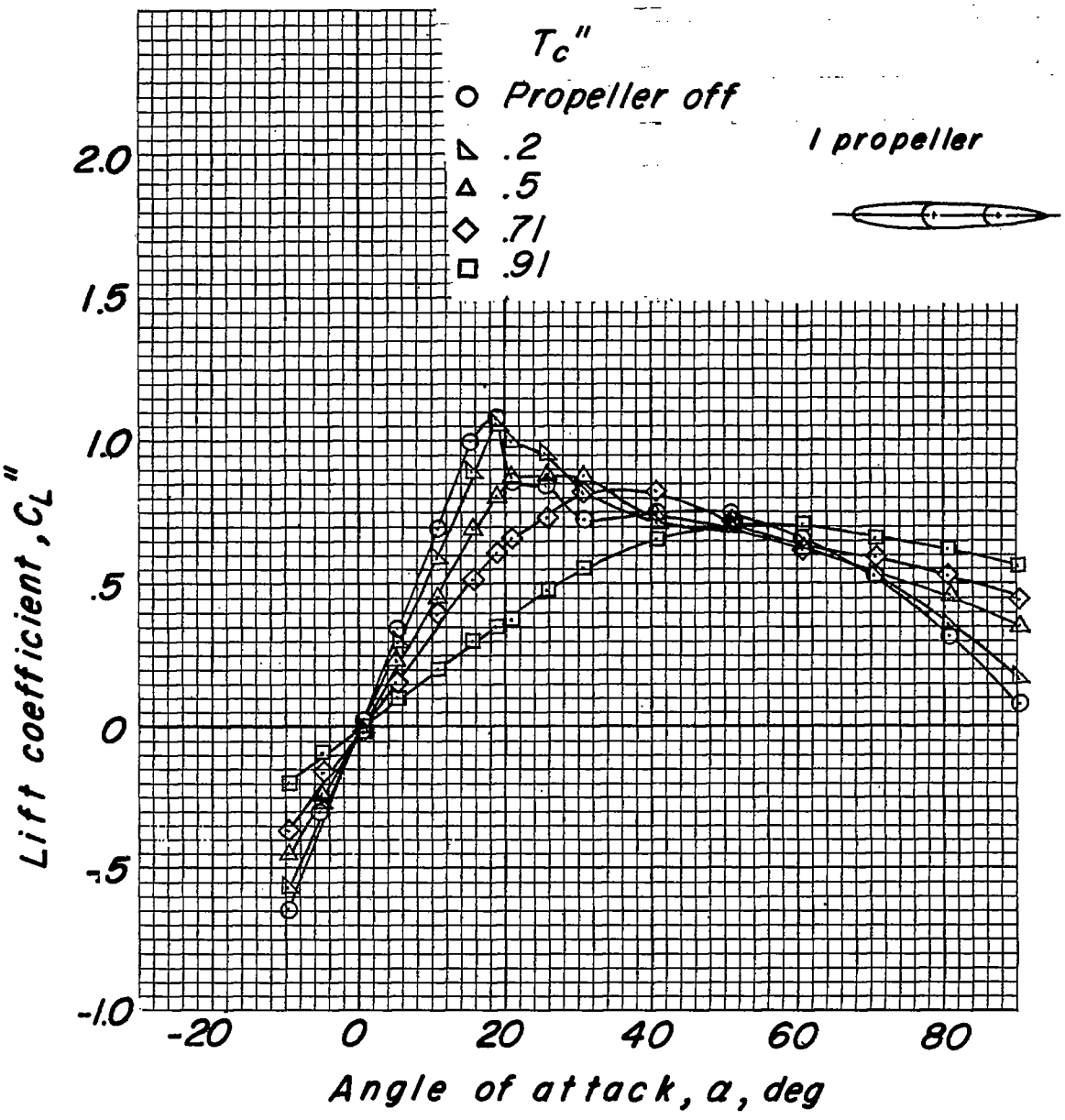

(a) Lift coefficient.

Figure 23.- Effect of thrust coefficient on aerodynamic characteristics of model. Inboard propeller only. $\delta_{f_{30}} = 0^\circ$; $\delta_{f_{60}} = 0^\circ$.

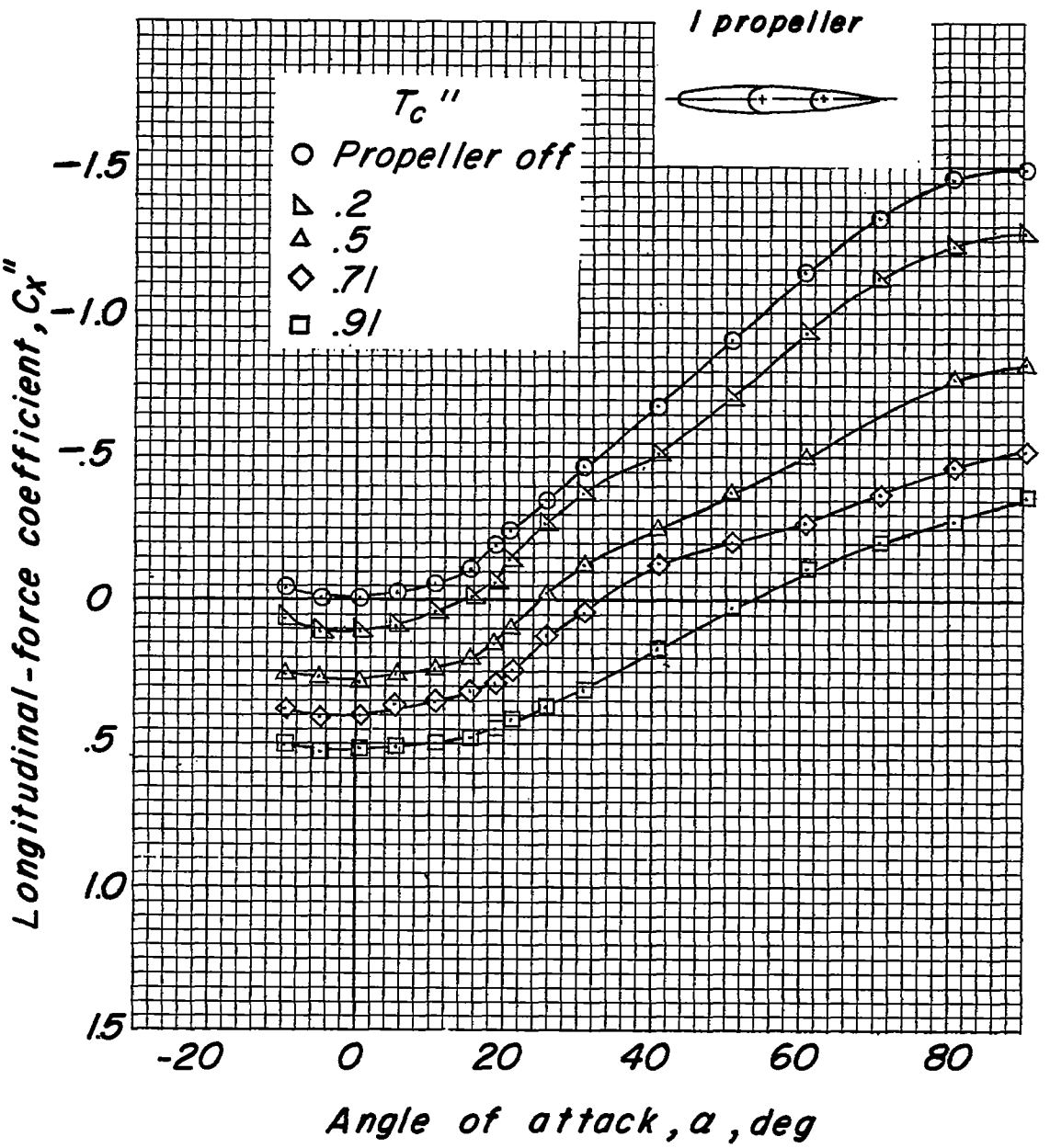

(b) Longitudinal-force coefficient.

Figure 23.- Continued.

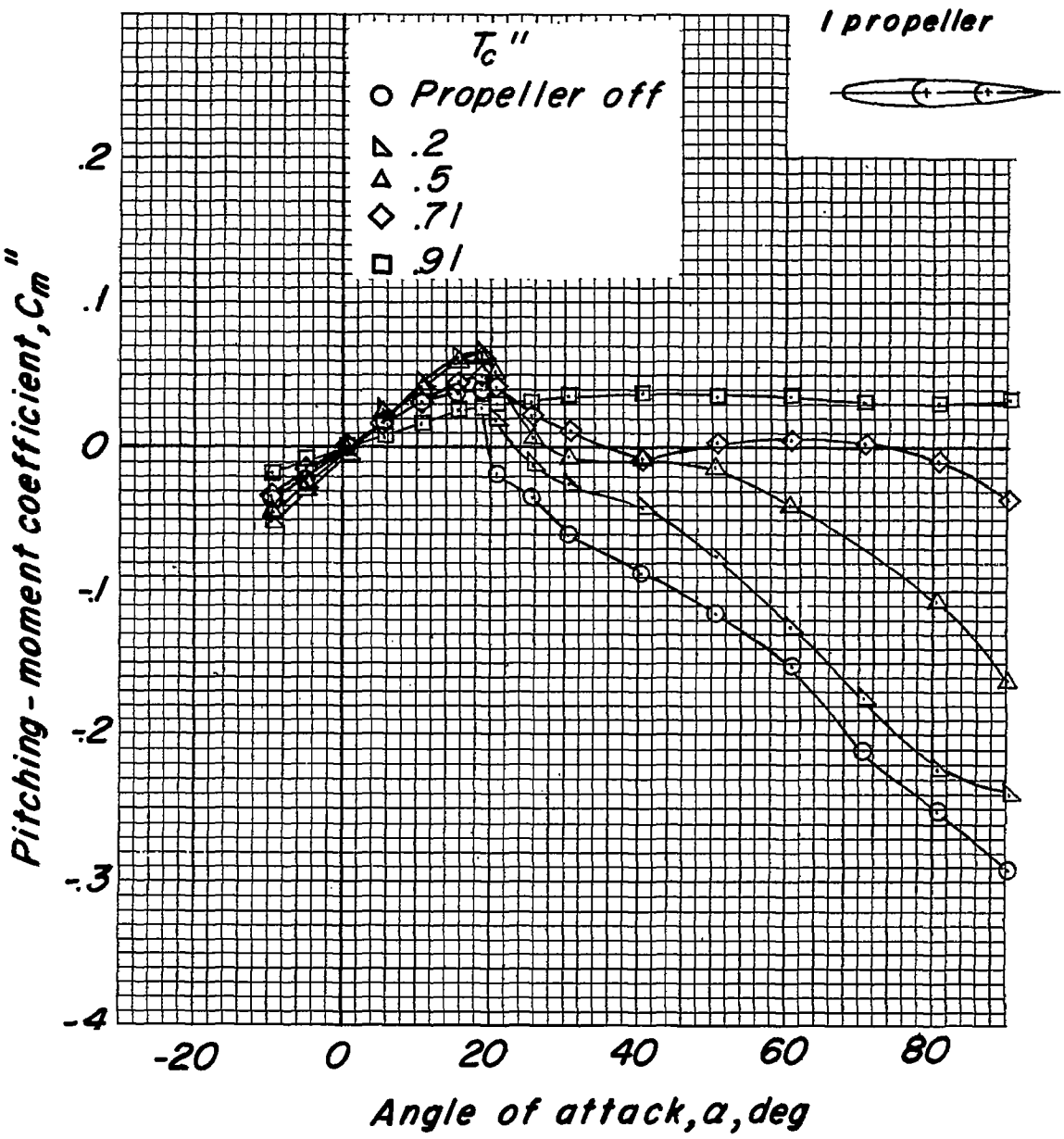

(c) Pitching-moment coefficient.

Figure 23.- Concluded.

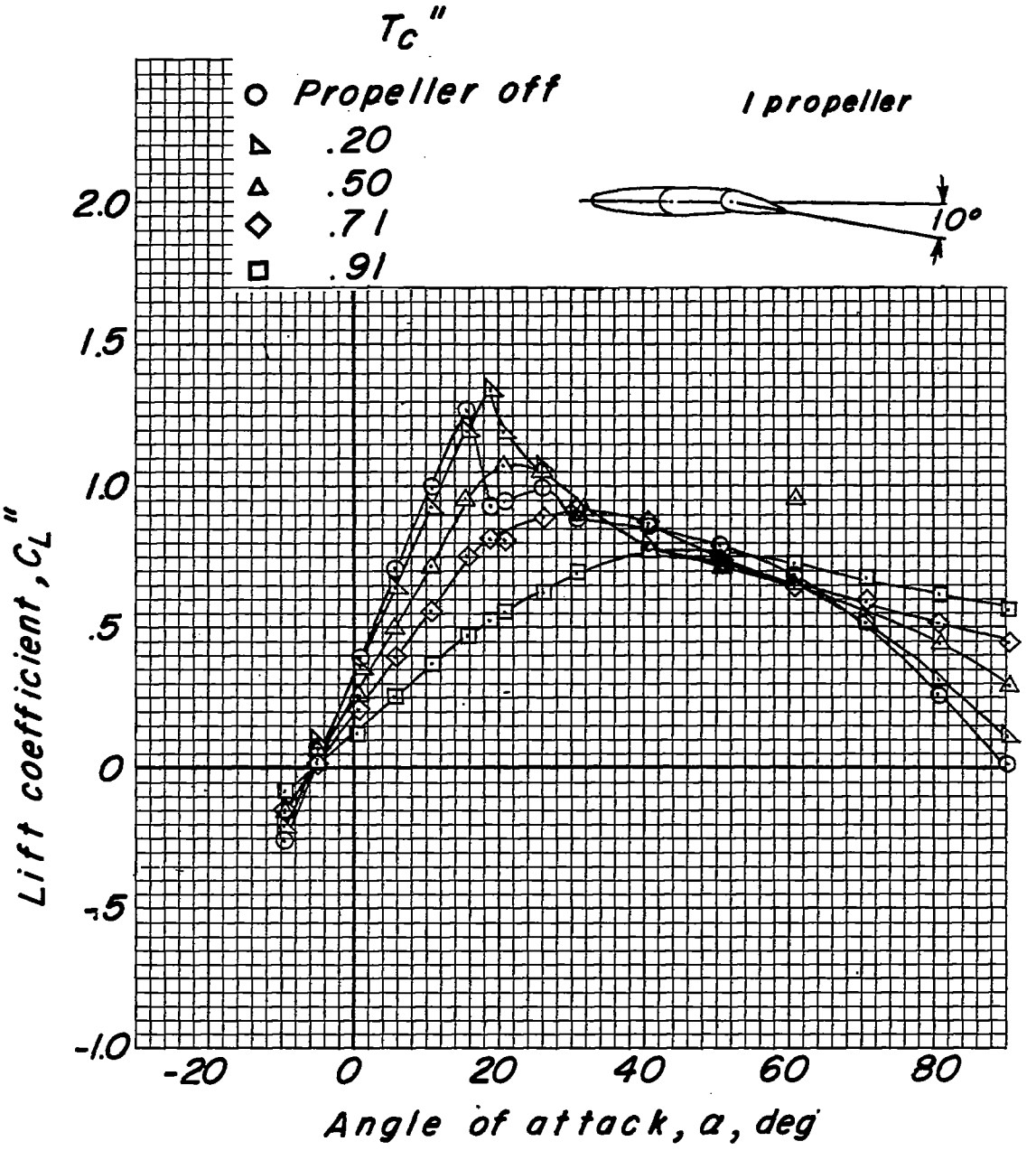

(a) Lift coefficient.

Figure 24.- Effect of thrust coefficient on aerodynamic characteristics of model. Inboard propeller only. $\delta_{f_{30}} = 10°$; $\delta_{f_{60}} = 0°$.

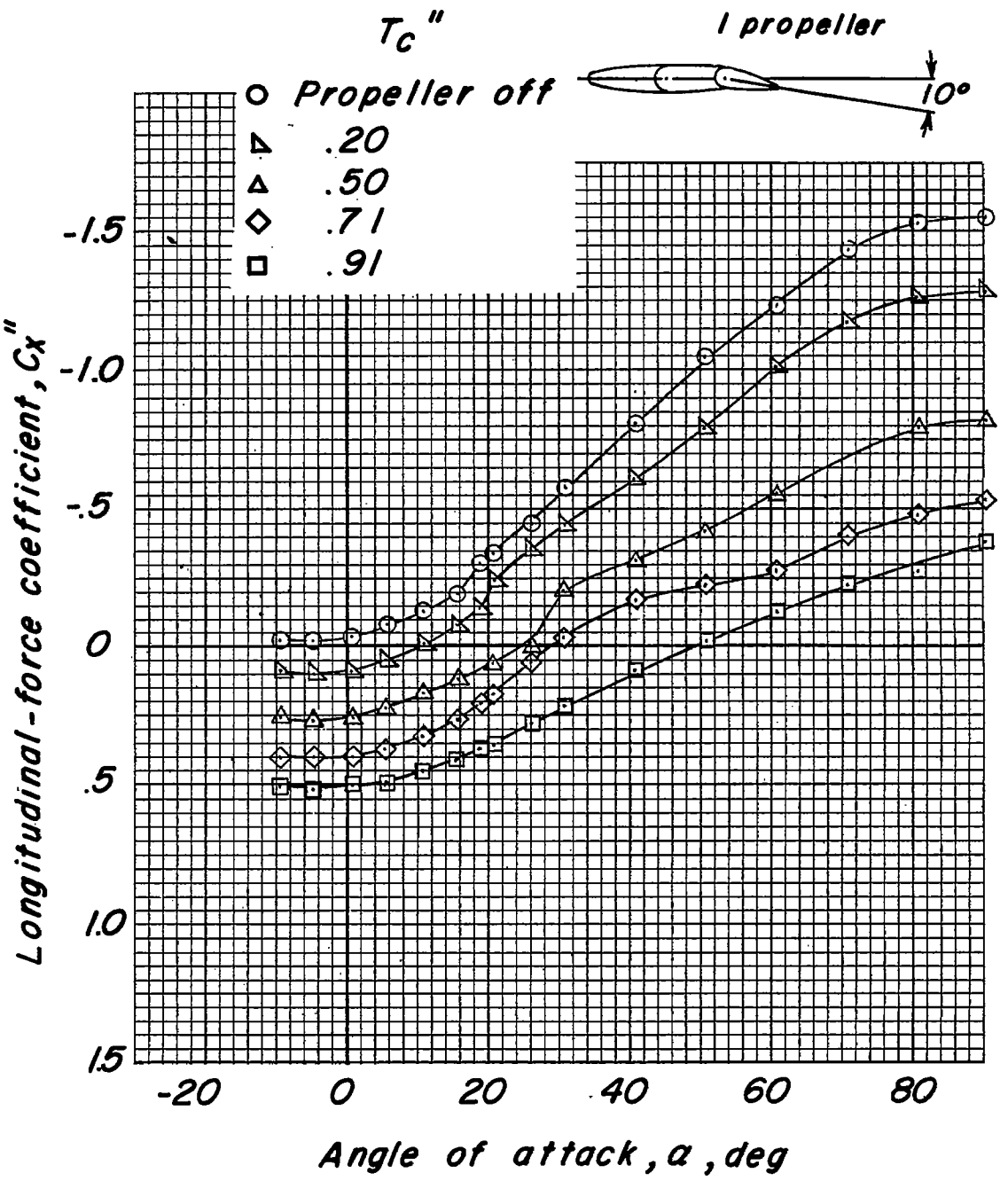

(b) Longitudinal-force coefficient.

Figure 24.- Continued.

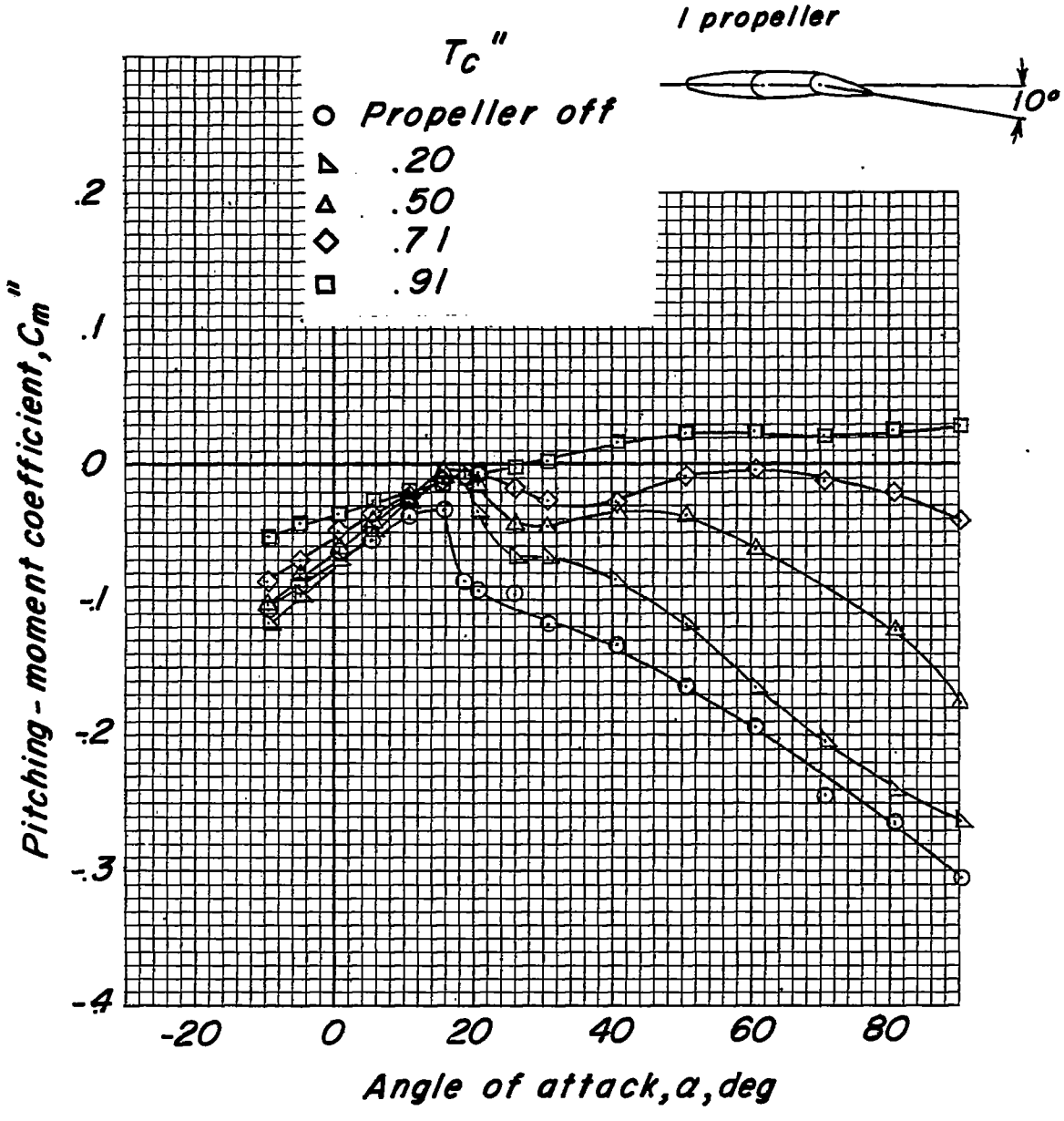

(c) Pitching-moment coefficient.

Figure 24.- Concluded.

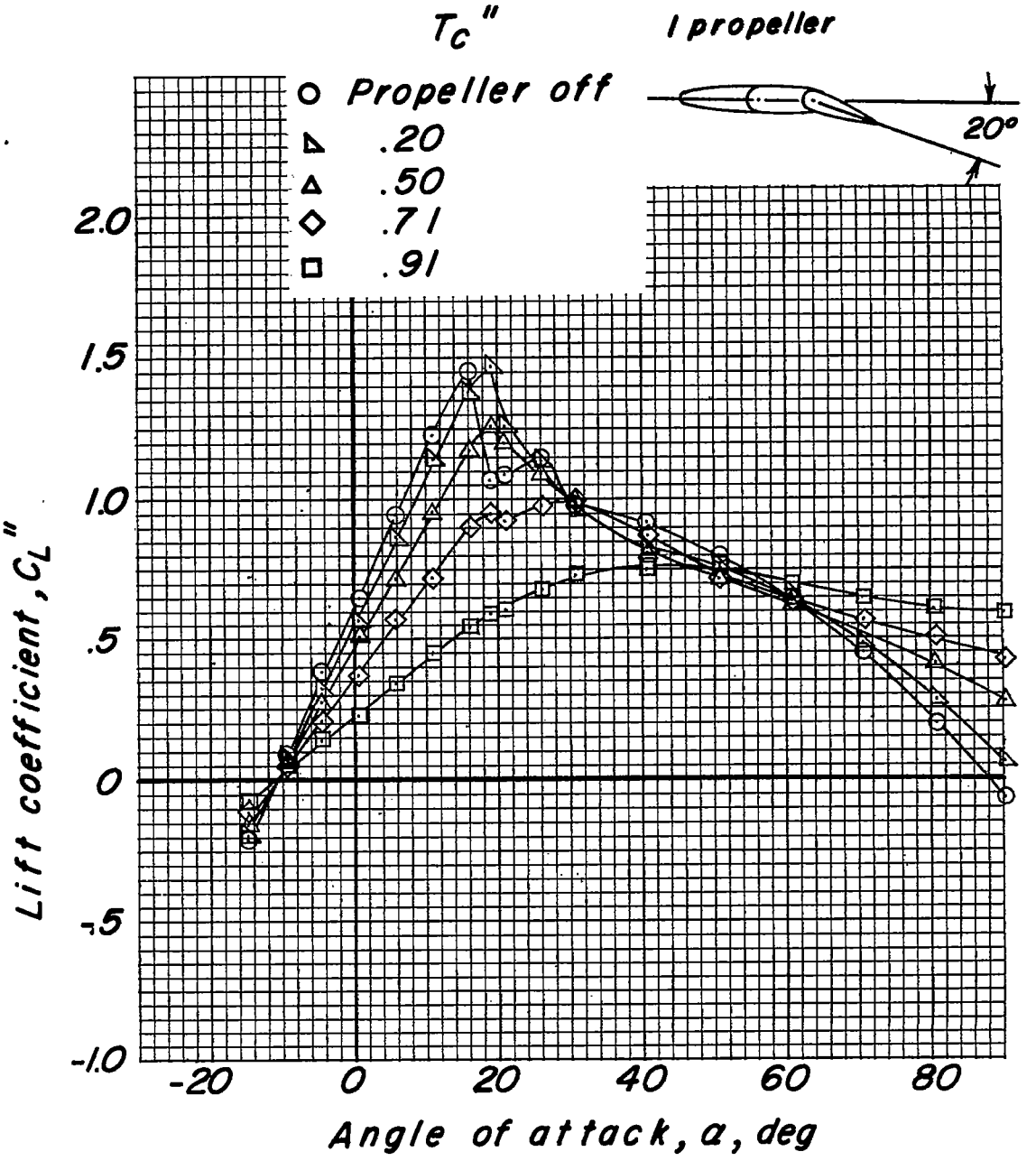

(a) Lift coefficient.

Figure 25.- Effect of thrust coefficient on the aerodynamic characteristics of the model. Inboard propeller only. $\delta_{f_{30}} = 20°$; $\delta_{f_{60}} = 0°$.

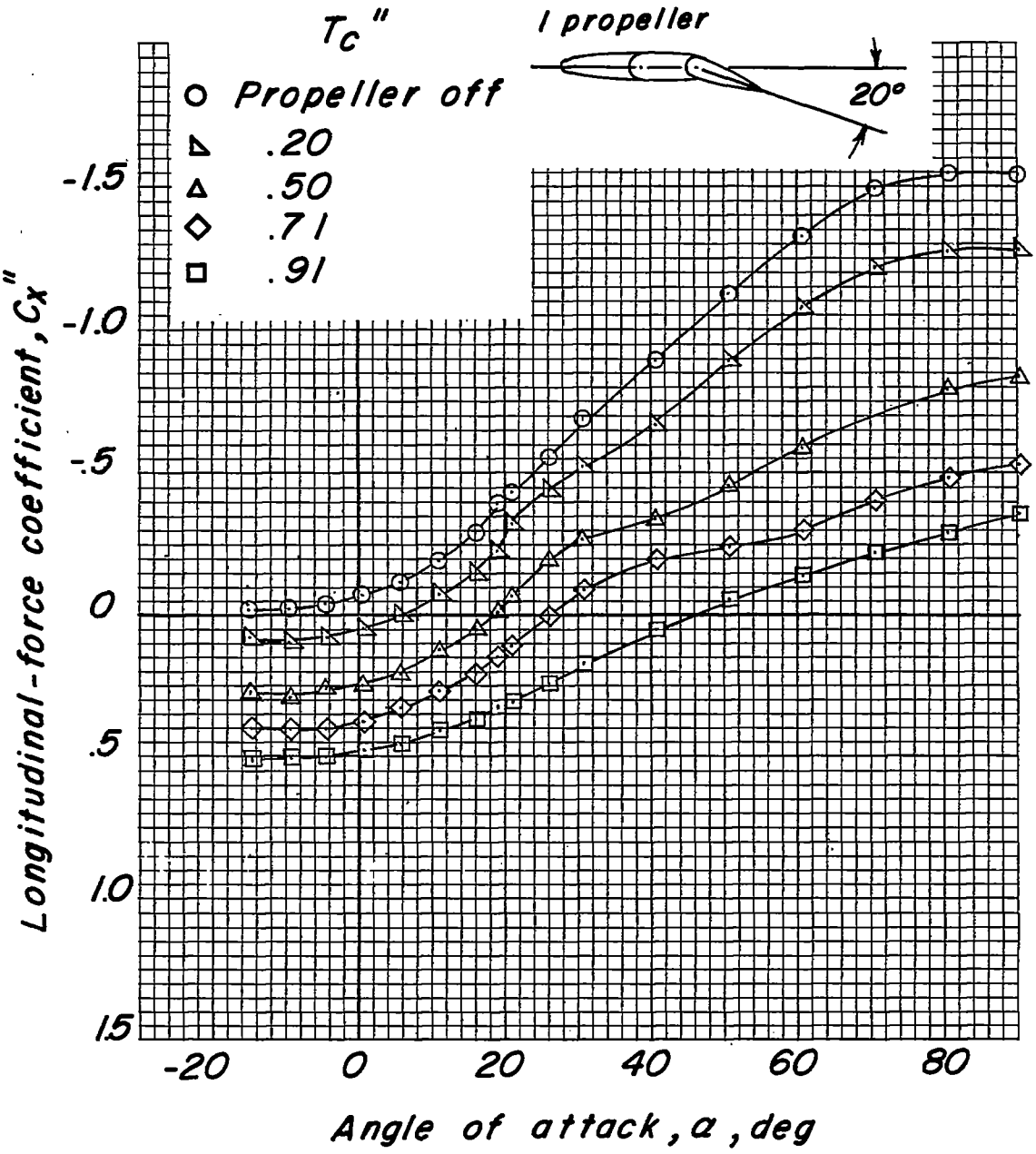

(b) Longitudinal-force coefficient.

Figure 25.- Continued.

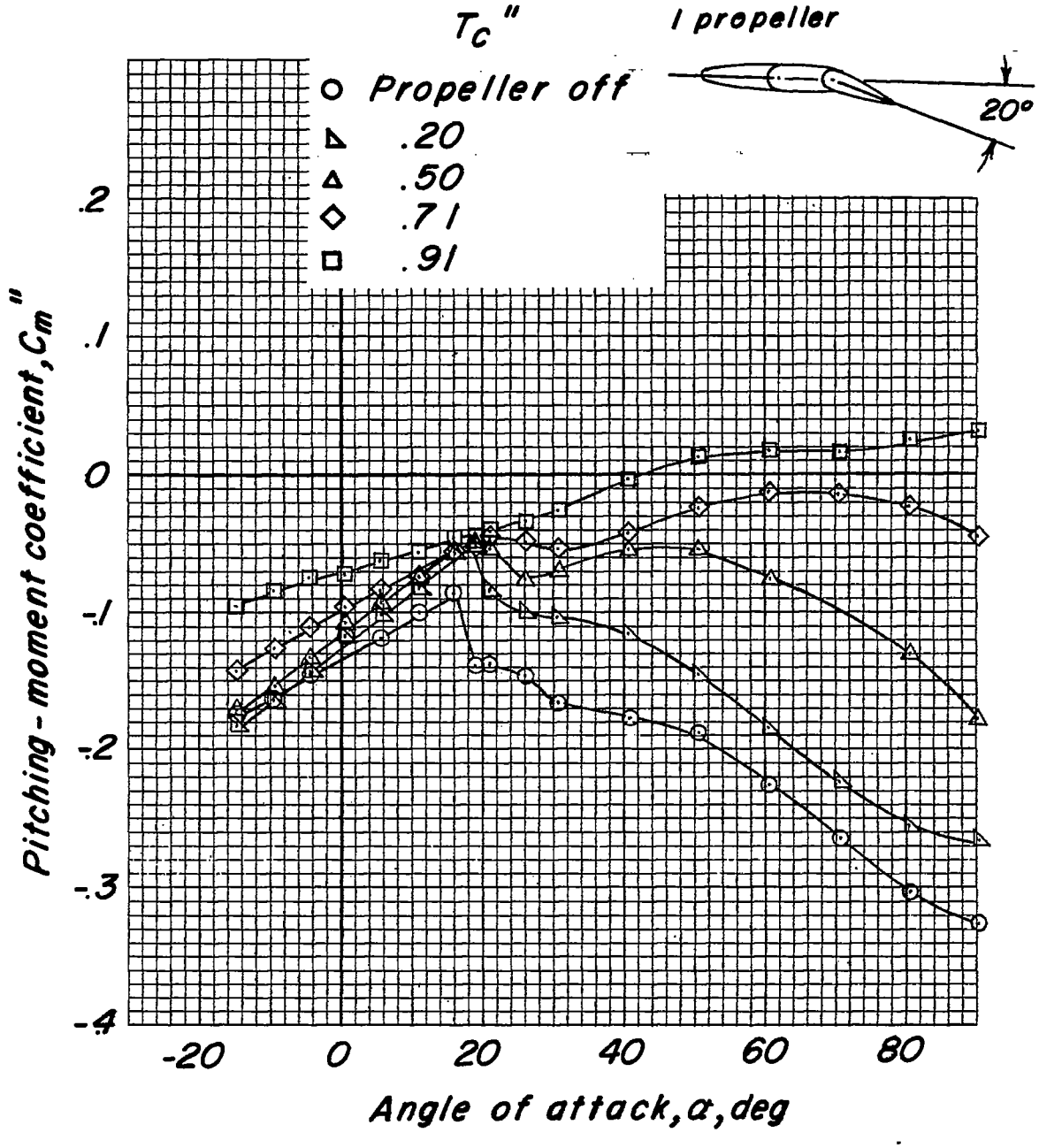

(c) Pitching-moment coefficient.

Figure 25.- Concluded.

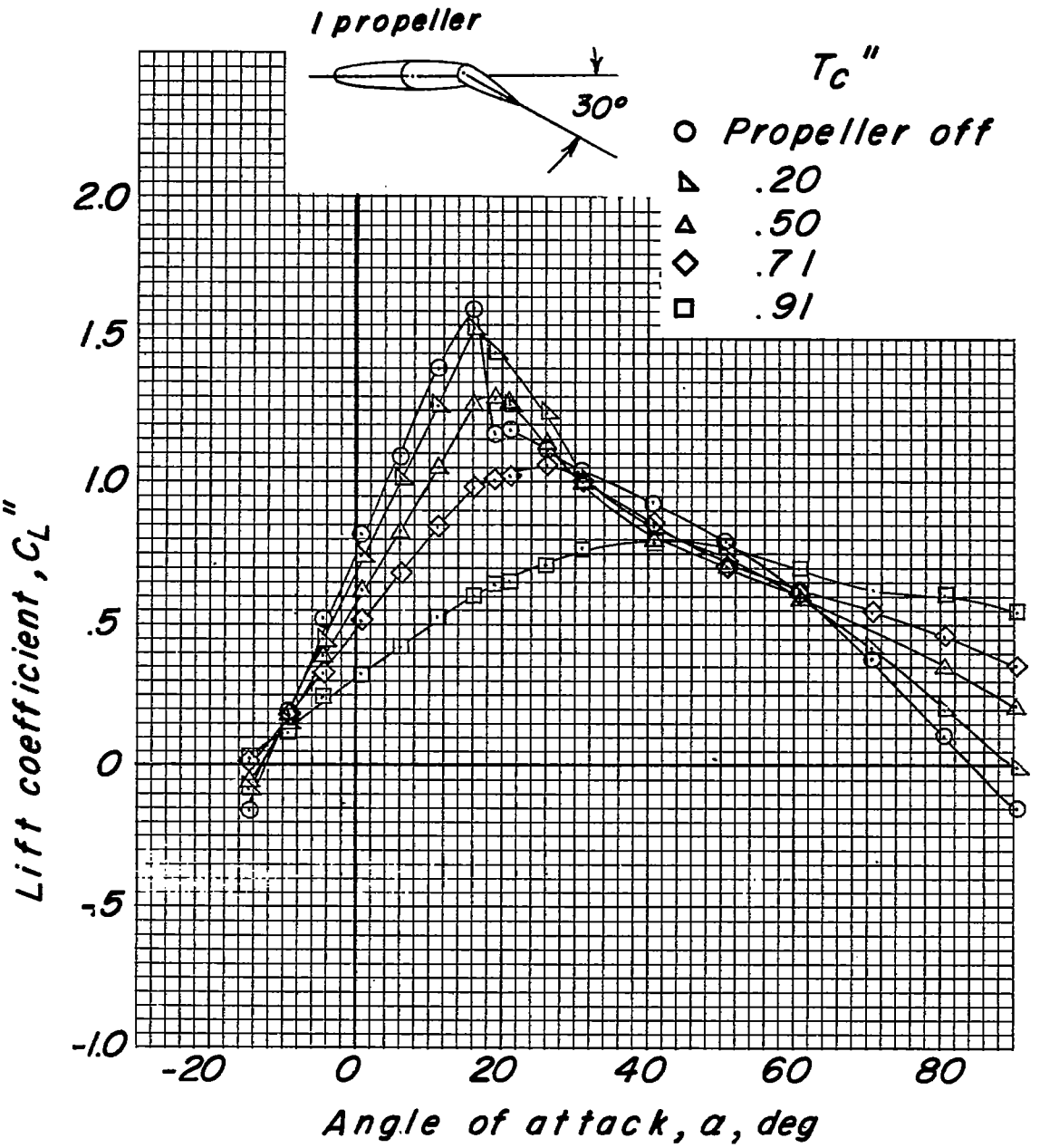

(a) Lift coefficient.

Figure 26.- Effect of thrust coefficient on aerodynamic characteristics of model. Inboard propeller only. $\delta_{f_{30}} = 30^\circ$; $\delta_{f_{60}} = 0^\circ$.

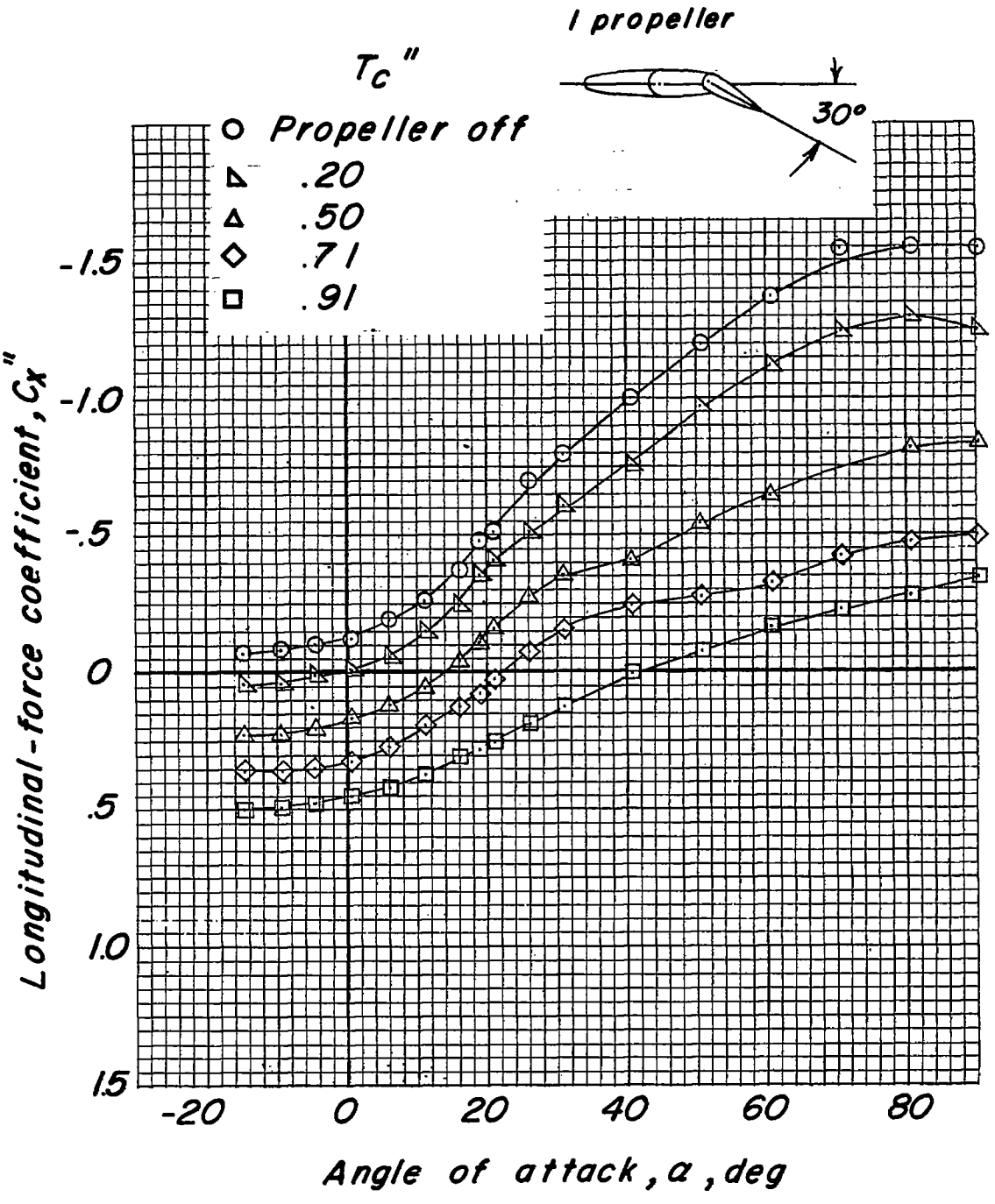

(b) Longitudinal-force coefficient.

Figure 26.- Continued.

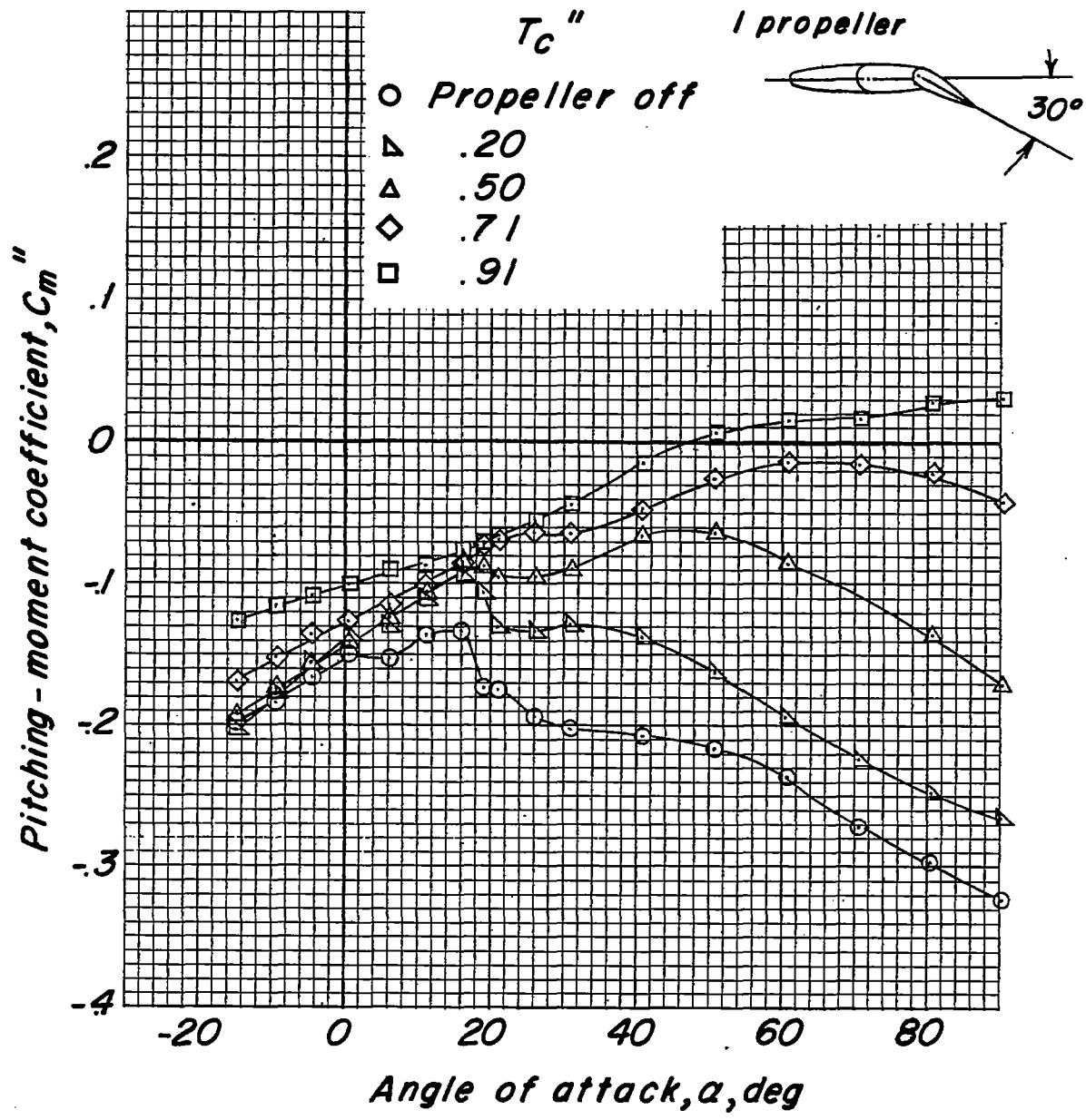

(c) Pitching-moment coefficient.

Figure 26.- Concluded.

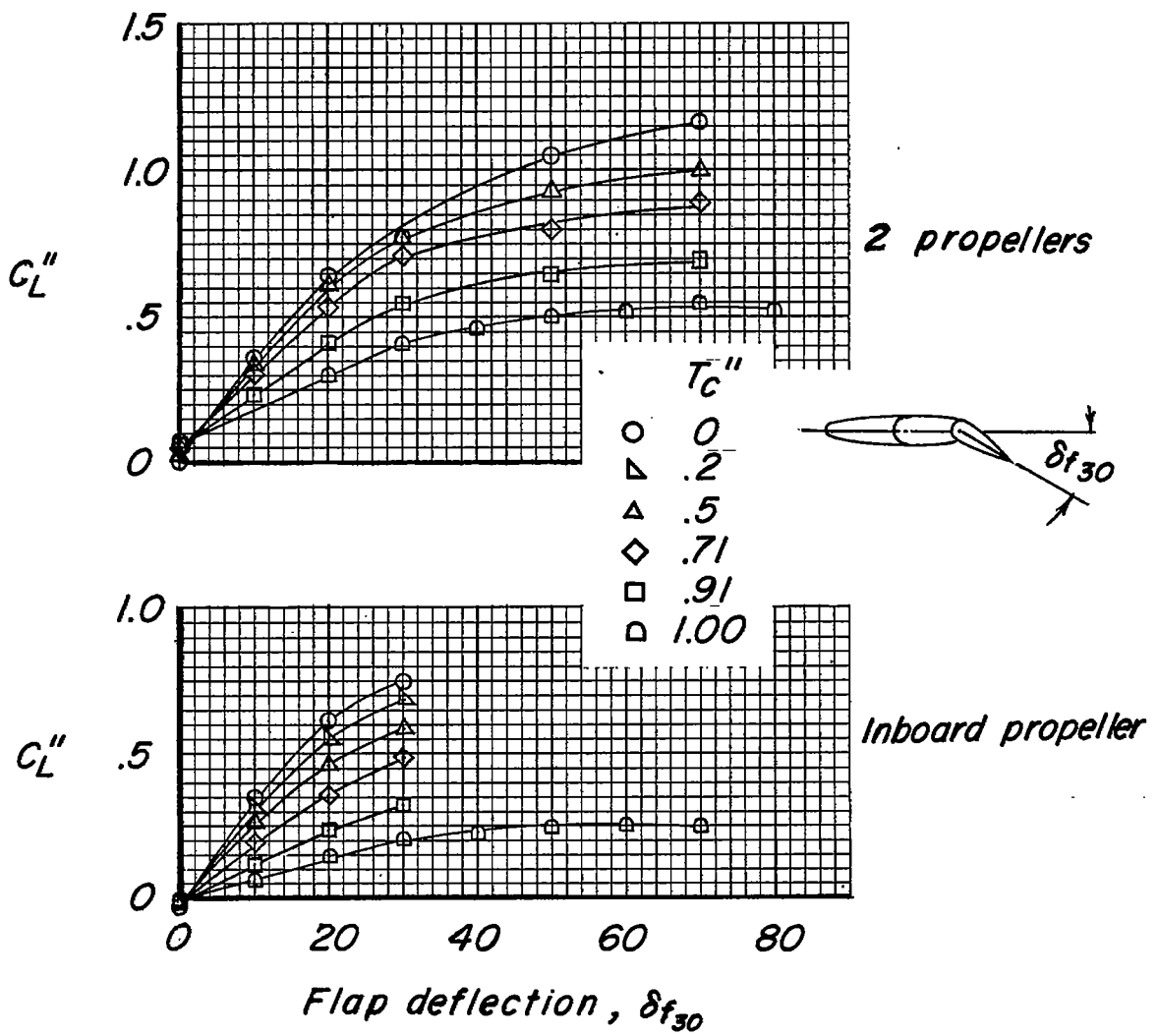

Figure 27.- Variation of lift with thrust coefficient and flap deflection at $\alpha = 0$. $\delta_{f_{60}} = 0^\circ$.

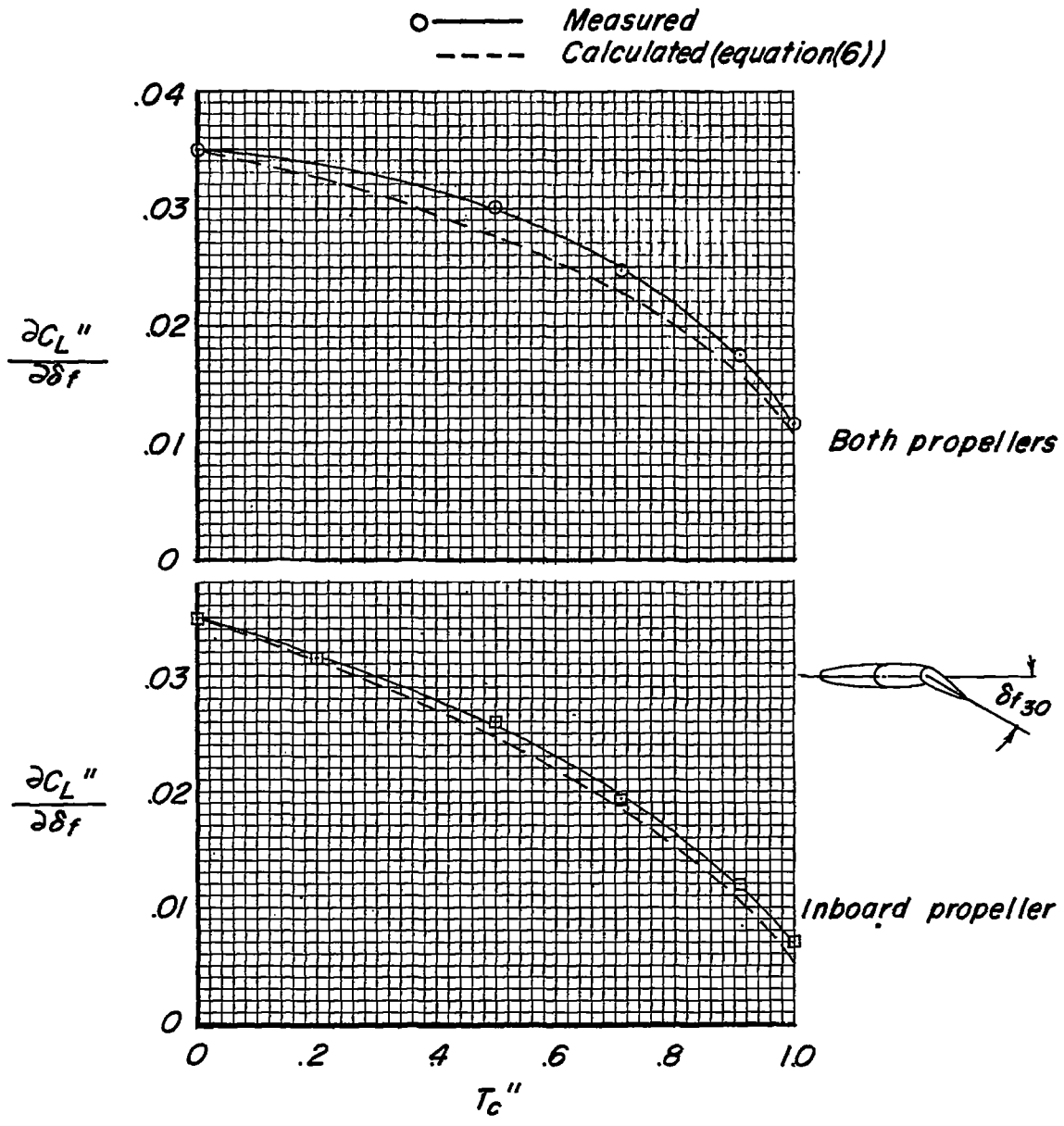

Figure 28.- Variation of $\frac{\partial C_L''}{\partial \delta_f}$ with thrust coefficient. $\alpha = 0^\circ$.

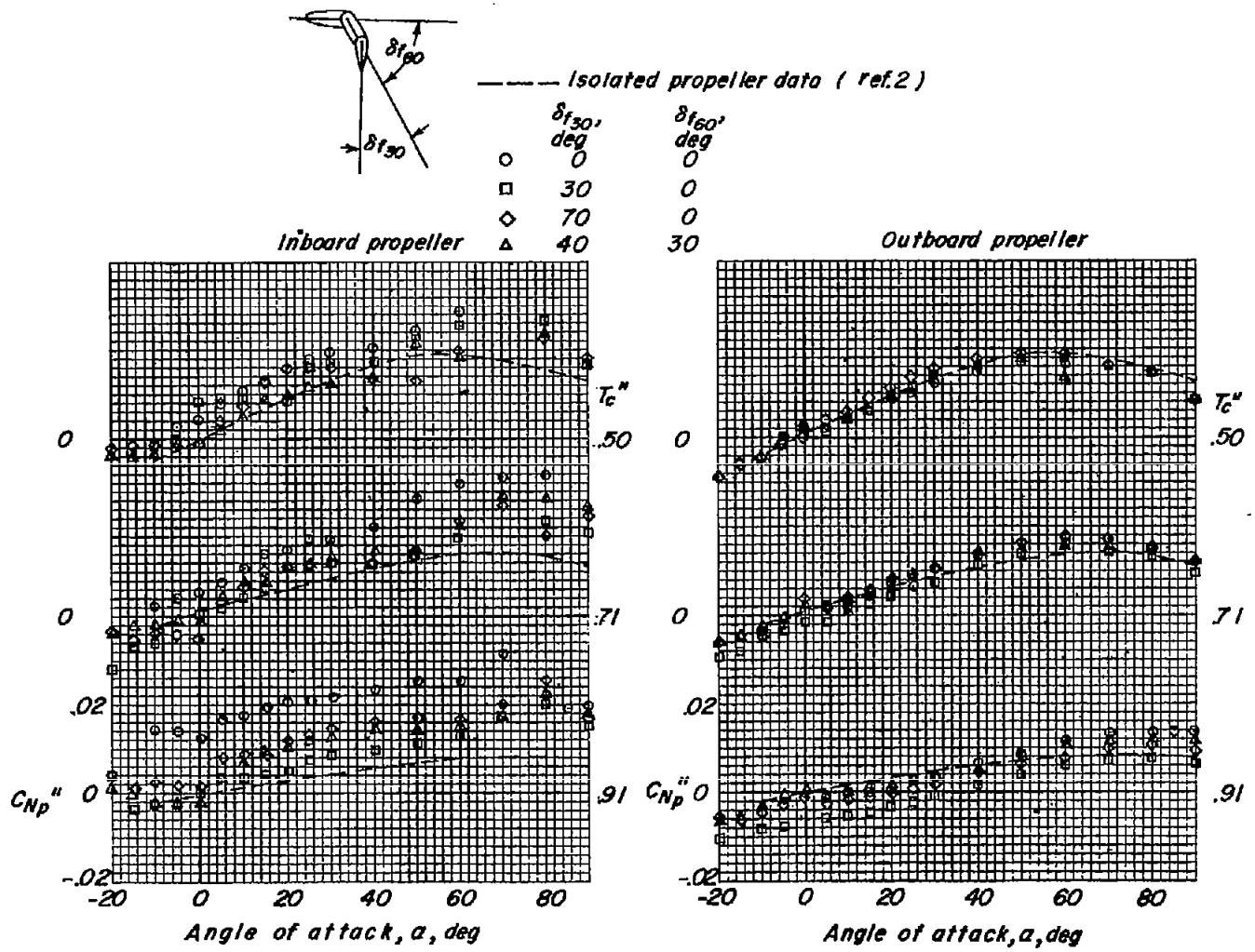

Figure 29.- Effects of flap deflection and angle of attack on propeller normal-force coefficient C_{N_p}''.

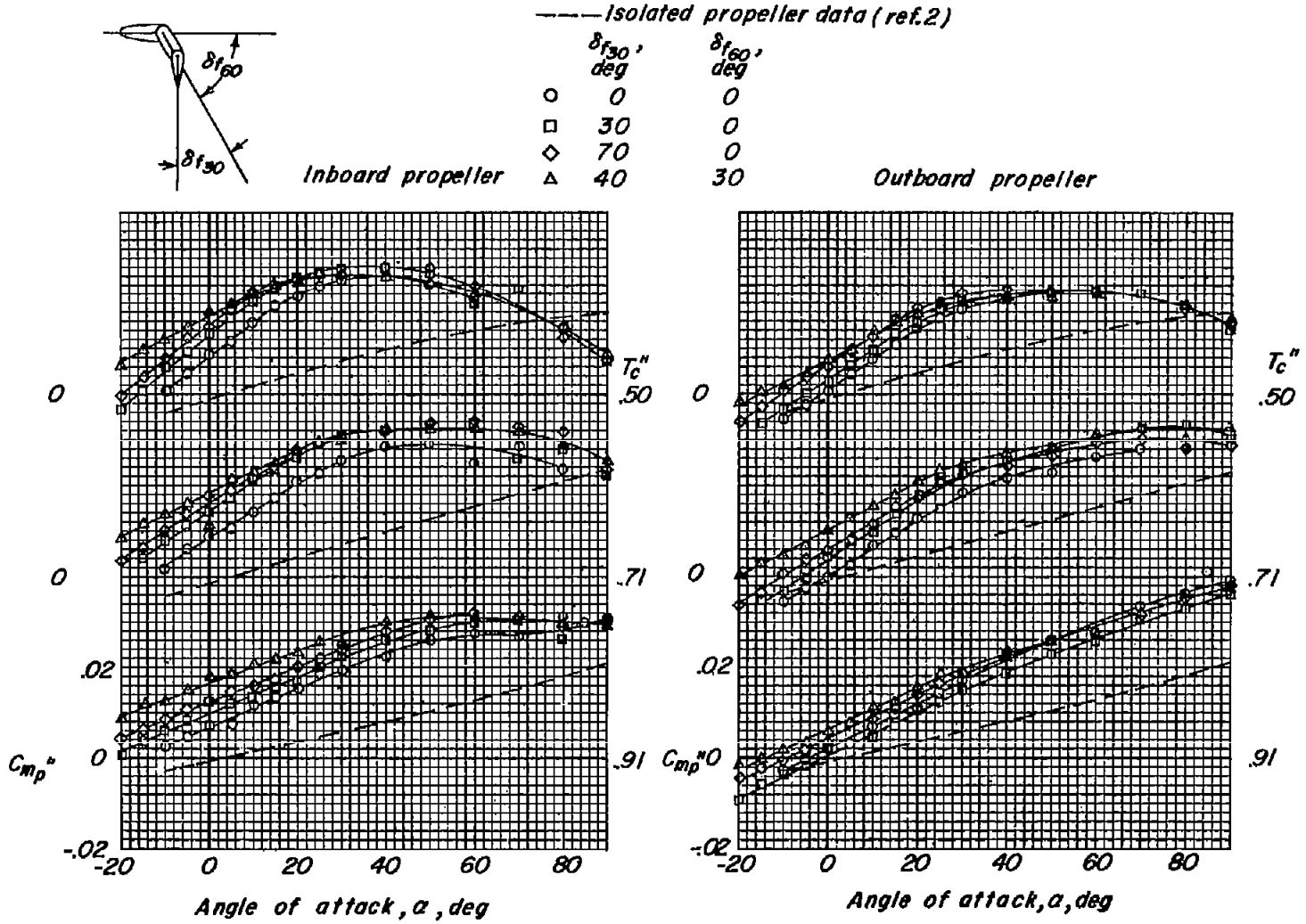

Figure 30.- Effect of flap deflection and angle of attack on propeller pitching-moment coefficient (measured about the intersection of the thrust axis and propeller-disk plane).

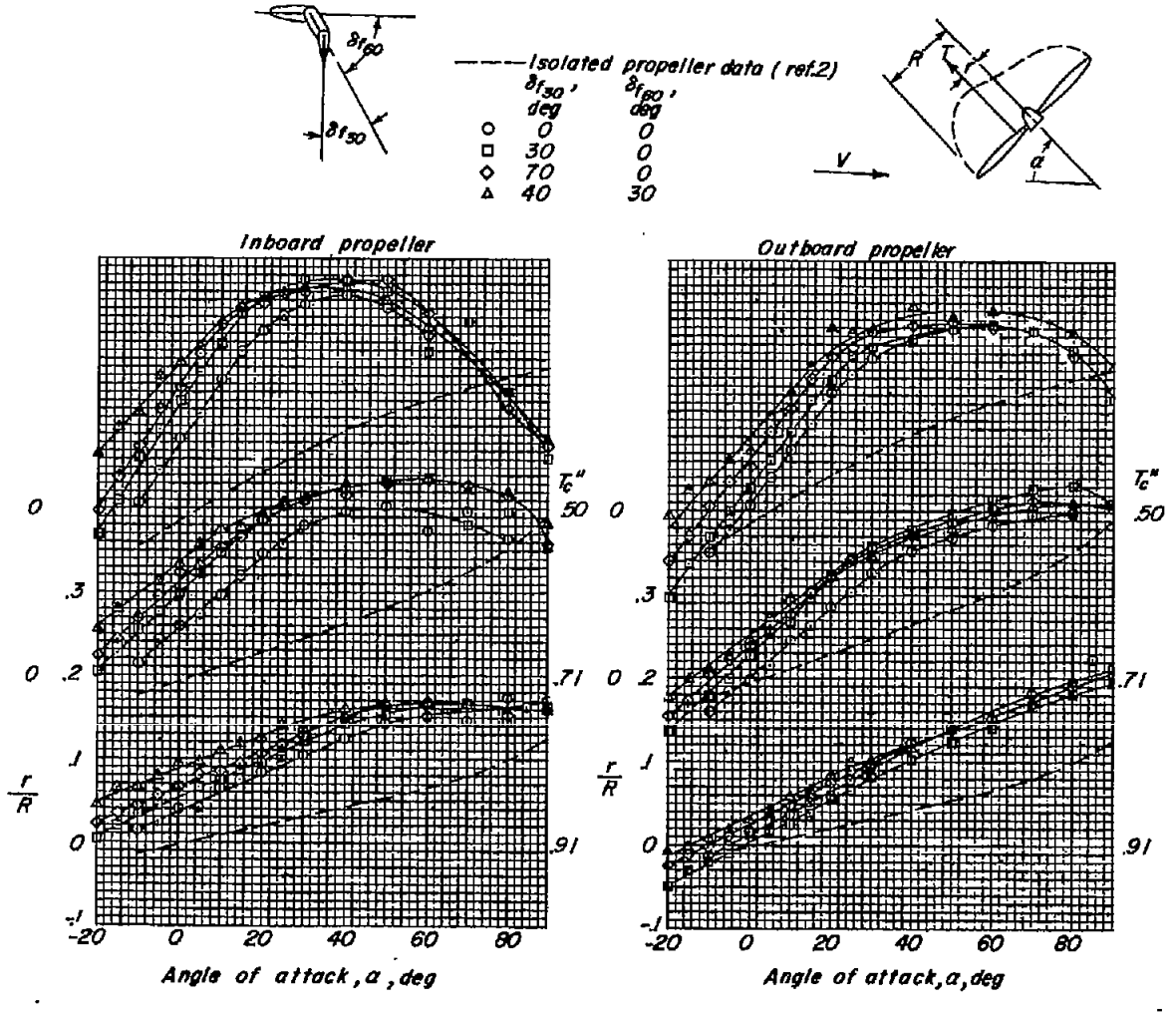

Figure 31.- Effect of flap deflection and angle of attack on effective location of thrust (determined from propeller pitching-moment data of figure 30).

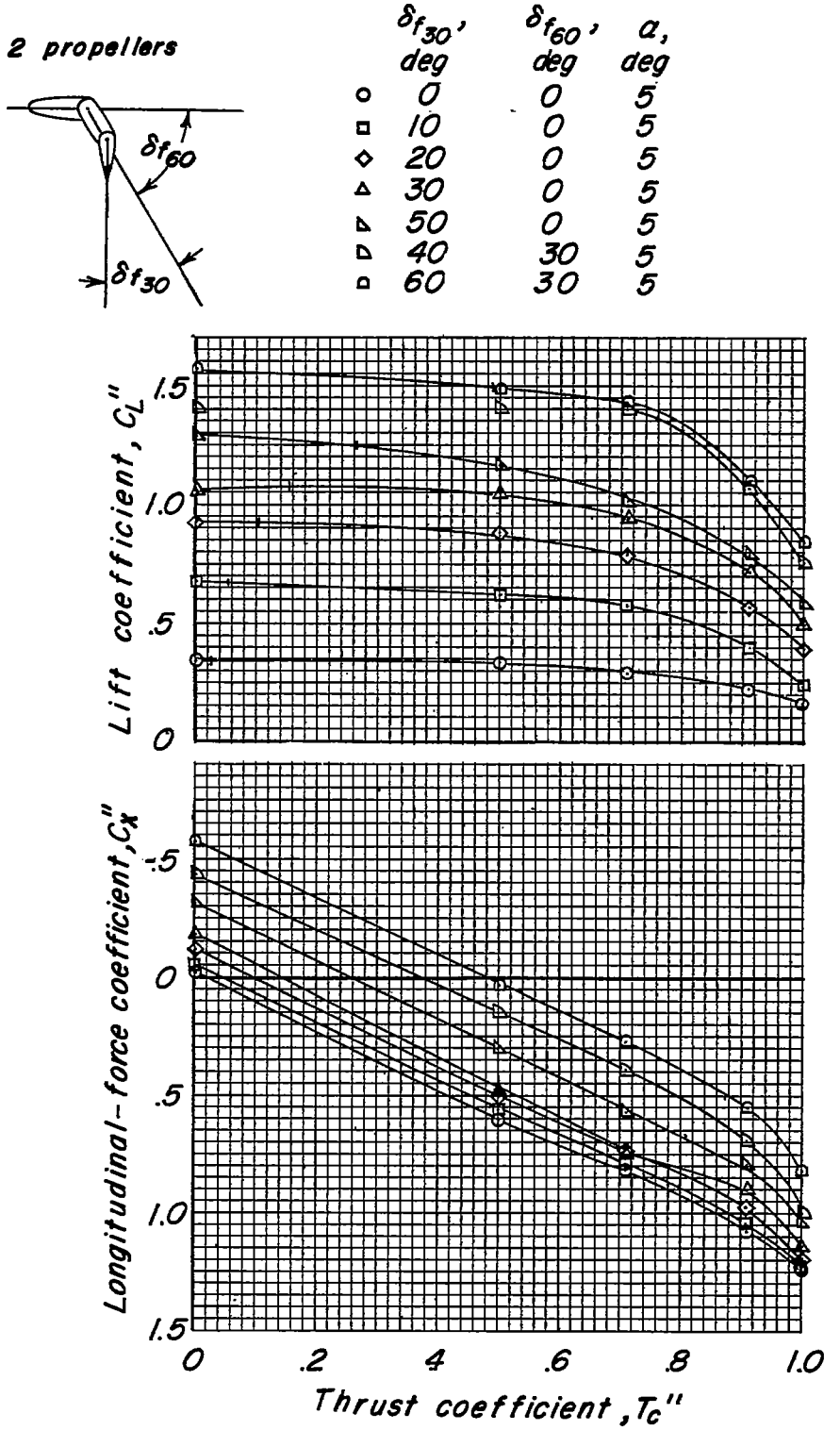

Figure 32.- Variation of longitudinal-force coefficient and lift coefficient with thrust coefficient for various flap configurations.

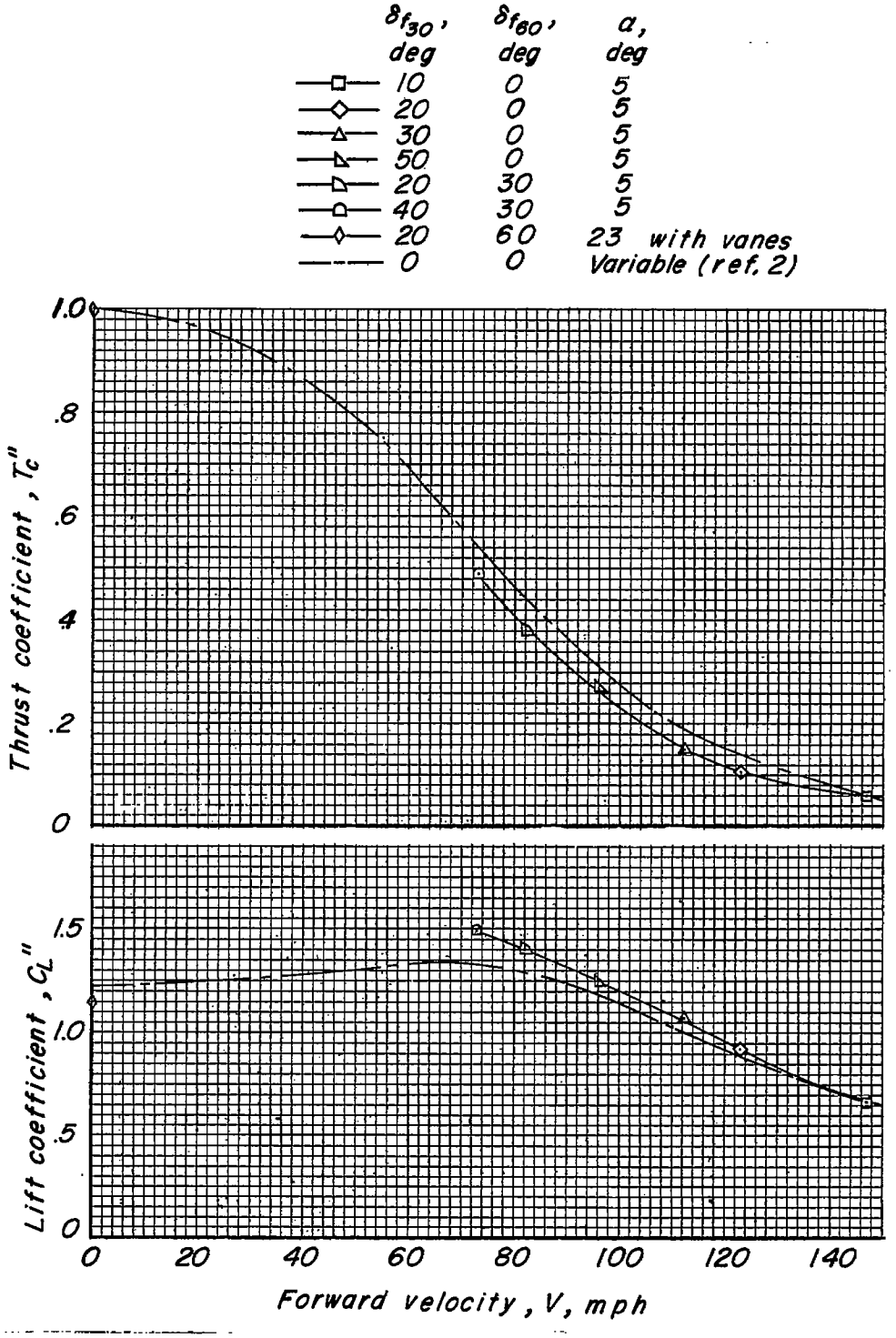

Figure 33.- Variation of thrust coefficient required and lift coefficient available with forward speed. $\frac{W}{S}$ = 40 pounds per square foot.

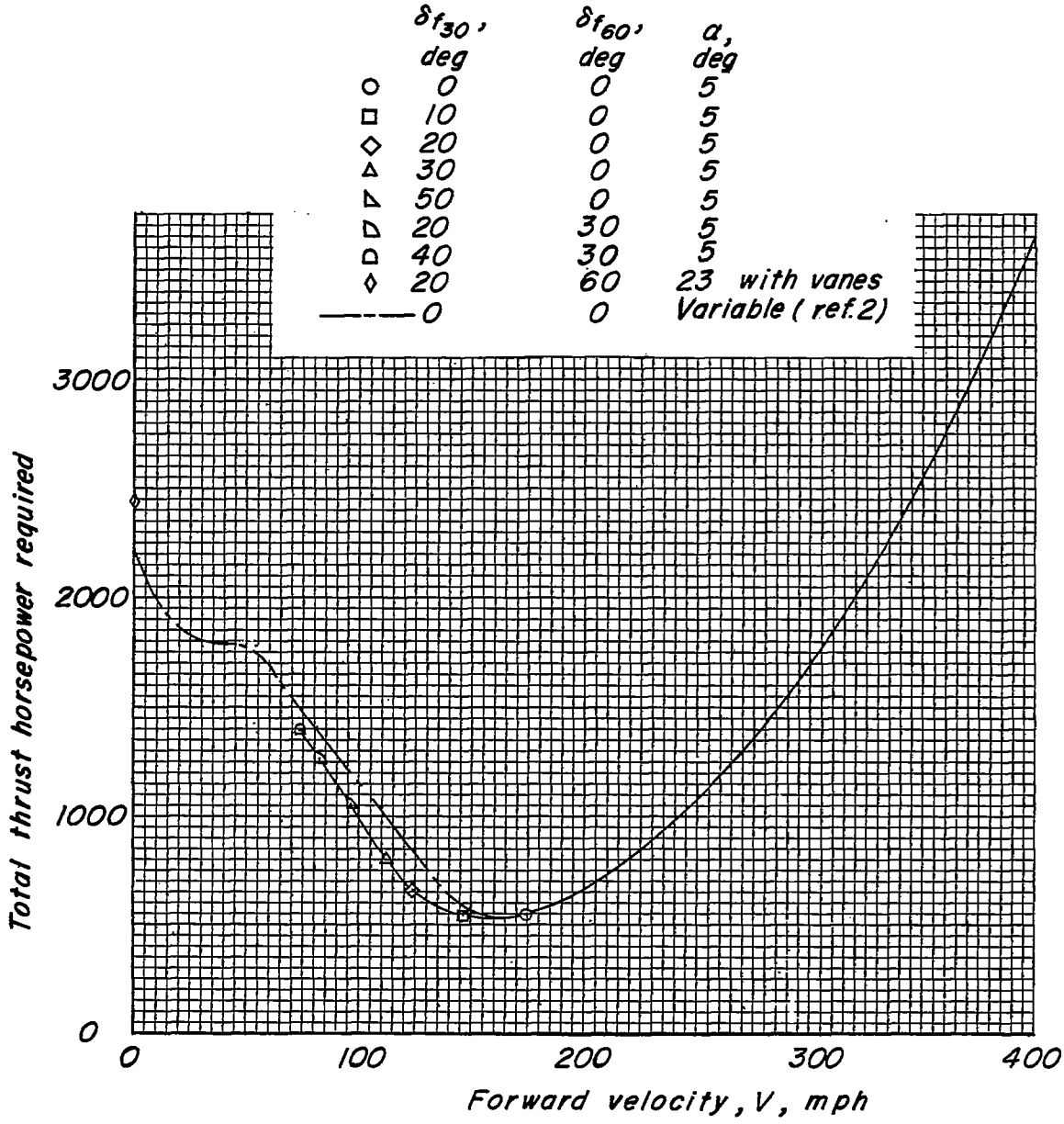

Figure 34.- Variation of total thrust horsepower required with forward velocity for a hypothetical airplane following an assumed flight plan. W = 14,760 pounds; S = 369 square feet; D = 12 feet.

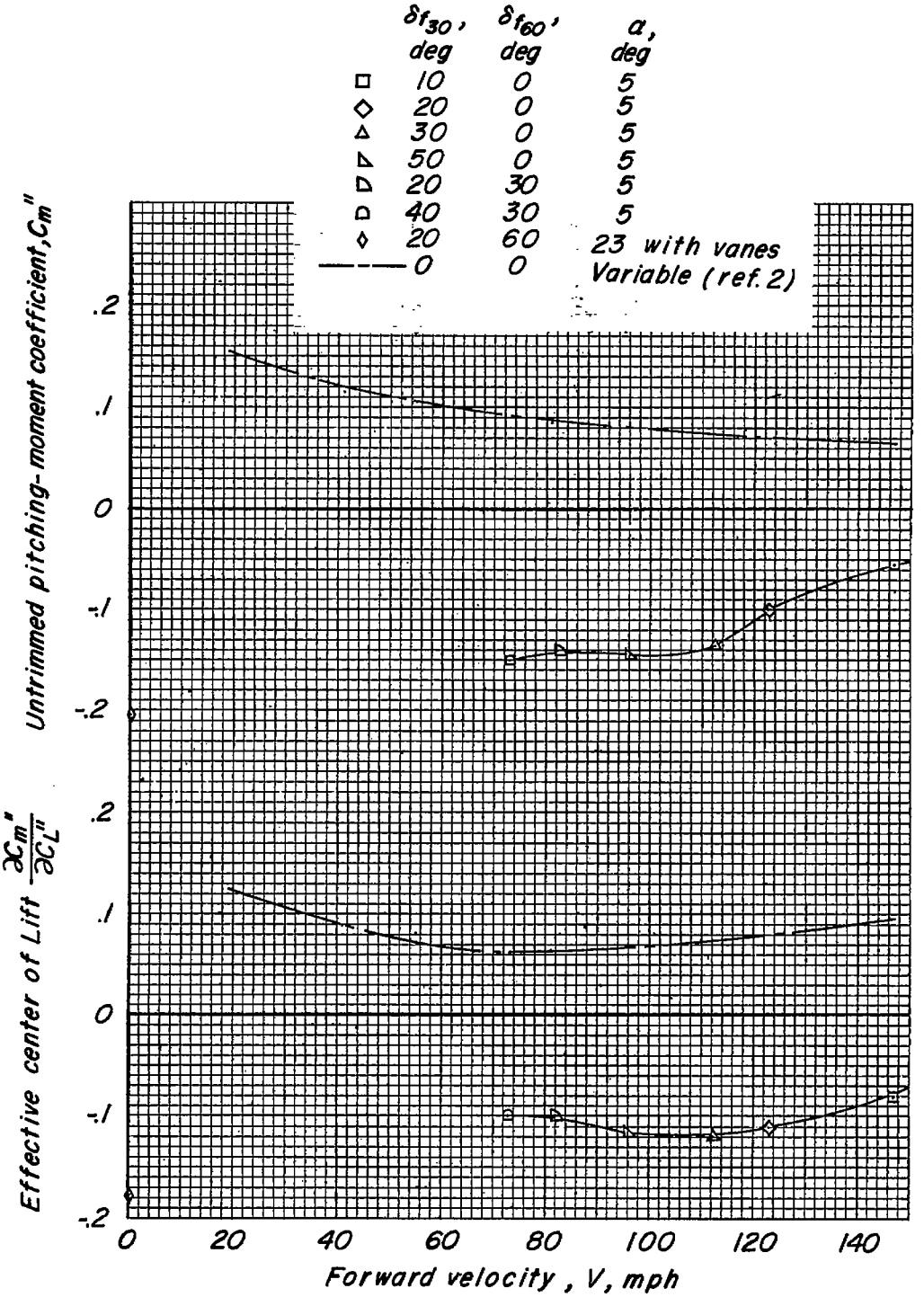

Figure 35.- Variation of the untrimmed pitching moment with forward velocity. $\frac{W}{S}$ = 40 pounds per square foot.

NACA-Langley - 12-13-54 - 1000